STRUCTURAL STUDIES OF THE KILLARNEY IGNEOUS COMPLEX, ONTARIO AND THEIR TECTONIC IMPLICATIONS

By

XIMO FAN, B.Sc., M.Sc.

A Thesis

Submitted to the School of Graduate Studies

in Partial Fulfilment of the Requirements

for the Degree

Doctor of Philosophy

McMaster University

STRUCTURAL STUDIES, KILLARNEY, ONTARIO

DOCTOR OF PHILOSOPHY (1995) MCMASTER UNIVERSITY

(Geology) Hamilton, Ontario

TITLE: Structural Studies of the Killarney Igneous Complex, Ontario and Their Tectonic Implications

AUTHOR: Ximo Fan, B.Sc. (Peking University)

M.Sc. (Institute of Geology, Academia Sinica)

SUPERVISOR: Dr. Paul M. Clifford

NUMBER OF PAGES: xv, 208

ABSTRACT

The Killarney Igneous Complex (KIC), one of a suite of plutons known as the Killarney Magmatic Belt along the Grenville Front Tectonic Zone (GFTZ), consists of granite, porphyry and volcanic rocks, forming a wedge between Huronian metasediments of the Southern Province and the Grenville Province gneisses.

Structural analysis of micro- and meso-scopic structural features of the KIC suggests that a set of subparallel faults observed in the research area are thrusting faults with substantial dextral horizontal movement. Various kinematic indicators are examined and proved very useful in determining the sense of shear accommodated by the faults. Palaeopiezometry indicates that the differential stress related to the thrusting ranged from 85 MPa to 146 MPa, with average of 100 MPa and standard deviation of 15 MPa, similar to the results obtained from other major thrusting zones. Fault-slip analysis reveals that the maximum compressive stress responsible for the thrusting came from the WNW direction, supporting the tectonic model that these faults were imposed by the indentation of the Superior craton.

Two fracture variations, namely, kinks and wedges, are found common in the KIC and are studied theoretically and practically. The study provides valuable insight into the palaeostress field and the regional structural development in the research area. Kink angles are found to be a reliable kinematic indicator, and are determined by the

ratio of the effective shear stress and the effective normal stress acting on their parent fractures. Wedge angles are found to be the prime factor controlling the fracture patterns developed within wedges; the formation of wedges was associated with the development of main faults.

These structural studies are integrated with previous work of geochronology into a tectonic model for the geological history of the KIC and the surrounding area. During the period of 1.75-1.65 Ga, the KIC was emplaced in a transtension zone due to the southeasterly indentation of the Superior craton or the northwesterly encroachment of the block of Grenville Province. After its emplacement, the KIC underwent two major compressional events: the first one imposed a regional foliation and lineation in the porphyry-volcaniclastic assemblages, at about 1.62 Ga; the second event, due to a renewed southeasterly indentation of the Superior craton or northwesterly encroachment of the Grenville Province, imposed the thrusting faults in the area, and effectively produced a transtension zone between the KIC and the Grenville Province, so providing the space and the thermal environment for the emplacement of the Bell Lake Granite (ca. 1.47 Ga).

ACKNOWLEDGEMENTS

I wish to express my sincere gratitude to my supervisor, Dr. P. M. Clifford who suggested the research area and provided cordial assistance and valuable guidance throughout the course of my study at McMaster. Dr. P. M. Clifford also negotiated funds for pertinent field trips.

I would like to thank Dr. W. A. Morris and Dr. R. G. Drysdale, who acted as members of my Ph.D supervisory committee and offered their advice and time throughout the project. My thanks also go to many other members of the Geology Department, too numerous to mention individually, for their assistance and various stimulating discussions.

Many thanks are extended to Mr. J. Worwood for his expert photography; to Mr. L. Zwicker for his excellent thin section preparation; to Mr. L. Ma for his enthusiastic field assistance.

Gratitude is also due to my wife, Shuhong, for her patience and continuous encouragement throughout my graduate studies.

Yates Fund and the GSA Travel Assistance Fund are acknowledged for supporting me to attend pertinent academic conferences. C. W. Sherman Graduate Scholarship, J. P. Bickell Bursary and the Departmental Graduate Scholarship of Geology are acknowledged for financial assistance towards this study.

TABLE OF CONTENTS

LIST OF FIGURES

LIST OF TABLES

CHAPTER 1, INTRODUCTION

The Canadian Shield contains several large structural provinces, each of which is characterized by a common period of most recent orogenesis. The youngest structural province of the Canadian Shield is the Grenville Province which forms a belt approximately 2000 KM long and 400 KM wide on the southeast margin of the shield. The northwest border of this province, the Grenville Front Tectonic Zone (GFTZ), truncates several older structural provinces, and also separates the Killarney Igneous Complex (KIC) from the gneissic rocks of the Grenville province. The Killarney Igneous Complex consists of granite, porphyry and volcanic rocks, forming a wedge between Huronian metasediments of the Southern Province and the Grenville Province gneisses. The KIC is one of a suite of plutons that form a continuous chain from the lakeshore of Georgian Bay to the northeast for approximately 80 KM along the Grenville Front Tectonic Zone.

For many decades, the Grenville Province, especially the Grenville Front Tectonic Zone, has attracted many geologists because of its particular tectonic location and mining significance. Even though, one may make different interpretations about the nature and status of GFTZ depending on where the research is done due to the complex nature of the Grenville Province. As Davidson wrote (1986), "despite a century's accumulation of knowledge and evolution of ideas about the Grenville Province, perhaps the only

consensus is that it represents the youngest orogenic belt in the Canadian Shield."

Besides the nature and status of GFTZ, the position of GFTZ is also a matter of controversy. In Killarney area two positions for the Front have been proposed: (1) along the northwest edge of the Killarney Igneous Complex (Frarey and Cannon, 1969; Frarey, 1985), hence, the KIC is included in the Grenville Province; (2) along the southeast edge of the KIC associated with a mylonite zone, therefore excluding the KIC from the Grenville Province (Lumbers, 1975; Card and Lumbers, 1977; Clifford, 1986, 1991). The latter notion has now been accepted by most geologists because of the structural features within the mylonite zone.

The ultimate objective of this study is to provide one more stepping-stone towards a better understanding of the geological history of the KIC and shed some light on the tectonic evolution of the GFTZ. The study focuses on structural analysis, mesoscopically and microscopically, in the vicinity of the Killarney village, and this thesis can be subdivided into four parts.

Part one (chapter 1 and chapter 2) introduces the study and the geological setting of the research area, and briefly reviews previous work done in the region.

Part two (chapter 3 and chapter 4) discusses meso- and micro-scopic structural features in a semi-brittle shear zone, consisting of tens of subparallel very high angle reverse faults with substantial dextral shear displacement, in the Killarney Igneous Complex, and investigates various kinematic indicators and their applications.

Part three (chapter 5 and chapter 6) studies two typical structural variations,

namely, kinks and wedges, in the research area, and numerically models the stress field responsible for their formation. In addition, the tectonic implications of these secondary structures are interpreted and integrated into the regional structural development.

Part four (chapter 7 and chapter 8) proposes a tectonic model for the tectonic evolution of the KIC and the surrounding area based on these structural studies and geochronology from other sources, and summarizes the conclusions drawn from this study and presents some suggestions for future research.

CHAPTER 2, GEOLOGICAL SETTING AND PREVIOUS WORK

2.1, Location and Access

The research area is chosen in, more or less, the middle of the Killarney Igneous Complex (KIC), and lies along the lakeshore of Lake Huron, to the east of Killarney village. Outcrops are excellent here, and can be reached by foot or by boat.

Access into Killarney village is easy by highway 637, which joins highway 69 just 40 KM south of Sudbury, Ontario. Highway 637 crosses the Grenville Front and bisects the complex before ending in the village (Figure 2.1).

2.2 Geological Setting of the Research Area

The KIC is the most southwesterly exposure of the suite of intrusions known as the Killarney Magmatic Belt (Easton, 1992), including the Chief Lake Batholith, the Bell Lake Granite and the Killarney Igneous Complex, collectively, formerly called the "Killarney Batholith" or "Grenvillian Front Granites" (Card, 1978), lying along the Grenville Front from Georgian Bay on Lake Huron to the northeast as far as Coniston (Figure 2.1).

The northwest edge of the KIC is in intrusive contact, partially faulted, with

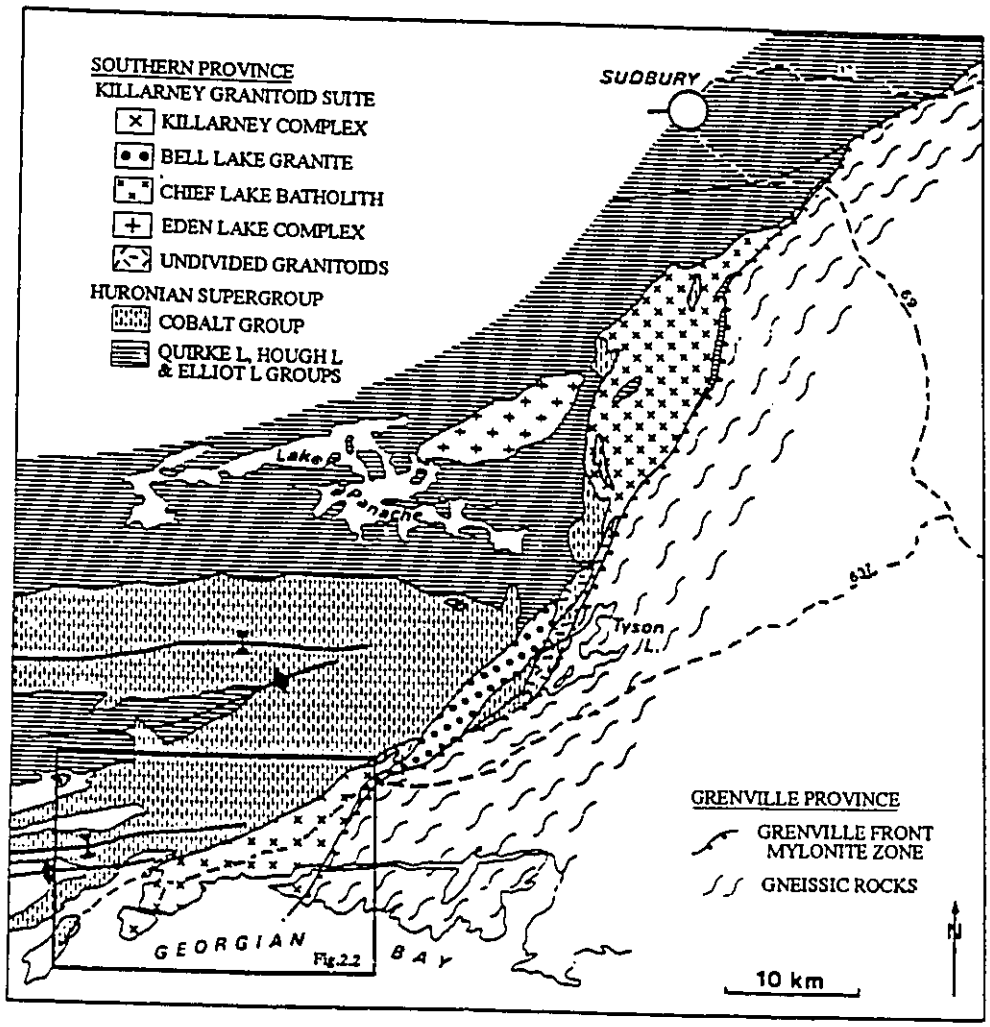

Figure 2.1, General geology of the Grenville Front region between Sudbury and Georgian Bay (after Davidson, 1986b).

Huronian metasedimentary rocks, while most of its southeast edge is separated by a mylonite zone of the GFTZ from the gneissic rocks of the Grenville Province. Based primarily on the appearance of foliation in the assemblage of porphyry and volcanic rocks, the complex can be divided into two parts (Figure 2.2): 1) unit Ka, is predominantly massive, pink, homogeneous, leucocratic granite, and includes numerous xenoliths in the vicinity of Killarney Bay. Rocks are generally not foliated in the unit; 2) unit Kb, is an assemblage of foliated fine-grained porphyritic felsite which typically contains 1 to 2 mm quartz and feldspar phenocrysts, fine-to medium-grained porphyritic granitoid rocks, zone of equigranular rhyolite and felsic volcaniclastic rocks. This study primarily focuses on unit Kb.

2.3, Previous Work

Grenville Province has been studied for over a century, but, as mentioned in chapter 1, the progress of our understanding of its origin has been slow and incomplete due to its complex nature. Several regional studies have been carried out in the past two decades, such as those of Wynne-Edwards (1972), Lumbers (1978), and Stockwell (1982), etc. Based upon different structural and metamorphic styles, Wynne-Edwards (1972) divided the Grenville Province into several subprovinces, such as: (1) the Grenville Front Tectonic Zone (GFTZ); (2) Central Gneiss Belt (CGB); (3) Central Granulite Terrane (CGT); and (4) Central Metasedimentary Belt (CMB) (Figure 2.3).

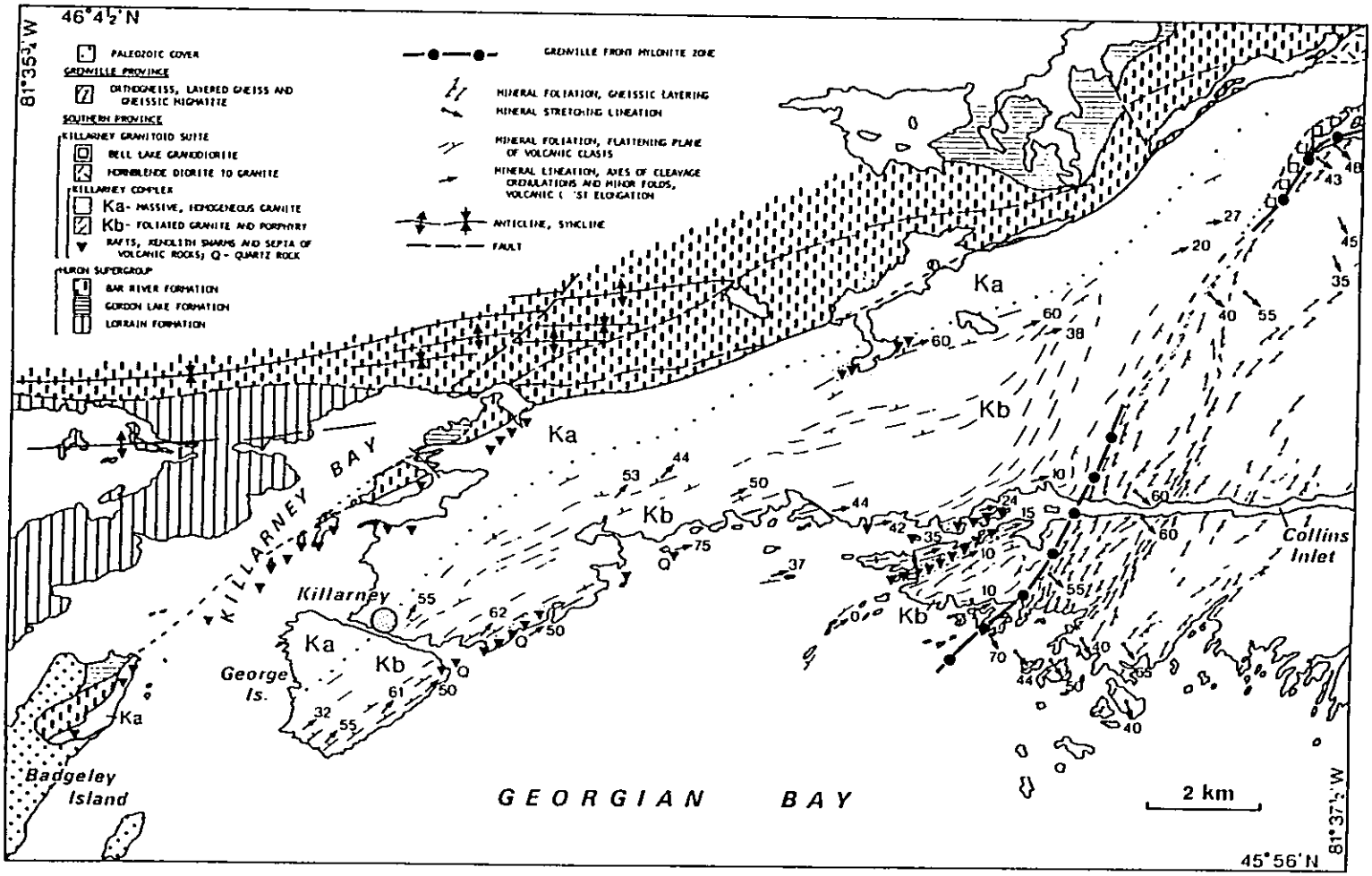

Figure 2.2, Geology of the Killarney Igneous Complex and the surrounding area.
(From Davidson, 1986b)

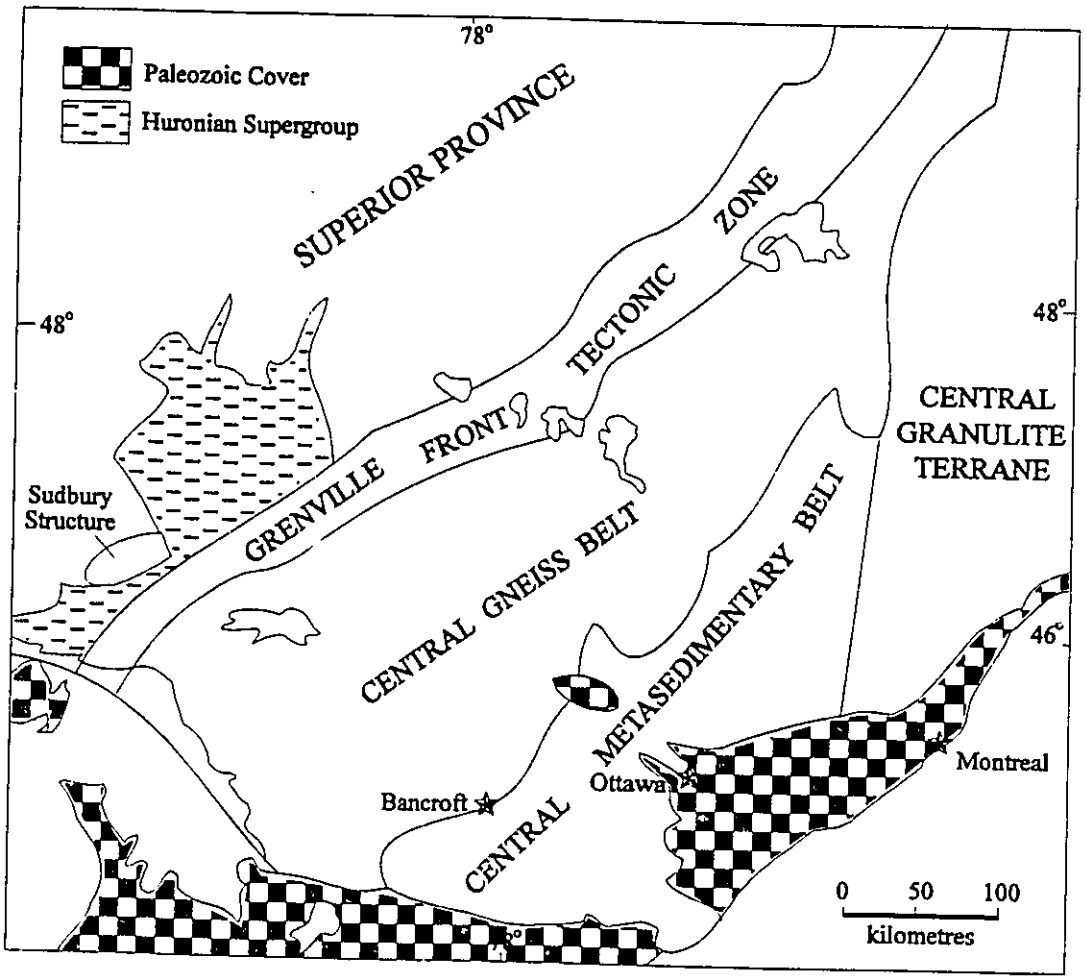

Figure 2.3, Main tectonic divisions of the Grenville Province.
(Modified from Easton et al, 1987)

The GFTZ forms a belt 15 to 80 KM wide, trending northeasterly for about 2000 KM in Canada. The dominant rock type in the zone is mylonite, having a strong and persistent northeast trending foliation and southeast plunging lineation. The Grenville Front, first named by Derry (1950) has long been recognized as a major tectonic feature of the Canadian Shield, but the exact definition of the Grenville Front is still open to question. The problem partially arises from the fact that the structural nature of the Front changes along its trend. Different segments of the Front have different structural features, marked by any one of the following or their combinations: 1) a reverse fault (Wynne-Edwards, 1972); 2) a zone of granitoid intrusions, spatially controlled by some long-lived structural elements (Brooks, 1967; Card et al, 1972); 3) a metamorphic/ultrametamorphic transition (Quirke et al, 1930; Grant, 1964).

Since the mid 1800's, many geologists including Murray (1849, 1857), Bell (1878, 1891, 1898) and Barlow (1893) have been particularly interested in the southeastern Grenville Front. Bell (1898) recognized the post-Huronian granites which he called the "Killarney Belt of Granites" which separate the metasedimentary rocks of the Southern Province from the gneisses of the Grenville Province, and produced the first map showing all the major rock units. Wilson (1918) first recognized the abrupt change in lithology from supracrustals to quartzofeldspathic gneisses across the Front in the Sudbury region and the prevailing high grade of regional metamorphism in the Grenville Province.

Collins (1916, 1925), Quirke (1917) and Eskola (1922) were the pioneers of

systematic mapping in southwestern Grenville Province and the adjacent area in the Southern Province. Collins (1925) established the structural and stratigraphic relationships of the Huronian rocks of the Southern Province, and recognized the Grenville Front, which he thought was the limit of Huronian strata. Later, Quirke and Collins (1930) studied the relationship between the Huronian sediments and the Grenville gneisses, and concluded that the "Killarney Belt of Granites" was the relic of Huronian sediments. But Lawson (1929), after studying the area, gave evidence for the intrusive nature of the granite. Although Quirke and Collins (1930) proposed that the intrusive nature of the granite at its northwest contact was due to melting and mobilization of the transformed rocks (granitization hypothesis), not many geologists believed that such an incredibly large transfer of material could happen. In addition, the porphyry in the Killarney area shows evidence of true igneous rock: porphyry dykes are found to cut the granite and other rocks (Lawson, 1939; Jones, 1930).

Card (1976) first reported volcanic rocks in large xenoliths near the margin of the granite in Killarney Bay. The xenoliths include dark grey plagioclase-phyric andesite, light grey porphyritic dacite, pale violet-pink rhyolite and porphyritic felsite. Later, volcanic rocks were also found elsewhere (Clifford, 1986; Davidson, 1986b) including felsic volcaniclastic rocks, coarse, heterolithic volcanic breccia and grey tuff with coarse clasts of collapsed pumice, etc.

Huronian rocks of the Southern Province in Ontario were intruded by gabbro sills (2,100-2,200 Ma)(van Schmus, 1965; Stockwell, 1982), and folded about east-trending

axes and metamorphosed to greenschist facies, locally higher, during the Penokean Orogeny (>1,850 Ma)(van Schmus, 1976). The emplacement of the Killarney Igneous Complex was referred as the "Killarnean Orogeny" by Stockwell (1982). Van Breemen and Davidson (1988) presented U-Pb zircon isotopic data to show that the granite of KIC was 1,742±1.4 Ma; porphyry of KIC, 1,732 Ma; volcanic breccia of KIC, 1,712 Ma. They also reported 1,471 Ma for the age of Bell Lake Granite, and 1,400 Ma for pegmatite. Krogh and Davis (1970) reported approximate ages of 1,665 Ma for the Chief Lake granite and of 1,523 Ma for the Bell Lake granite. Fahrig and West (1986) reported approximate ages of 1,220-1,250 Ma for olivine diabase dikes of the Sudbury swarm. Grenvillian orogeny has an U-Pb age of 1,150 Ma, obtained from zircon in pegmatitic leucosomes in gneiss just southeast of the Grenville Front east of Sudbury (Krogh and Wardle, 1984). Table 2.1 summarizes the above isotopic data done by previous workers. Because of the emplacement age of KIC, some workers have correlated it with anorogenic granite and felsic volcanic rocks of comparable age that underlie much of mid-continental North America south of the Penokean fold-belt of the Southern Province (van Schmus and Bickford, 1981; Davidson, 1986a).

It has long been realized that the styles and orientations of the structures are different in Huronian Metasediments, the KIC and the Grenville Front Tectonic Zone. The dominant structures in Huronian metasediments of Southern Province are east-striking folds produced by Penokean Orogeny (1,850 Ma) (Card et al, 1972). There is a set of foliation and lineation in the porphyry and volcanic rocks (Kb in Figure 2.2) of

Table 2.1. Summary of Isotopic Data Related to the Research Area

EVENTS	Dates	REFERENCE
Grenville Orogeny	1,000-1,200 Ma	Krogh and Wardle, 1984
Sudbury Diabase Dikes	1,220-1,250 Ma	Fahrig and West, 1986
Pegmatite	1,400 Ma	van Breemen and Davidson, 1988
Bell Lake Granite	1,471 Ma	van Breemen and Davidson, 1988
	1,523 Ma	Krogh and Davis, 1970
Chief Lake Granite	1,665 Ma	Krogh and Davis, 1970
	1,713 Ma	Krogh and Davis, 1969
Killarney Complex, Volcanic Breccia	1,712 Ma	van Breemen and Davidson, 1988
Killarney Complex, Porphyry	1,732 Ma	van Breemen and Davidson, 1988
Killarney Complex, Granite	1,742 Ma	van Breemen and Davidson, 1988
Penokean Orogeny	1,850 Ma	Card et al, 1972; van Schmus, 1976
Nipissing Diabase Dikes	2,100-2,200 Ma	van Schmus, 1965; Stockwell, 1982

the KIC while Killarney granite sensu stricto (Ka in Figure 2.2) is relatively clean (Davidson, 1986b). The foliation of KIC is defined by elongated quartz grains or grain aggregates of quartz. The foliation and lineation in KIC are quite different from those in the GFTZ where the foliation and lineation are defined by extremely flattened and stretched quartz and feldspar characterizing the mylonitic fabrics (Clifford, 1986, 1990; Davidson, 1986b). Furthermore, the attitudes of these foliation and lineation are sharply different over the region. The foliation in KIC approximately parallels to the GFTZ only where it is close to the zone (Figure 2.2). The lineation in KIC plunges generally at low to moderate angles to the east or east-northeast while the lineation in the mylonite zone always plunges moderately to steeply to the southeast. Pegmatites, 1,400 Ma of age (van Breemen and Davidson, 1988), and Sudbury diabase dykes (1,220-1,250 Ma)(Fahrig and West, 1986) found in KIC do not have the typical foliation and lineation of KIC, but have the mylonite fabrics when close to the GFTZ. It is clear that the foliation and lineation in the KIC and in the GFTZ are the products of two different deformation events, respectively. The flattening event responsible for producing the foliation and lineation in KIC has been tentatively correlated by Clifford (1991) with activity represented by a Rb-Sr whole-rock isochron age of 1,623 Ma (Wanless and Loveridge, 1972). This is regarded as a reset date by van Breemen and Davidson (1988) and is comparable to similar ages in the mid-continental terranes to the southwest (van Schmus, 1980). The mylonitic fabrics in the GFTZ are considered to be the product of the Grenville Orogeny, dated at 1,000-1,200 Ma (Krogh and Wardle, 1984).

CHAPTER 3 FAULTS AND RELATED FRACTURES

3.1 Introduction

Fracturing, or faulting, is a common type of rock deformation, essentially brittle in nature, when the rock is under stress and some critical stress exceeds the rock's cohesive strength. Fractures as a general term (including joints and faults) are therefore found almost everywhere on the earth, ranging from a broad variety of different scales. The study of fractures not only can help us to understand mountain-building and seismic activities currently going on in the earth's crust, but also can provide valuable information regarding palaeostress field and ancient tectonic events.

This chapter discusses faults and related fractures in the research area and their implications.

3.2 A Brief Review of Nomenclature

3.2.1 Classification of Faults

The word fault was initially derived from an eighteenth and nineteenth-century mining term for a surface across which coal layers were offset. According to Charles

Lyell (Principles of Geology, 3rd ed., 1834):

"Fault, in the language of miners, is the sudden interruption of the continuity of strata in the same plane, accompanied by a crack or fissure varying in width from a mere line to several feet, which is generally filled with broken stone, clay, etc."

The term fault has been fully accepted by geologists, and it is now defined as a fracture along which an appreciable displacement has taken place. That is in contrast to a joint which refers to a fracture along which there is no appreciable displacement taken place. It is clear that it is difficult to specify what "appreciable displacement" is, i.e. the definition of fault is scale-dependent. Although Ramsay and Huber (1987) once proposed the minimum value of displacement for a fault as 0.5 mm, most people prefer to use the term in accord with the scale of each study (e.g. Hatcher, 1990). However, a fracture is generally considered as a fault if the displacement along the fracture is easily visible to naked eyes.

There are three basic types of fault frequently found in nature:

(A) Normal Fault

A normal fault is an inclined dip-slip fault on which the hanging wall moves downwards relative to the foot wall (Figure 3.1a).

(B) Reverse Fault

A reverse fault is an inclined dip-slip fault on which the hanging wall moves upwards relative to the foot wall (Figure 3.1b). Low angle reverse fault (dips less than 45°) is usually termed thrust or thrust fault.

A. Normal Fault

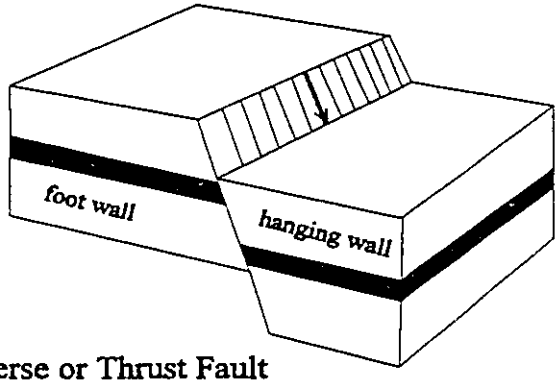

B. Reverse or Thrust Fault

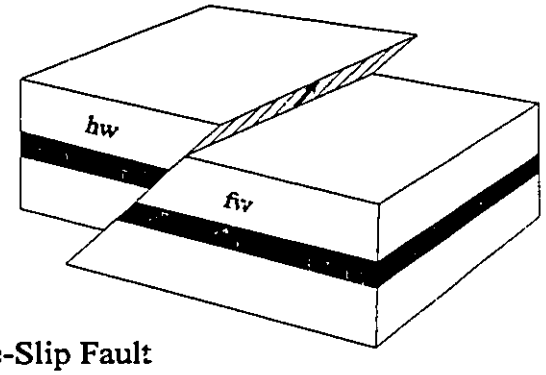

C. Strike-Slip Fault

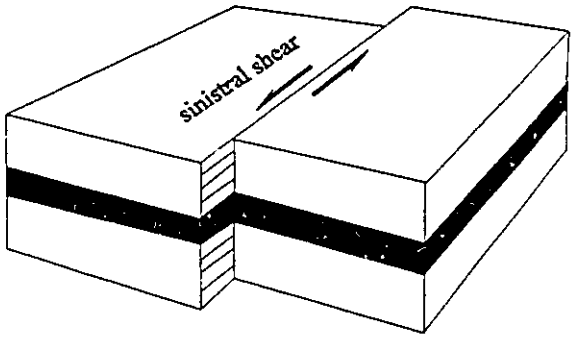

Figure 3.1, Illustration of three basic types of faults.
(after Ramsay and Huber, 1987)

(C) Strike-Slip Fault

A strike-slip fault is characterized by nearly horizontal slip parallel to the strike of vertical or steeply dipping fault. The movements on a strike-slip fault are classified either dextral (right-lateral), or sinistral (left-lateral), depending on the relative movement of the fault wall opposite to that of the observer (Figure 3.1c).

The combination of (A) and (C) is called oblique-normal fault while the combination of (B) and (C) is called oblique-reverse fault.

A large fault generally consists of a series of parallel sectors of smaller faults which may or may not contact to each other, forming a fault zone. A fault zone may also refer to a set of parallel or subparallel faults, which may be a few metres or more apart but developed by the same tectonic event.

3.2.2 Shear Zones

Shear zones are defined as planar or curviplanar zones of high deformation and are surrounded by rocks showing a lower state of finite strain. Ramsay (1980) has classified them as 1) ductile shear zones where the deformation state varies continuously from wall to wall through the zone, 2) brittle shear zones or faults where the walls are separated by a discontinuity or fracture surface, and 3) brittle-ductile shear zones where a combination of brittle and ductile deformation has taken place in different proportions (Figure 3.2).

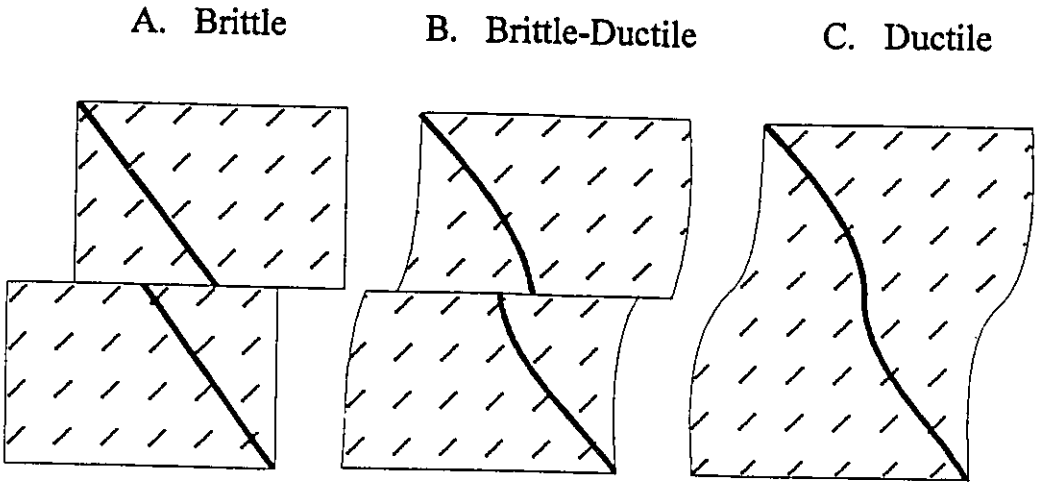

Figure 3.2, Illustration of different types of shear zones

3.2.3 Fault Rocks

Fault rock is a collective term used to describe the distinctive rock types found in zones of shear dislocation at both high and low crustal levels, whose textures arise at least in part from the shearing process.

Shearing along a fault plane at high crustal level generally results in the fracturing and breaking of wall rock fragments due to the process of cataclasis. Non-cohesive fault rocks produced by cataclasis are known as fault breccia, or gouge if the comminuted material is granulated to fine flour (<0.1 mm). Although breccia and gouge are non-cohesive materials, they may become impregnated and sealed by crystal growth in the voids to produce cemented breccia or cemented gouge. The cohesive products of cataclasis are generally named cataclasites, which can be further divided into several subdivisions (e.g. Sibson, 1977; Ramsay and Huber, 1987). Cohesive cataclasites may form at depth up to 10 KM.

Pseudotachylite is a massive rock that frequently appears in microbreccias or surrounding rocks as black or dark coloured glass or cryptocrystalline material, resulting from rapid movement occurred along a fault surface located in the upper crust.

Fault zones developed at depth exceeding about 10 KM are characterized by another type of very fine-grained fault rock called mylonite. The term mylonite was first used by Lapworth (1885) to describe a fault rock found within the Moine Thrust Zone

of northern Scotland. The name originally came from the greek *mylon*: to mill. Lapworth used it to describe the finely laminated "schist" which he thought were the result of crushing and grinding of the larger size original crystals in the Moine Thrust Zone. It is now understood that these small grains were derived from dynamic recrystallization of plastically deformed grains, and not by simple cataclasis. Therefore, mylonite is now used as a general term for fine-grained coherent rocks with at least microscopic foliation, with or without porphyroclasts, characterized by intense syntectonic crystal-plastic grain size reduction and invariably showing at least minor syntectonic recovery/recrystallization (Wise et al, 1984). The crystal grains in mylonites usually show characteristically preferred optic orientations because of the plastic deformation mechanism. Mylonites, like cataclasites, can be further subdivided into several subdivisions according to the proportions of recognizable parent material and dynamically recrystallized matrix (e.g. Sibson 1977; Wise et al, 1984; Ramsay, 1987).

As a relatively simple field criterion, the distinction of foliated versus non-foliated texture can be used to separate mylonitic and cataclastic rocks.

3.3 Faults in the Research Area

3.3.1 Main Faults

3.3.1.1 Orientation

In the research area, the main structural grain is controlled by a set of parallel or subparallel faults classified as main faults (Figure 3.3), which are very consistent and cut almost all other fractures. Main faults are exposed on the order of KM along the lakeshore east of Killarney village before being covered by vegetation to the northeast and by water to the southwest.

The orientation of main faults is consistent. As listed in Appendix A, the strike of main faults only varies from 236° to 245°, with average of about 240°, and the dip only varies from 78° to 84°, with average of about 80°. This study follows the right-hand rule in recording fault orientation, i.e., the dip is on the right hand side of the strike azimuth. Thus, the average orientation of main faults is recorded as 240°/80°.

3.3.1.2 Distribution

A fracture density survey is done on an excellent outcrop (Main Site) opposite to the Lighthouse. In Table 3.1, main faults are classified as moved-fractures in order to be distinguished from those unmoved-fractures which have the same orientation as main faults but do not show any clear evidence of shear movement. Those unmoved-fractures are probably incipient main faults. Had the tectonic event been stronger the unmoved-fractures might have become main faults.

Apparently, the density of main faults is very consistent compared with that of unmoved-fractures throughout the outcrop (Figure 3.4). The interval of main faults is

Figure 3.3, A view of main faults in Main Site.

Table 3.1, DENSITY OF M (moved) & UM (unmoved) FRACTURES

Location(ft from ZERO)	No. of M-fractures	No. of UM-fractures	Zone Width(m)	M-density(f/m)	UM-density(f/m)
0	8	4	8.84	0.9	0.45
50	23	28	21.64	1.06	1.29
100	30	40	24.38	1.23	1.64
150	20	31	18.29	1.09	1.69
200	23	29	24.08	0.96	1.2
250	26	36	24.08	1.08	1.5
300	24	20	22.55	1.06	0.89
350	21	34	25.91	0.81	1.31
400	31	35	28.96	1.07	1.21
450	26	50	30.48	0.85	1.64
500	17	26	19.2	0.89	1.35
Mean				1.0	1.3
S.D.				0.12	0.36

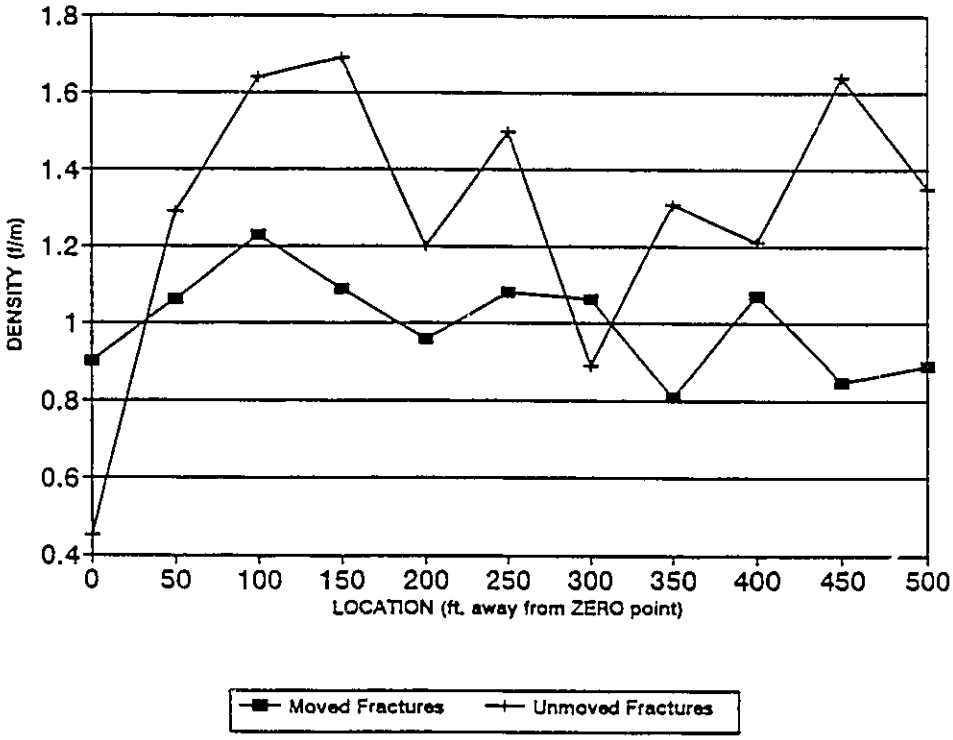

Figure 3.5, Fracture density in Main Site.

constantly around 1 m, but the interval of unmoved-fractures has a wide range of from 0.6 m to 2.2 m, which indicates that the incipient main faults have not been continuously developed yet across the outcrop while the real main faults almost all cut through the region.

3.3.1.3 Surface Features

In response to shearing on fault planes, a common feature on fault surface is growth of fibrous minerals or grooves aligned parallel to the movement direction. They are usually arranged to yield a series of steps with the step-down side in the movement direction of the opposing fault block. The striated surfaces are called slickensides, and the strongly oriented linear features on them are called striations, or slickenlines. Aligned fibrous minerals on fault surfaces are known as slickenfibers. These surface features all indicate the line of relative movement on a fault plane, but steps may also provide information on the movement direction. Jagged-edged steps across slickensides, facing to the direction of movement of the adjoining wall, result from plucking. The feature is formed by tearing away pieces of the face (Tjia, 1967). It is believed that slickensides most frequently record only the last movement event on the fault.

Where exposed, main faults in the research area commonly show smooth, polished slickensides (Figure 3.5), and striations as well as jagged-edged steps on them

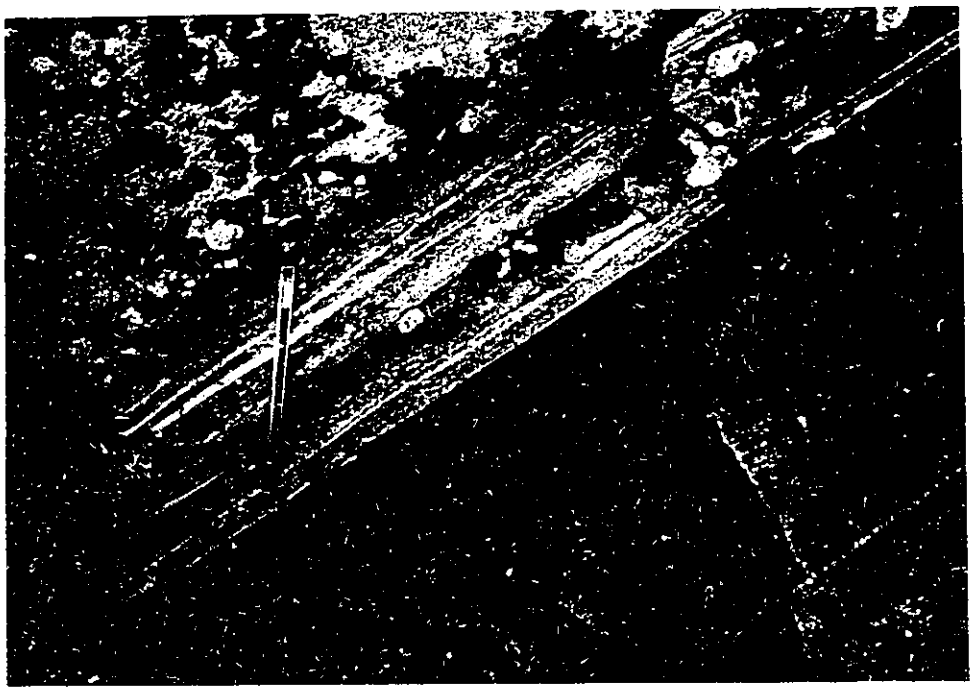

Figure 3.5, Exposed slickenside of main fault #5.

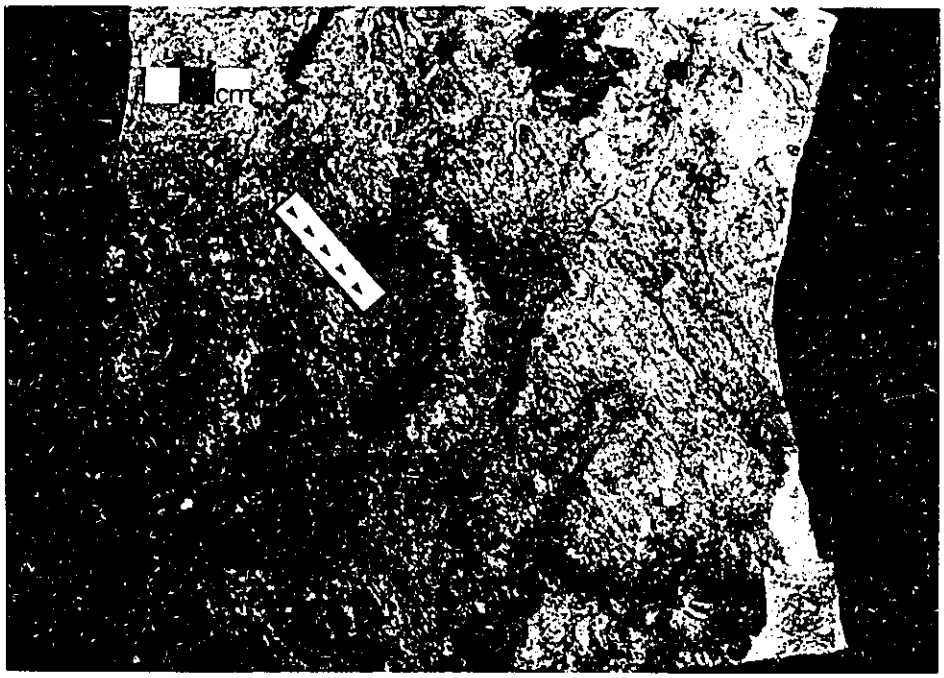

Figure 3.6. Jagged-edged steps on the slickenside. The arrows show the sense of movement of this rock relative to the block once on top of it.

(Figure 3.6). The striations are of two types: ridges and grooves, resulting from scratching and gouging of the fault surface; and slickenfibers, resulting from the growth of fibrous minerals, mainly chlorites in this area.

The pitch of the striations is constantly at about 65° SW on fault planes. The steps indicate that the hanging walls moved upwards relative to the foot walls. The surface features suggest that main faults are oblique, very high angle reverse faults, with dextral strike slip.

3.3.1.4 Displacements

Displacement along faults separates rocks that originally belonged together. By matching points that were once in contact but are now separated by the fault plane, the total displacement, or net slip across the fault can be determined in principle. Slip is generally represented by a vector defined by the direction and amount of the displacement of one block relative to the other. Net slip can be given in terms of two displacement components on the fault surface, strike slip and dip slip (Figure 3.7).

In practice, determining the movement vector in any sector of a fault surface is not easy. What can be measured directly from outcrops is separation--the amount of apparent offset of a faulted surface, such as a bed or a vein, measured in a specified direction. Strike separation is measured parallel to the strike of the fault, and dip separation is measured parallel to the dip of the fault. It should be pointed out that strike

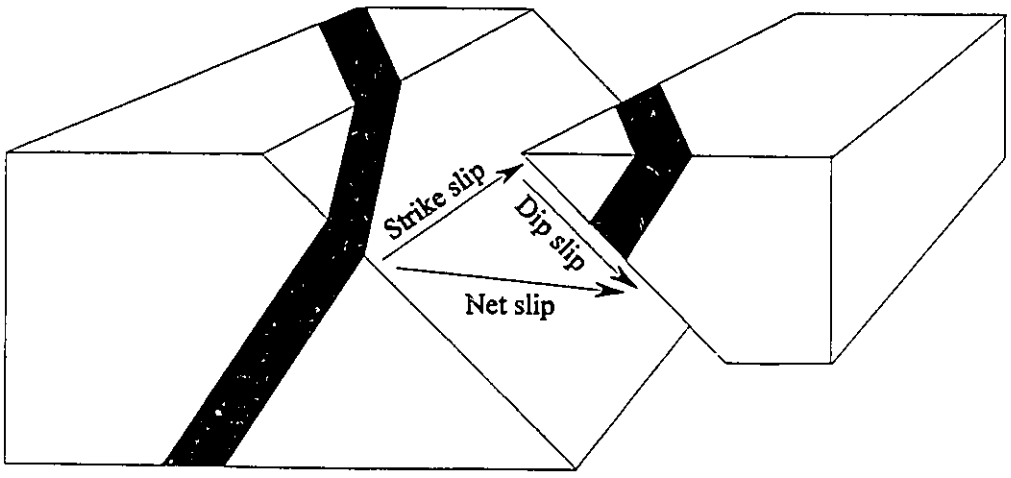

Figure 3.7, Illustration of slip components on a fault plane

separation is not the equivalent of strike slip. They will only be equal in faults which have no dip slip or where a fault cuts a vertically oriented marker horizon striking normal to the fault plane. Similarly, dip separation is not the equivalent of dip slip. If the movement sense of the two sides of a fault can be constrained by observations of subsidiary structures, such as fault grooves and striae, on or around the fault surface, the slips can be estimated from the separations, providing the orientations of the fault and the displaced marker horizon are known.

Almost all main faults show dextral separations revealed by displaced quartz veins or minor fractures on the ground surface (an approximately horizontal plane), with a few exceptions such as fault #07 and #06 in Figure 3.8c and 3.8e which show sinistral separations on the ground. Figure 3.9 shows a dextral separation of a fracture along fault #9. Figure 3.10 shows a series of dextral separations of a fracture along fault #6, #7 and #8.

As discussed in previous section, main faults have polished slickensides containing steps and striations. The steps indicate main faults are oblique reverse faults, and the pitch of striations is about 65°SW. By combining the fault surface features with the separations of minor fractures and quartz veins caused by the movement of main faults, and the orientations of these structures involved, the net slip, strike slip and dip slip of main faults can be estimated from graphic solutions with stereonet and geometric analysis (Ragan, 1985).

The slips of some main faults are presented in Table 3.2. The faults are

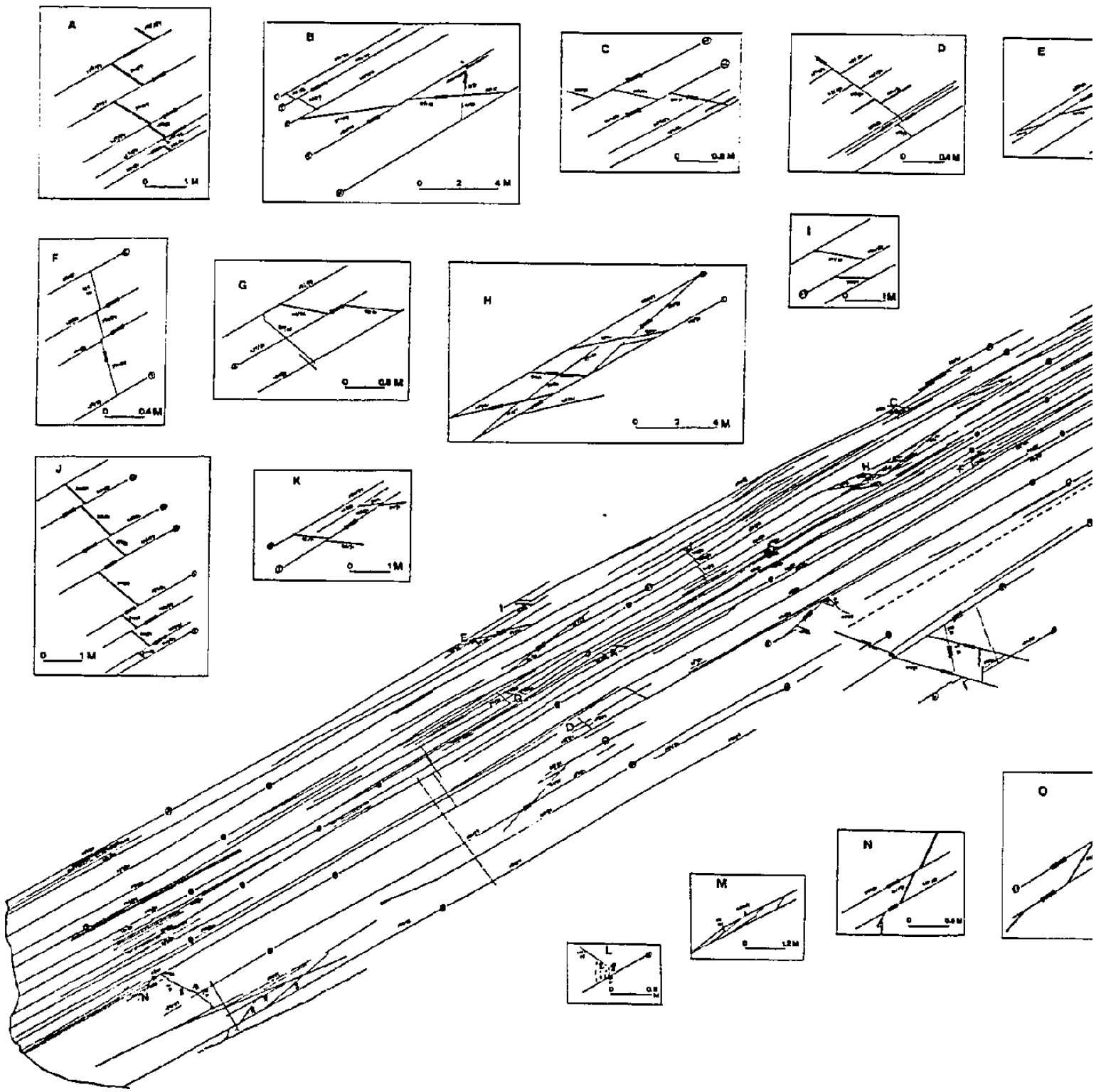

Figure 3.8, Structural map of Main Site.

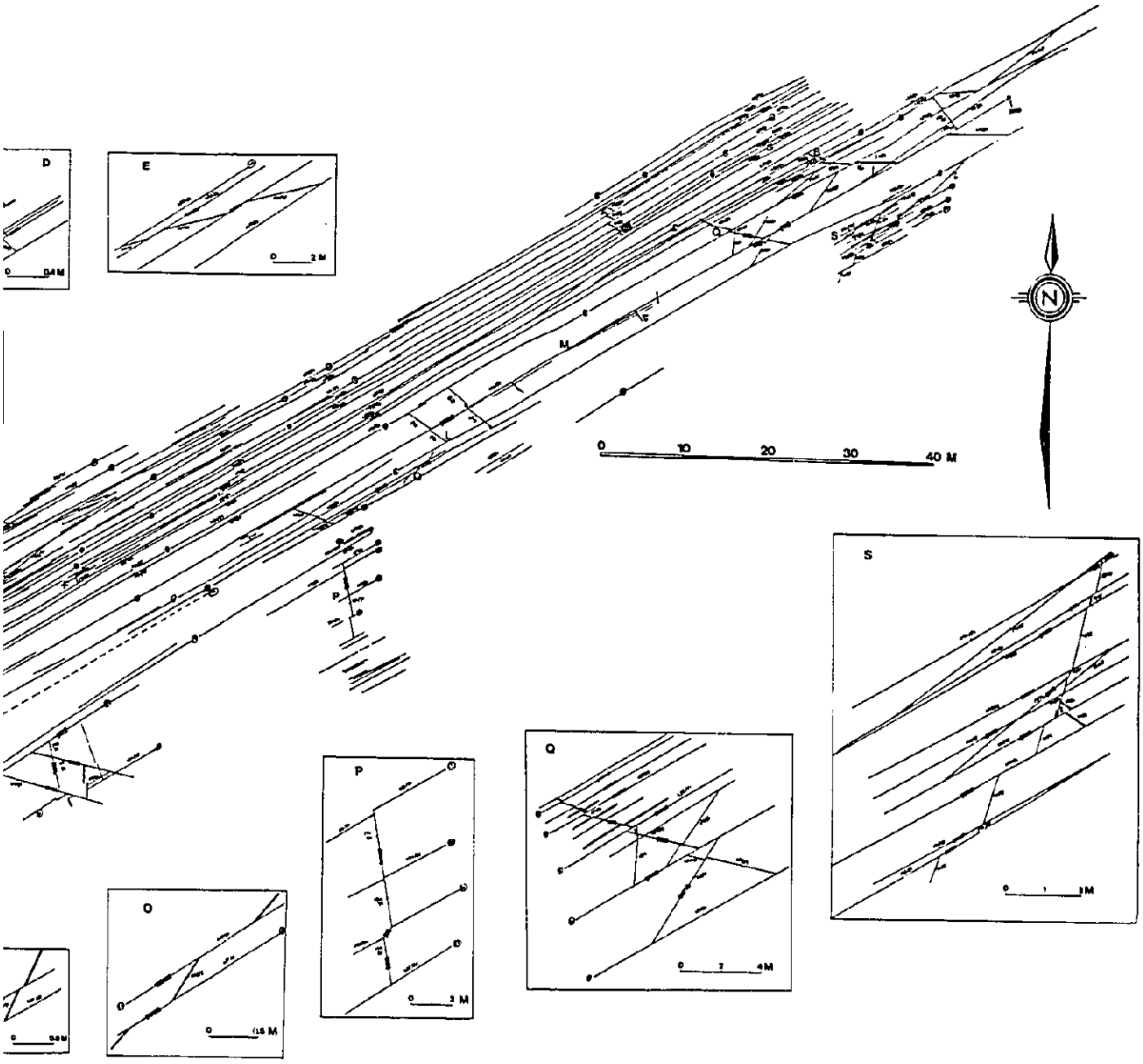

fracture

quartz vein

diabase dike

f Main Site.

Figure 3.9, Showing dextral separation caused by fault #9.

Figure 3.10, Showing dextral separation caused by fault #8, #7, and #6.

dominated by thrust dip-slips, and accompanied with dextral strike slips. Apparently, the fluctuation of slips on different faults is quite large, so the following estimation of shear strain in the fault zone based on the average net slip only provides a rough idea on the order of the strain from the data available in the outcrop.

The total net slip of these 14 documented faults is 16 metres, and the average net slip of an individual fault is then approximately 113 cm. About 50 main faults have been identified in a zone about 35 metres wide, almost all of which have slickensides, indicating that they all had similar movement although only some of them have documented slips. Others do not cut any reliable markers or their displacements of any reliable markers are yet to be discovered in the exposed outcrop. An approximate estimation of the total net slip for the fault zone can be carried out

$$\Sigma NS = 50 \times 113cm = 5650cm = 56.5m$$

which gives a rough notion about the order of the total slip accommodated by the fault zone exposed in Main Site.

The shear strain of the fault zone is determined by

$$\gamma = \frac{\Sigma NS}{W Sin\varphi} \qquad \ldots\ldots\ldots (3.1)$$

where W is the width of the zone measured on the ground surface, and φ is the dip angle of the main faults.

So,

$$\gamma = \frac{56.5}{W Sin 80^0} \approx 1.64$$

This value corresponds to an angular shear of about 60 degrees.

In considering the fact that some faults might not be counted in the field, the value calculated above is the minimum shear strain for the zone, realized purely by shearing on each individual fault, i.e., brittle deformation. The fault zone contains some extremely high brittle strain portions--the faults, and non-brittle strain portions between these faults because of the strain partitioning during deformation. As discussed in a later section, the fault zone also accommodated ductile deformation as revealed by mylonites. The total shear strain of the zone therefore should be much higher than the value estimated above if the ductile shear strain is taken into consideration, though probably as the result of two or more deformation episodes.

3.3.1.5 Brecciation and Mylonization

Breccia and mylonite, as discussed in section 3.2.3, are common types of fault rocks. Brecciation is believed to occur at high levels in the crust (<5 KM depth) while mylonization occurs at lower levels (about 10 KM depth or more).

Table 3.2, Slips of some main faults

Fault #	Net Slip (cm	Strike Slip (cm)	Dip slip (cm)
01	295	135	263
02	27	13	24
03	31	15	28
0	205	94	183
1	98	47	87
5	43	19	38
7	60	27	53
8	100	45	88
9	108	48	95
10	298	125	270
12	113	47	103
13	40	18	36
14	128	58	115
50	36	15	33
Mean	113	50	101
S. D.	88	40	80

Several outcrops of breccia are presented in the research area, especially in South Bay. Figure 3.11 shows incipient breccias constrained by main faults. Figure 3.12 and Figure 3.13 show more advanced breccias, not far away from those shown in Figure 3.11, in South Bay. These breccias are all cohesionless in appearance, representing a fairly high level brittle deformation.

Fault rocks related to main faults are mainly mylonites in Main Site (Figure 3.14 and Figure 3.15), suggesting a deeper level ductile deformation. A detailed discussion of mylonites is presented in Chapter 4.

Fault rocks imply that the strain gradient decreased westwards from Main Site to South Bay. The relatively undeformed homogeneous granite (Ka in Figure 2.2) lies to the west of South Bay. Other supporting evidence for this strain gradient is that main faults are much more intensively developed in Main Site, whereas, in South Bay, main faults are only sparsely presented.

3.3.2 Related Fractures

In addition to main faults, there are a lot of minor faults and joints developed in the area, which do not extend far. Some of them pass across a few main faults, and may show some displacement due to the movement of main faults (e.g. Figure 3.9 and Figure 3.10) while many others only exist between main faults and do not traverse those main faults.

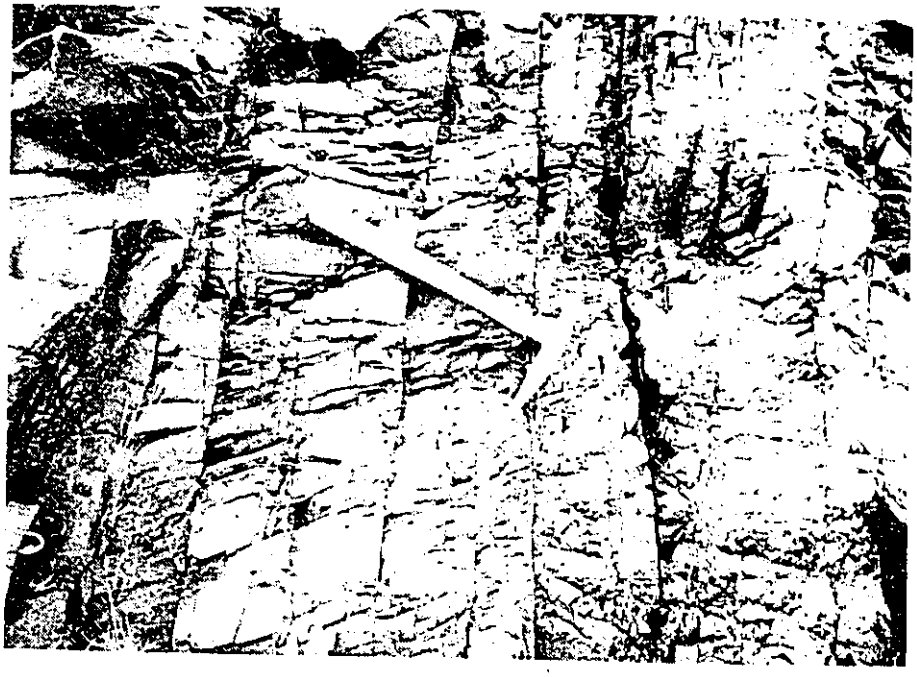

Figure 3.11, Showing incipient breccia in South Bay.

Figure 3.12, Showing breccia in South Bay.

Figure 3.13, Showing breccia in South Bay.

Figure 3.14, Banded mylonite between faults.

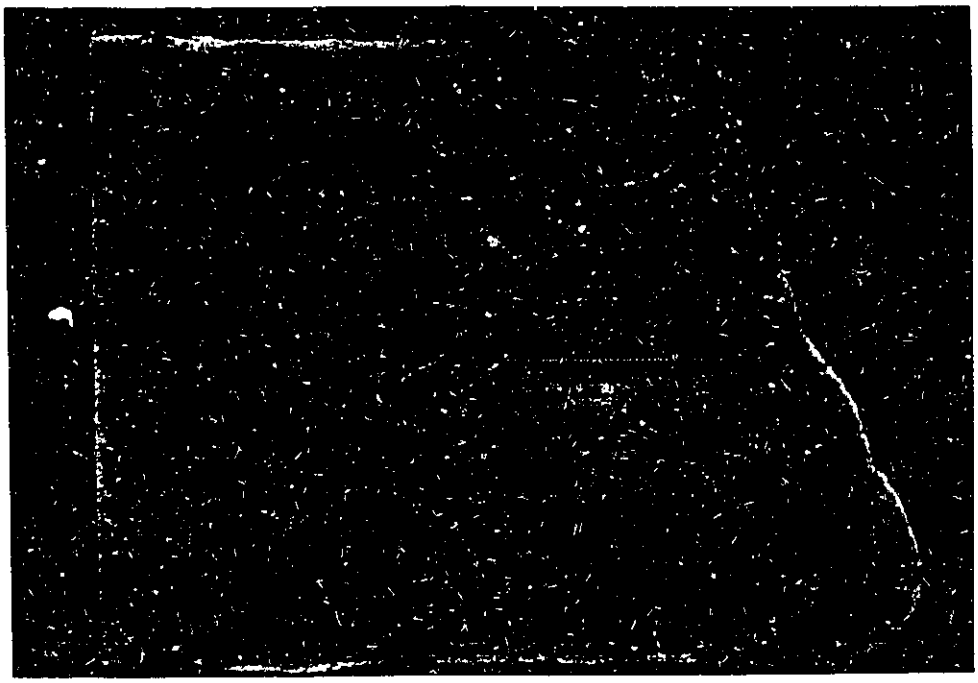

Figure 3.15, Hand sample of the banded mylonite.

Appendix B lists the attitudes of these minor fractures measured in Main Site. A rose diagram showing the fracture orientations in the area is produced in combining the data of Appendix A and Appendix B (Figure 3.16). Clearly, there are four distinct sets of fractures revealed by the diagram. Set I, striking about 240°, corresponds to main faults, and is the most dominant set. Set II, set III and set IV represent minor fractures, striking about 105°, 300°, and 345°, respectively. Field observations indicate set II and set IV are shear fractures; fractures of set II show dextral sense of shear (e.g. Figure 3.8c,h,q) while those of set IV show sinistral sense of shear (e.g. Figure 3.8f,p). Fractures of set III are tensile fractures, with quartz veins filling them (e.g. Figure 3.8a,j,s).

Although the relative sequence of their formation cannot be established solely from field observations, the main faults (set I) cut and displaced all other sets of fractures (e.g. Figure 3.8a,f,h,j,q,s) and therefore formed at the latest. In general, the main faults in this area are the last formed structures. They control the main structural grain of the area.

In contrast, fractures in relatively undeformed homogeneous granite in Killarney village, a few kilometres west of South Bay, are all vertical joints, and very short (no longer than a few metres). The joints show no distinct pattern in terms of size and orientation (Appendix C and Figure 3.17).

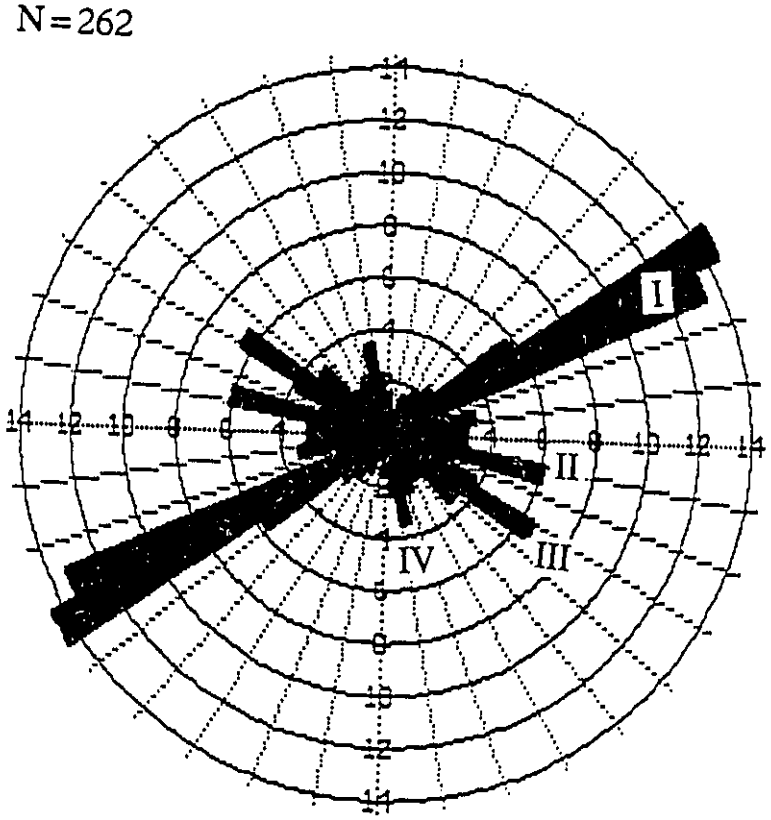

Figure 3.16, Fracture orientations in Main Site.

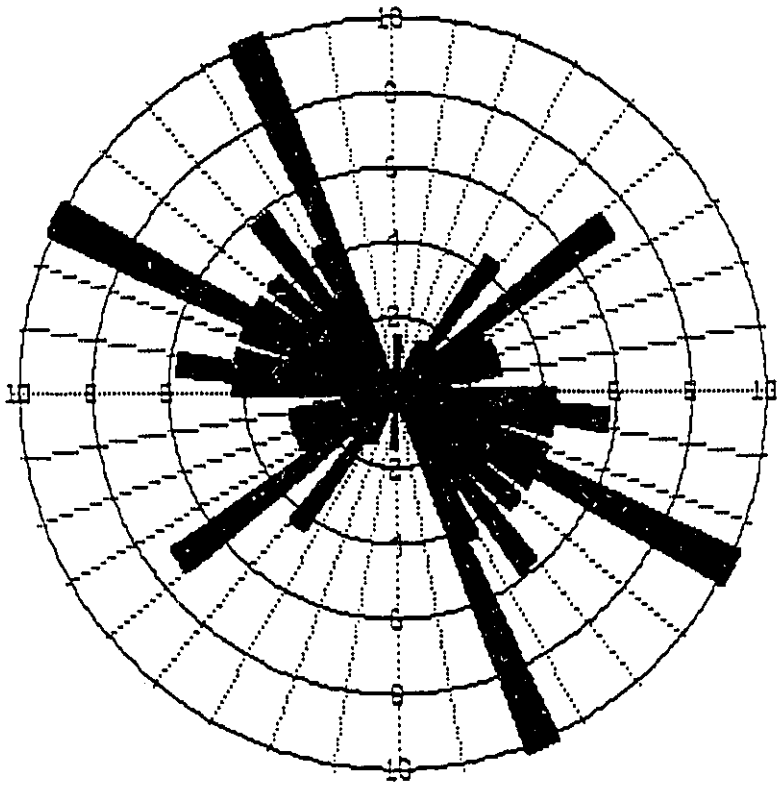

Figure 3.17, Fracture orientations in undeformed area.

3.4 Orientation of the Palaeostress Field

3.4.1 The Coulomb Criterion

About two centuries ago, Coulomb (see Handin, 1969) realized that there are two factors affecting shear failure:

(A) the cohesive shear strength of the material,

(B) the normal stress across the potential shear plane.

This is now called the Coulomb fracture criterion, or Coulomb criterion, and is described by the equation

$$|\tau| = \tau_o + \sigma \tan\phi \quad or \quad |\tau| = \tau_o + \mu\sigma \qquad \ldots\ldots\ldots (3.2)$$

where τ=the critical shear stress on the potential shear plane,

σ=the normal stress across the potential shear plane,

τ_o=the cohesive shear strength of the material,

ϕ=the angle of internal friction,

μ=the coefficient of internal friction,

$\mu = \tan\phi$.

The Coulomb criterion can be depicted graphically on a Mohr circle diagram

(Figure 3.18), in which θ is the angle between the normal to the shear plane and the maximum compressive stress while α represents the angle between the shear plane and the maximum compressive stress. From the figure, the relationships between θ and ϕ, α and ϕ can be expressed as follows,

$$\pm\theta = 45° + \phi/2 \qquad \text{.....(3.4)}$$

$$\pm\alpha = 45° - \phi/2 \qquad \text{.....(3.5)}$$

Equation(3.5) indicates that the shear fractures usually do not form along the planes of maximum shear stresses which are oriented at $\pm 45°$ to the maximum compressive stress, instead the angle between the shear fractures and the maximum compressive stress depends on the angle of internal friction, which varies from 20° to 40° depending on materials, but 30° is a common value used by most workers (e.g. Ragan, 1985; Twiss and Moores, 1992).

3.4.2 Palaeostress Field Deduced from Fault-Slip Analysis

Fault-slip analysis, or striation analysis, is the method used to estimate the principal stress orientations from data consisting of the orientation of fault planes and their corresponding slip directions, which are normally derived either directly from field measurements of faults and their associated striations or indirectly from the first motions of earthquakes. The basis of the fault-slip analysis is the Coulomb criterion.

During the last decade, a substantial number of studies have been carried out in

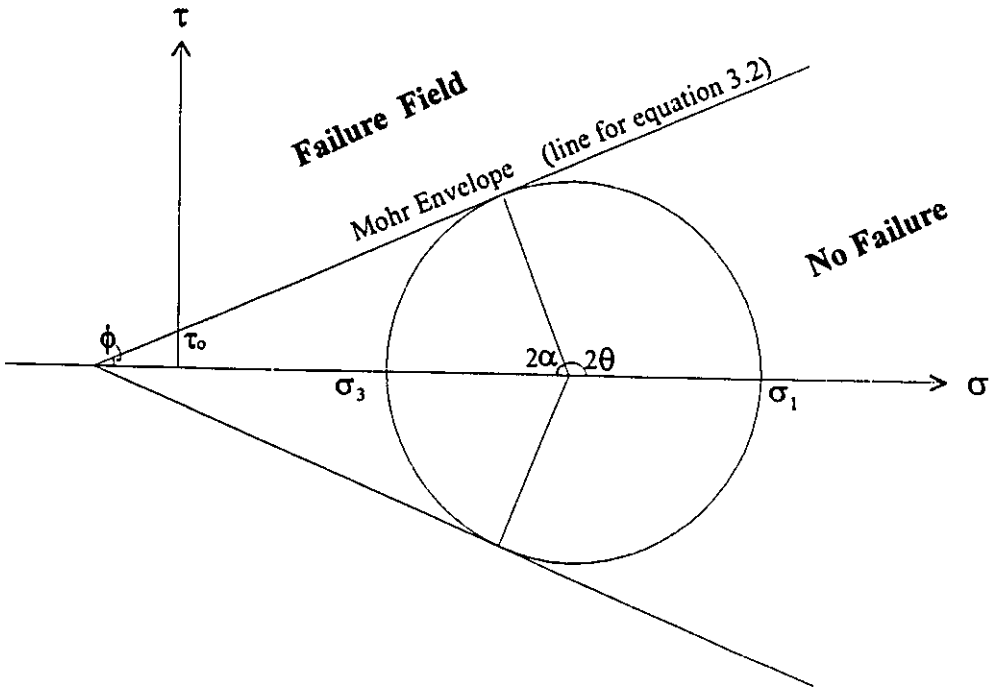

Figure 3.18, The Coulomb criterion of shear failure

applying the fault-slip analysis to deduce the orientation of palaeostresses (e.g., Angelier, 1984, 1990; Lisle, 1987, 1988; Bergerat and Vandycke, 1994). Some computer programs, such as ROMSA by Lisle (1988), are developed to locate the axes of principal stresses on a stereonet if the data of fault planes and slip directions are relatively widespread. However, the orientation of main faults and the direction of striations on the fault planes are very consistent in the research area, so the attitude of palaeostresses can be easily derived graphically on a stereonet by hand.

The data of orientation of main faults are presented in Appendix A which, combined with the slip direction on the fault planes, provide information necessary to estimate the orientation of the palaeostress field. The main stream of main faults is oriented at about 240°/80°, and the striations are pitching 65°SW on the fault planes. The orientation of the palaeostress field is derived from a stereonet graphic solution (Figure 3.19), assuming the angle of internal friction is 30°. From Figure 4.19, the approximate orientation of the principal stresses were,

σ_1: 298°/42°; σ_2: 55°/25°; σ_3: 162°/34°

i.e., the maximum compressive stress came from WNW direction.

The perfect case for fault-slip analysis is in homogeneous isotropic rocks. The presence of discontinuities and heterogeneities, e.g., foliation and mylonite zones in the region, obviously disturbs the stress distribution. Fortunately, numerous heterogeneities and anisotropies are found in fact to have little influence, especially those that geometrically correspond to symmetries of stresses distribution (Angelier, 1984). Other

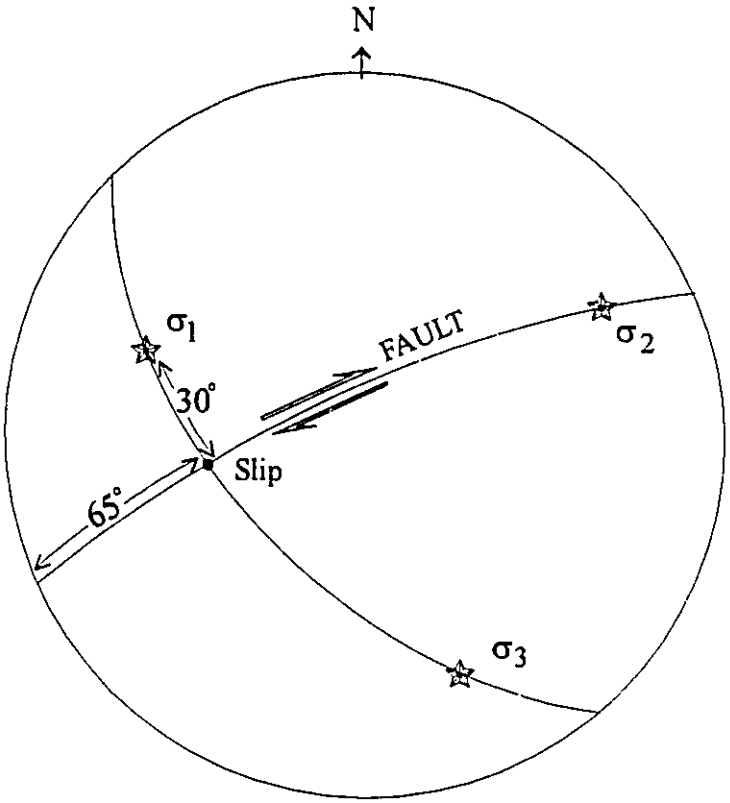

Figure 3.19, Palaeostress field deduced from fault-slip analysis in stereographic projection (equal area projection, lower hemisphere).

σ_1: 298/42 σ_2: 55/25 σ_3: 162/34

heterogeneities may locally play an important role, such as modification of stress distribution close to faults or geometrical constrains on fault block movements, but they appear more or less cancel one another in large fault slip populations. These restrictions have little effect in most practical cases because deformation remains typically brittle and rapid. Therefore, the principal stress axes deduced above should represent a fairly good approximation to the real palaeostress field.

3.5 Age of Faulting

The Killarney Igneous Complex, dated at about 1.71-1.74 Ga (van Breemen and Davidson, 1988), shows evidence that it has been subjected to several events after its formation. A hydrothermal alteration resulted in silicification of the volcaniclastic assemblages (Clifford, 1986), and a flattening and stretching event followed the hydrothermal activity and imposed a regional foliation and lineation in the porphyry-volcaniclastic assemblages. The flattening and stretching event was perhaps related to the activity dated at about 1.623 Ga (Wanless and Loveridge, 1972). This date is based on analysis of mica in the KIC; the same mica that defines the foliation.

Main faults in the research area were superimposed on the regional foliation produced by the flattening and stretching event, apparently because of the weakness of these foliated planes, which set the older limit for the age of faulting. The younger limit for the age of faulting is defined by a set of Sudbury diabase dikes, dated at about 1.22-

1.25 Ga (Fahrig and West, 1986). The dikes straightly cut through main faults (see Figure 3.8), and show no sign of deformation here.

Therefore, the faulting and mylonization occurred between 1.6 Ga to 1.2 Ga due to the WNW compression. Mylonites and breccias accompanied with some main faults indicate that there have been at least two phases of deformation involved after the formation of regional foliation: the earlier phase of deformation probably occurred in a relatively deep level and produced the mylonite zones, corresponding to ductile or semi-ductile shear zone; the later phase of deformation occurred in a shallower level after erosion of the upper cover and produced the brittle shear zones-main faults. These two phases might belong to the same tectonic event with maximum compressive stress coming from the WNW direction, but at different stages.

CHAPTER 4 MICROSTRUCTURE ANALYSIS

4.1 Introduction

Microstructures are referred to structures observable in thin sections. Although many of these structures are expressed in hand samples, e. g., foliation, s-c fabrics, etc., the development of these features occurs at a grain or subgrain scale and therefore can only be fully characterized in thin sections. Fabric is used by geologists as a general term for the internal arrangement of the constituent particles of the rock, including texture, packing, preferred orientation and homogeneity, and reflects the primary formation of the rock and secondary processes such as deformation and metamorphism (Suppe, 1985). The fabrics this study concerns are those produced through deformation.

For the purpose of microstructure analysis, two thin sections are cut from each of 60 oriented samples collected across the study area in such a way that one section is cut parallel to the lineation and perpendicular to the foliation; the other is cut perpendicular to both lineation and foliation.

4.2 Penetrative Fabric

Penetrative fabrics refer to those fabrics which are developed everywhere

throughout a rock mass, affecting every grain.

In the research area, penetrative fabrics are revealed mesoscopically by a set of foliation, striking northeasterly and dipping steeply to the NNW, and a set of lineation, plunging generally at a moderate angle to the northeast; they are marked microscopically by flattened and stretched quartzs and preferred orientation of mica (Figure 4.1). The groundmass is generally composed of a mixture of quartz, K-feldspar, a little plagioclase and mica, with minor amounts of sphene, zircon, chlorite and epidote.

Penetrative fabrics are best preserved in the rock mass between individual main faults; around these faults the fabrics have been extremely disturbed and re-deformed into mylonitic fabrics (see next section). Figure 4.1 shows some microscopical deformation features in samples collected a few metres away from main faults. In general, the common deformation features of quartz grains are undulatory extinction, serrated boundaries, deformation bands, elongated subgrains and dynamic recrystallization, in addition to their irregular shapes, while feldspars only exhibit brittle deformation features, mainly microfractures.

Microstructural strain features in quartz have been studied by many workers (White, 1976, 1977; Carreras et al 1977; Burg and Laurent, 1978; Burg, 1986). The first optical strain feature to occur for a quartz under deformation is undulatory extinction, mainly resulting from the formation of closely spaced dislocation walls (White, 1976). The next optical strain features developed in quartz grain are deformation bands and deformation lamellae. With increasing strain, elongate and

Figure 4.1, Photomicrograph of penetrative fabrics, showing elongated quartz grains (Q), preferred orientation of mica (M), and feldspar (F) with microfracture. The thin secton is cut perpendicular to foliation and parallel to lineation.

equidimensional subgrains and dynamically recrystallized grain form, and then quartz ribbon aggregates develop. Quartz usually begins to behave in ductile fashion at the onset of greenschist facies metamorphic condition while feldspar, another common mineral in granitic rocks, remains strong, deforming in brittle regime until metamorphic condition reaches amphibolite grade (White, 1975; Hanmer, 1982). At the higher levels of deformation, feldspars may show undulatory extinction, deformation bands, bent twins or kinked bands.

Microstructural deformation features revealed by quartzs and feldspars in the research area suggest that the greenschist facies metamorphic condition was not exceeded during the formation of the penetrative fabrics, a conclusion supported by metamorphic index mineral assemblages. Index minerals such as muscovite, biotite, chlorite and epidote are present in thin sections.

Obviously, the event producing the penetrative fabrics occurred after the emplacement of KIC (ca. 1,700 Ma), but before the intrusion of pegmatites (ca. 1,400 Ma) which show no penetrative fabrics in the region. It is tentatively referred to a flattening-stretching event at the age of 1,623 Ma (Wanless and Loveridge, 1972; Clifford, 1990).

4.3 Mylonitic Fabrics

4.3.1 Introduction

In the research area, obvious mylonitic fabrics are developed only in zones along some main faults. Mylonite zones range from several centimetres to several decimeters wide, where mylonitic fabrics were superimposed on the penetrative fabrics, and almost parallel to them. Mylonitic fabrics result from severely deformed features of quartzs and feldspars, and the rock contains more muscovite and chlorite. Along some main faults, e.g., fault #10 and #5 (see Figure 3.8), the rock has been deformed to banded mylonite, in which grey muscovite-rich bands about 6-10 mm wide and dark salmon feldspar-rich bands about 2-4 mm wide alternate (see Figure 3.15 and Figure 3.16). In general, the mylonites have better developed ductile deformation features than the overall penetrative fabrics, including quartz ribbon and bent twins of feldspars, etc., in addition to undulose extinction and deformation bands of quartz, recrystallization of quartz grains and formation of subgrains.

The analysis of mylonitic fabrics has proved particularly useful in assessing the kinematics of deformation events (Lister and Williams, 1979, 1983; Schmid, 1982; Simpson and Schmid, 1983). The criteria most useful in determining shear sense are asymmetric porphyroclast systems, s-c fabrics, displaced broken grains, and preferred optical orientations, all of which will be discussed later. Observations regarding the shear sense should be made in thin sections cut parallel to the shear direction and perpendicular to the flattening plane, which generally correspond to the sections parallel to the lineation and perpendicular to the foliation.

4.3.2 Kinematic Significance

4.3.2.1 Asymmetric Porphyroclast System

In many shear zones, mylonites contain large and relatively flow-resistant grains commonly referred to as "porphyroclasts" or "augen" surrounded by more ductile and finer-grained matrix. Those porphyroclasts most commonly are feldspars, less commonly micas or larger, not yet fully recrystallized, quartz grains. Mylonitic foliation planes are asymmetrically distributed around the porphyroclasts so that the grains have a retort-shape with tails of finer-grained recrystallized materials. The geometry of a porphyroclast and its tails is referred as a "porphyroclast system", which has been divided by Passchier and Simpson (1986) into two types: σ- and δ-type. The σ-type porphyroclast system has wedge-shaped recrystallized tails whose median line lies on opposite sides of a reference plane parallel to the tails and containing the symmetry axis for the system, while δ-type typically has narrow recrystallized tails whose median line crosses the reference plane adjacent to the porphyroclast (Figure 4. 2). Such porphyroclast systems have long been used to deduce the sense of shear on shear zones (Eisbacher, 1970; Choukroune et al, 1977; Etchecopar, 1977; Lister et al, 1978; Berthe et al, 1979; Simpson et al, 1983). Figure 4.2 shows the use of stair-stepping of tails away from the central clast of both porphyroclast systems to determine the sense of shear.

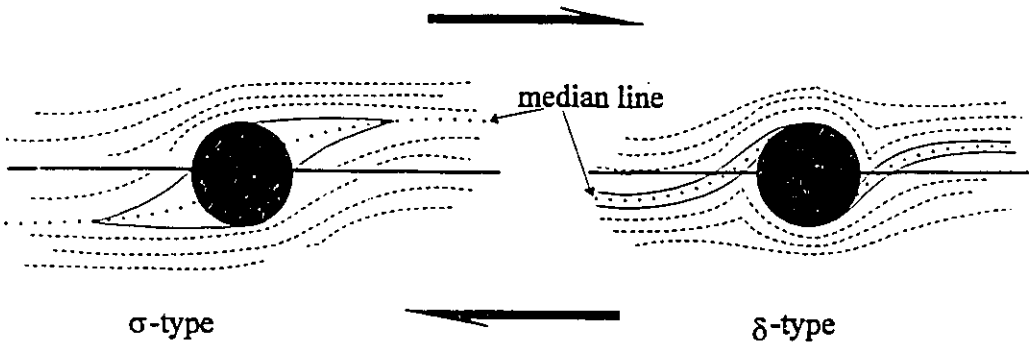

Figure 4.2, Porphyroclast systems with dextral sense of shear

Experimental studies indicate that the ratio of recrystallization rate and deformation rate is one of the most important factors in determining which porphyroclast system will develop. σ-type is characteristic of shear zones with low shear strain where the recrystallization rates are higher than the deformation rates; δ-type is only developed at high shear strain values where the recrystallization rates are lower than the deformation rates (Passchier and Simpson, 1986).

Samples collected immediately from the surfaces of main faults or in the mylonite zone along main faults exhibit σ-type porphyroclast systems. Figure 4.3 shows the mylonitic fabrics in an oriented sample from the surface of main fault #6, in which some large-sized feldspars are surrounded by finer-grained quartzs and sericites with tails of fine recrystallized quartz grains, defining σ-type porphyroclast systems which suggest the sense of shear on fault #6 was dextral. Figure 4.4 and Figure 4.5, also from fault #6, show similar σ-type porphyroclast systems. Samples collected from mylonite zone of fault #10 reveal σ-type porphyroclast systems as well, indicating dextral sense of shear (Figure 4.6 and Figure 4.7). There is no δ-type porphyroclast system found in any thin sections from the research area.

The dextral sense of shear deduced from porphyroclast systems confirms what has been determined in the field according to the relative displacement of small fractures and quartz veins caused by the movement of main faults (see chapter 3). The fact that there are only σ-type porphyroclast systems formed in the area suggests that the shear strain was not very high and the recrystallization rate was higher than the deformation rate

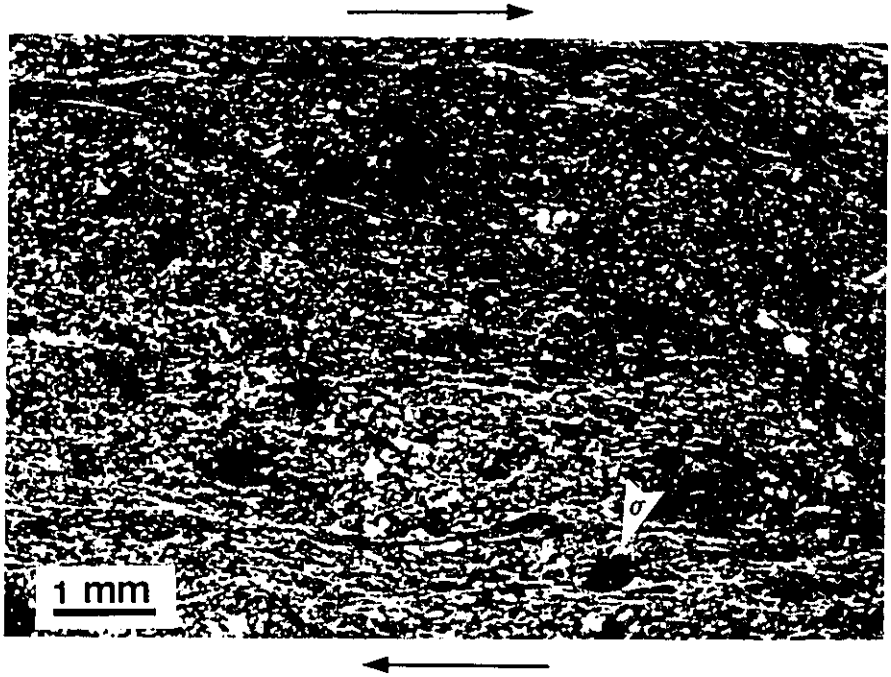

Figure 4.3, Photomicrograph of mylonitic fabrics with σ-type porphyroclast systems, indicating dextral sense of shear.

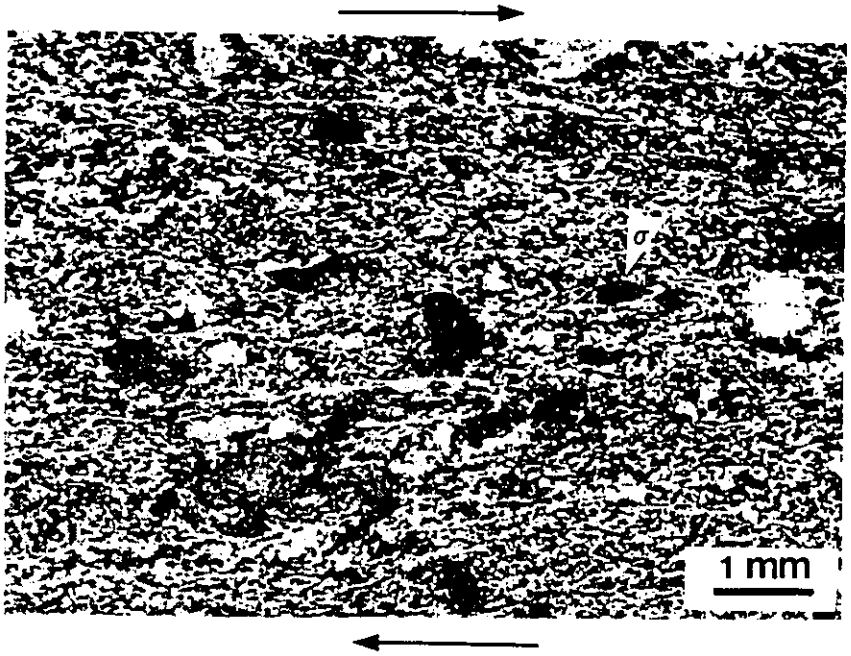

Figure 4.4, Photomicrograph of mylonitic fabrics with σ-type porphyroclast systems, indicating dextral sense of shear.

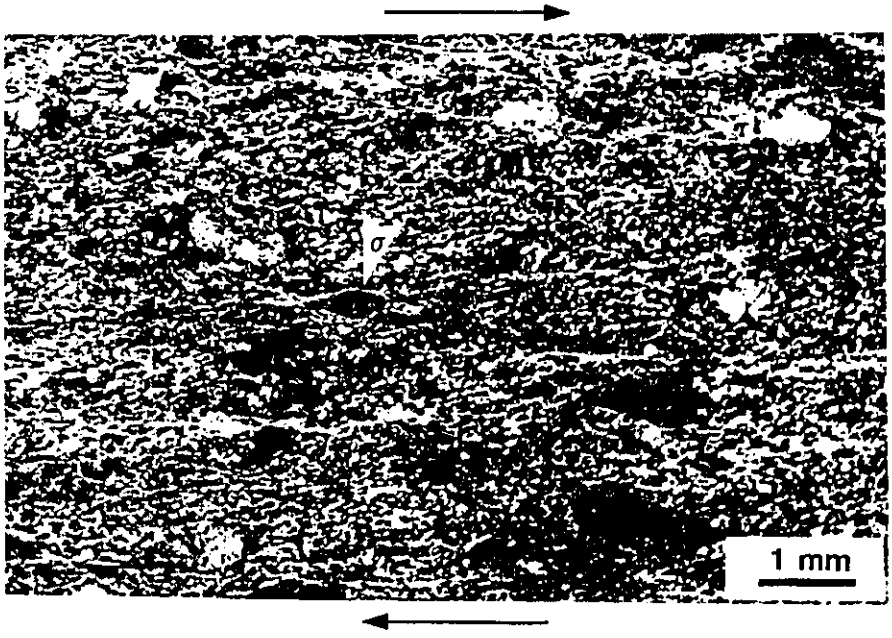

Figure 4.5, Photomicrograph of mylonitic fabrics with σ-type porphyroclast systems, indicating dextral sense of shear.

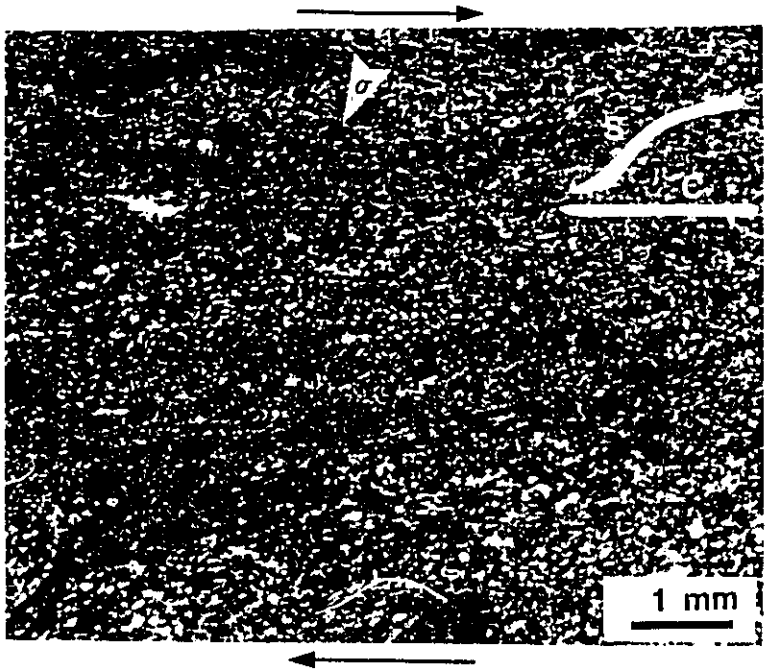

Figure 4.6, Photomicrograph of mylonitic fabrics with σ-type porphyroclast systems and s-c fabrics, indicating dextral sense of shear.

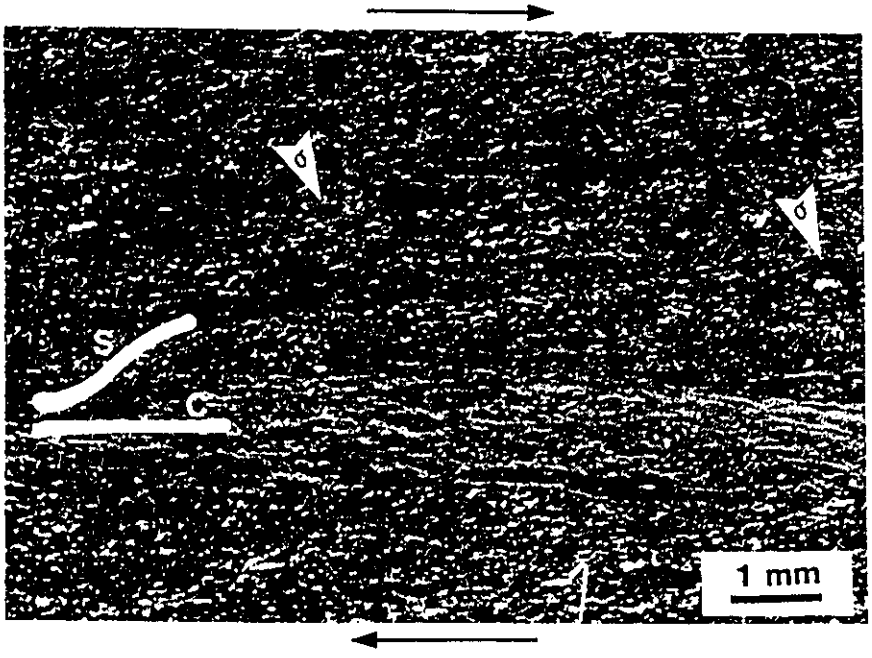

Figure 4.7, Photomicrograph of mylonitic fabrics with σ-type porphyroclast systems and s-c fabrics, indicating dextral sense of shear.

during the mylonitization.

4.3.2.2 S-C Fabrics

Studying the progressive development of planar fabrics within granitic rocks along a shear zone, Berthe and others (1979) observed two sets of planar fabrics which they called as c- and s-surfaces, referring (in French) to "cisaillement", shear in French, and "schistosite", schistosity, respectively. The s-surfaces are defined by the preferred orientation of old grains such as foliation, and are perpendicular to the short axis of the finite strain ellipsoid, i.e., they mark the planes of finite flattening (Ramsay et al, 1970). As proposed by Berthe et al (1979), however, the s-surfaces do not necessarily match the planes of finite flattening of the bulk rock due to the later discrete shearing along the c-surfaces, which are initiated and remain aligned parallel to the main shear zone boundaries with progressive deformation, having the same sense of shear as the over-all shear zone. Due to inhomogeneous strain distribution (strain partitioning), the zones of high and low strain run parallel to the shear zone and give a banded appearance, marked partially by c-surfaces, to the rock (Ramsay and Huber, 1987). Microscopically, the c-surfaces are marked by thin layers of recrystallized, polymineralic aggregates with a reduced grain size.

The s-surfaces are initially oriented at an angle of 45° to the c-surfaces and curved into the c-surfaces, so the angular relationship between the two surfaces defines the sense

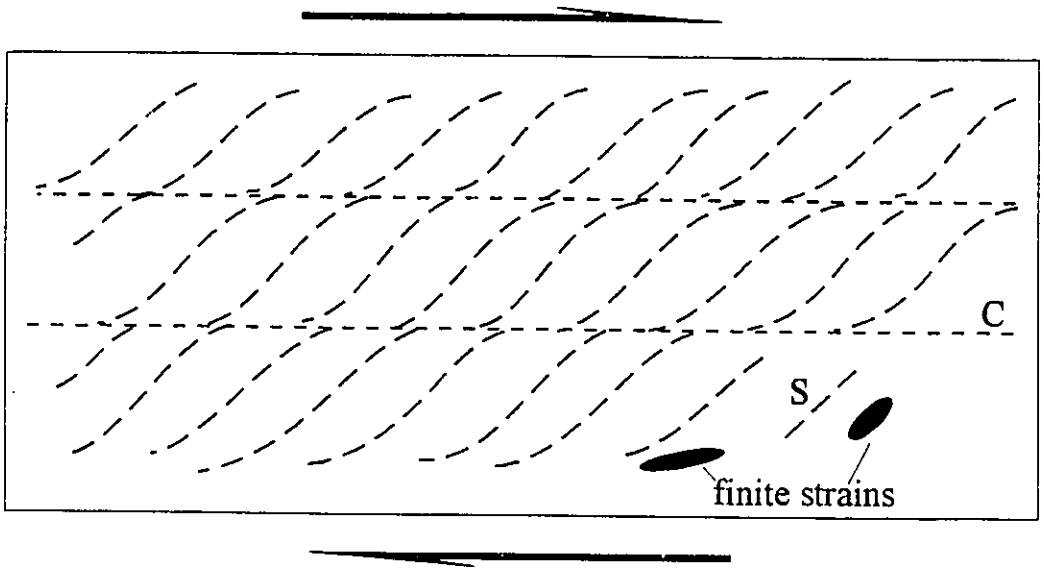

Figure 4.8, S-C fabrics in a shear zone with dextral sense of shear.

of shear along the shear zone (Figure 4.8).

With progressive deformation, the angle between c- and s-surfaces decreases and s-surfaces curve into near parallel to the shear zone boundaries (Simpson and Schmid, 1983). In an advanced stage of deformation, c- and s-surfaces may coincide while a few isolated porphyroclasts, usually feldspars, with sigmoidal pressure-shadow tails still define a geometry of s-c fabrics. The angular relationship of the c- and s-surfaces has been proven to be a reliable indicator of the shear sense for the main shear zone (e.g., Berthe, 1979; Simpson and Schmid, 1983; Ramsay and Huber, 1987).

S-C fabrics are observed not only in thin sections (Figure 4.9 and Figure 4.10), but also on hand samples (Figure 4.11) collected from the mylonite zone along main faults. The s-surfaces here are revealed by elongated quartz grains and preferred orientation of mica and feldspar, while the c-surfaces are defined by thin layers of finer-grained recrystallized quartz and sericite. The angular relationships of s-c fabrics all indicate that the sense of shear accommodated by main faults was dextral (Figure 4.9-4.11). S-C fabrics are observed in mylonites from main faults #10, #9, #6, #5 and #03, though some other main faults (e.g., #8, #7) are also accompanied by mylonitic rocks, the shear strains in these rocks might be not high enough to produce s-c fabrics. The angle between the c- and s-surfaces is found to be around 15°-30°, suggesting an intermediate stage of deformation was reached during the mylonitization.

4.3.2.3 Crystallographic Preferred Orientation

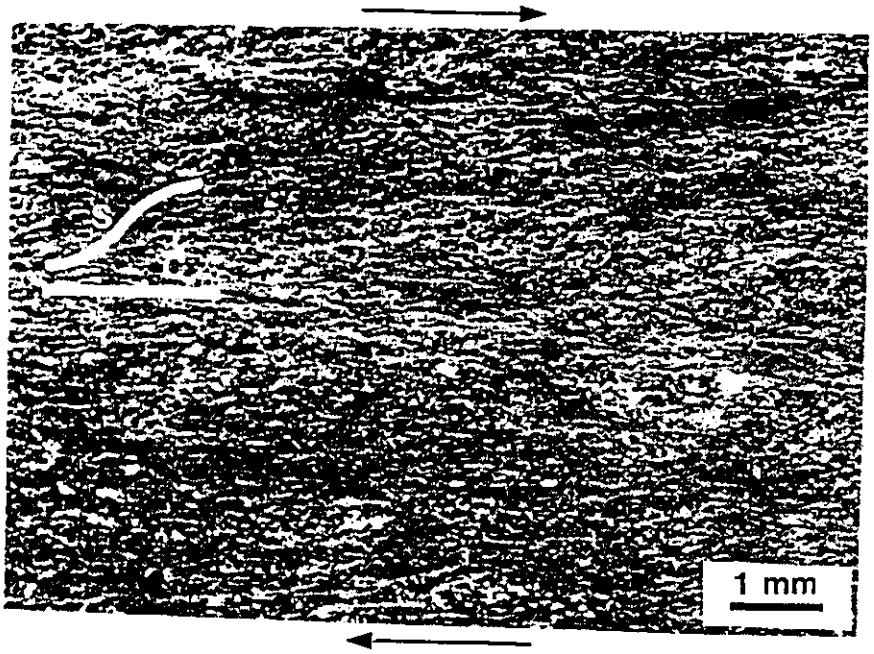

Figure 4.9, Photomicrograph of mylonitic fabrics with s-c surfaces, indicating dextral sense of shear.

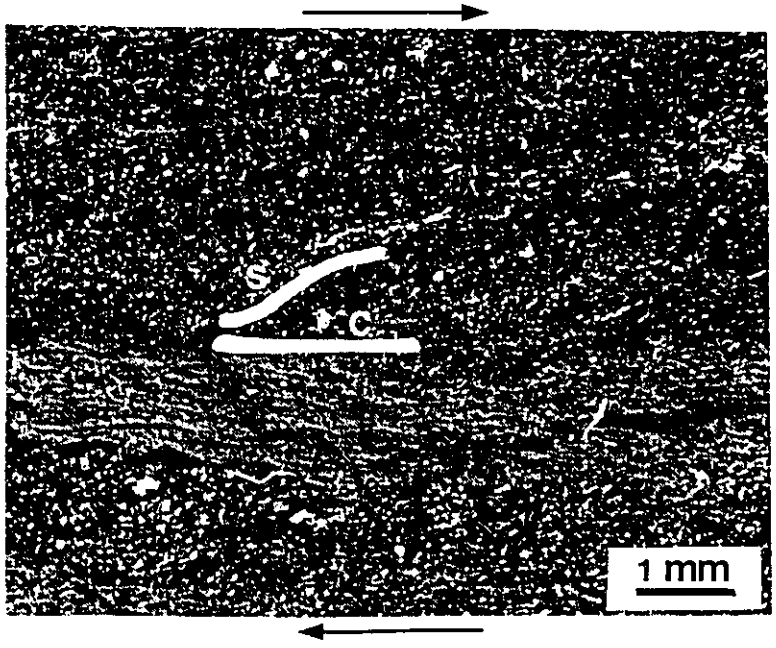

Figure 4.10, Photomicrograph of mylonitic fabrics with s-c surfaces, indicating dextral sense of shear.

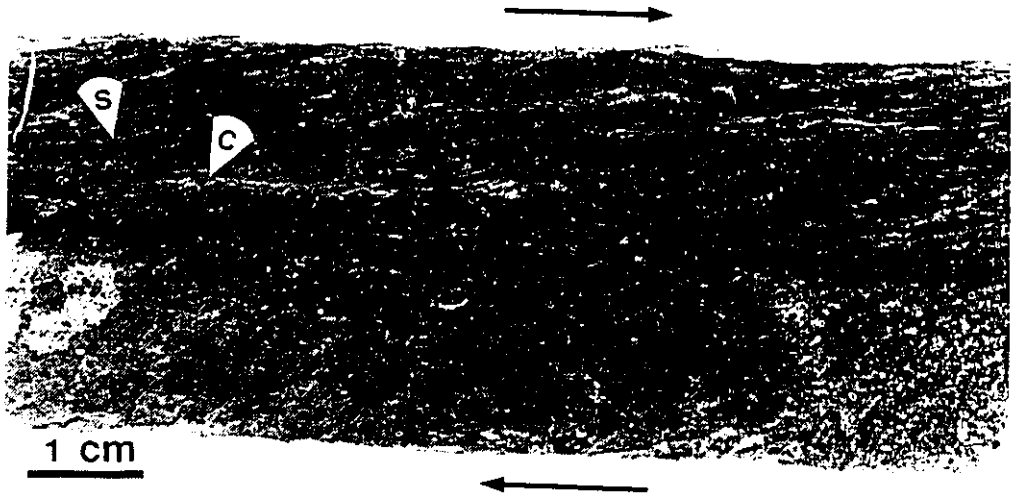

Figure 4.11, Polished surface of a hand sample of mylonite with s-c surfaces, indicating dextral sense of shear.

The development of crystallographic fabrics mainly results from reorientation of crystal axes, during ductile deformation, in response to the kinematic framework and the particular combination of crystallographic glide systems active during deformation (Lister et al, 1978; Law, 1985). Considerable work based on naturally deformed rocks (Schmid and Casey, 1986; Law et al, 1986) and deformation experiments (Tullis et al, 1973) has contributed much towards the understanding of crystallographic fabrics. Quartz, a common mineral in granitic rocks and mylonites, has received much attention from geoscientists; quartz c-axis fabrics especially have been a subject of several regional deformation studies (Lister and Dornsiepen, 1982; Law et al, 1986; Fueten, 1992), deformation experiments (Tullis et al, 1973; Kirby, 1977) and numerical modelling (Lister, 1979; Lister and Paterson, 1979) due to the fact that the c-axes can be readily measured on a Universal-stage mounted on a microscope. It is found that quartz c-axes developed along non-coaxial strain paths are asymmetric in respect to the macroscopic fabrics (e.g., foliation and stretching lineation) and their symmetry departs from an orthorhombic character in terms of fabric skeleton and intensity distribution. Furthermore, these asymmetries are formed to reflect the deformation path, and therefore can be used as kinematic indicators in structural analysis.

Measured quartz c-axes are usually plotted as poles in a stereo net, and then contoured in the net in order to see their asymmetries. The orientation of the highest count value is referred to as the mode while other highs are referred to as peaks in contoured c-axis pole figures. Lister and Williams (1979) propose that the skeletal

outlines of c-axes can be used to derived the sense of shear (Figure 4.12). These skeletons are extracted from contoured c-axis pole figures by connecting the loci of point maxima across the contour lines, and are classified into single girdles and crossed girdles (Figure 4.12). Single girdles are the most easily identified fabrics where the lowest contour roughly follows a single, steeply dipping girdle which may contain one or several distinct peaks resulting from the alignment of one or several glide planes with the shear plane (Simpson and Schmid, 1983). The angular width of single girdles should be relatively small and the contours must extend almost continuously across the net, otherwise the skeletons should be classified by their point maxima rather than as single girdles.

Crossed girdles are subdivided into Type I and Type II crossed girdles. Skeletal outlines of Type II crossed girdles are centred about the Y axis, while individual branches of Type I crossed girdles intersect away from the Y position (Figure 4.12), where Y represents the intermediate axis of the strain ellipsoid. One complicating factor for recognizing crossed girdles is that patterns may have developed c-axis maxima but have no significant concentration of c-axes along the girdles. In these cases, the skeletons are better classified by their point maxima.

Fairbairn (1949) first identified c-axis fabrics by point maxima. Lister and Dornsiepen (1982) adapted Fairbairn's use to the X-Z plane (Figure 4.13), where X is the stretching lineation and Z the foliation normal. Point maxima provide an exact means to describe the orientation of c-axis peaks in a fabric diagram.

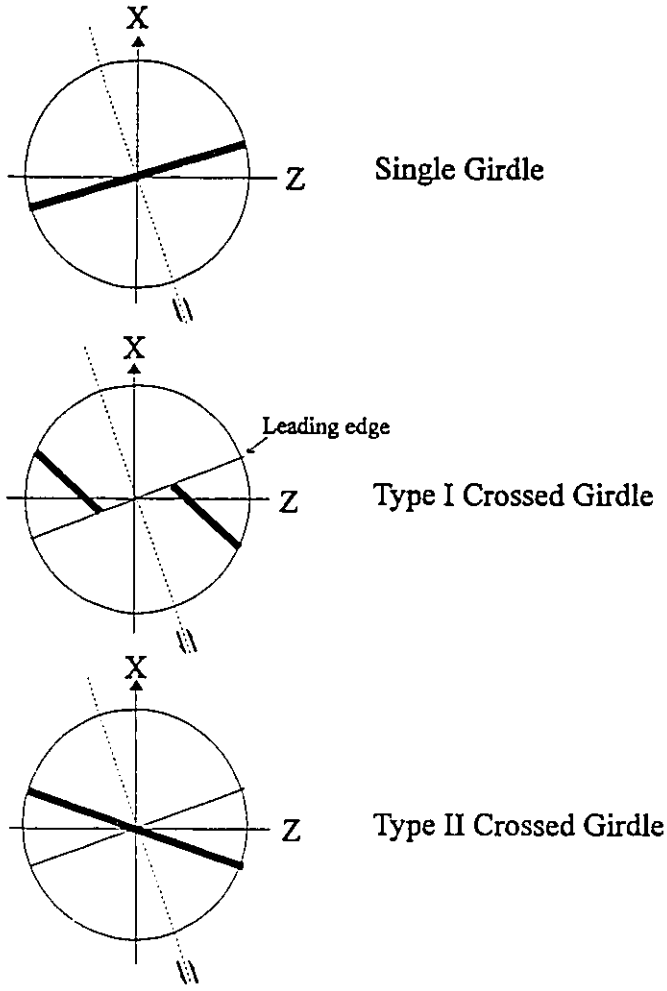

Figure 4.12, Skeletons of c-axis fabrics (Modified after Lister &Williams, 1979).

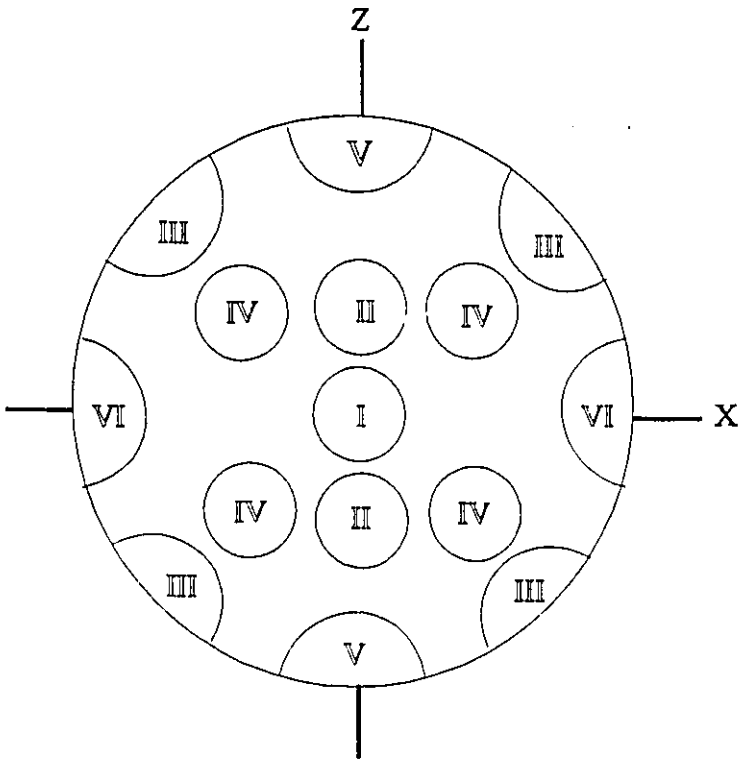

Figure 4.13, Point maxima of c-axis fabrics (Modified after Lister & Dornsiepen, 1982).

The asymmetries of the girdles and point maxima with respect to the foliation and shear plane are used as kinematic indicators. Etchecopar(1977), based on his two-dimensional model of progressive deformation, suggests a c-axis maximum normal to the shear plane and oblique to the foliation, considering that the basal plane <a> in quartz is a particularly important glide system, especially at low temperatures (Tullis et al, 1973). If other glide systems such as glide on the rhombs <r> or the prisms <m> operate as well, c-axis submaxima along a single asymmetric girdle are to be expected on the basis of Etchecopar's model. On the other hand, Lister and Hobbs (1980) used a three-dimensional model for quartz deformation and obtained Type I crossed girdles. The mechanism of fabric development assumed in this model is fundamentally different from that of the two-dimensional model (see Lister, 1982 for a discussion). They proposed the use of skeletal outline as a kinematic indicator, namely, the leading-edge principle. The leading-edge is a sharply defined boundary into the pole-free area around the extension axis (see Figure 4.12), and is expected to be oriented perpendicular to the shear plane according to their simulation. It is found in this study that the orientation of the mode is particularly important in determining the sense of shear, and is oriented close to the direction of the maximum compressive stress. This is in agreement with the angular relationship detected by Hobbs (1968) in experimentally deformed and recrystallized single quartz crystals. Hobbs (1968) found that dislocation slip within single crystals loaded oblique to the c-axis resulted in a rotation of the host c-axis towards the direction of the maximum compressive stress.

Petrofabric analysis of quartz c-axis has been carried out from specimen collected in the research area, using an optical microscope and Universal-stage. Wherever possible at least 200 quartz grains were measured in each thin section. The c-axis data are presented on equal area, lower hemisphere stereographic projections. All c-axis diagrams are plotted in the X-Z plane which contains the stretching lineation (X) and pole (Z) of foliation, except specimen KF-7, which was collected from an undeformed area without foliation and lineation. In all these stereographic projections (except KF-7), the foliation is vertical and lineation within the foliation horizontal. The intermediate axis Y is in the centre of the net, the Z at the top and the X is at the intersection of the equatorial axis with the perimeter of the net. In geographical terms, all fabric diagrams are viewed towards northwest.

All c-axis plots were contoured using a computer software entitled Rockworks (version 3). Numerical densities of c-axes were calculated using a spherical Gaussian weighting function described by Robin and Jowett (1986), which results in much smoother and more realistic density contours. Following the suggestion of Kamb (1959) for the size of a counting circle, the Kurtosis (k) of the Gaussian function is chosen so that $E=3s$, where E is the Expected Value of the counts for a data set of N points, and s is the Standard Deviation of the counts if the N data points are drawn randomly from an isotropic population. All contour lines are plotted in terms of standard deviation, for example, a contour line marked by 4.5 equals to 4.5 times of the standard deviation.

Thin sections cut from mylonites show distinctive c-axis fabrics, mainly in point

maxima fashion. Well-defined maxima III fabrics are observed in samples collected from main fault #6 and #5, along which rocks were deformed into banded mylonites (e.g., Figure 3.16). Mesoscopic kinematic indicators (e.g., displaced quartz veins) and other microscopic kinematic indicators (e.g., s-c fabrics) all suggest the faults had right-handed sense of shear, which is confirmed by the c-axis fabrics (Figure 4.14 and Figure 4.15). The mode of c-axes is located within the northwest quadrant in these figures, close to the direction of the maximum compressive stress determined in chapter 3 with an estimated orientation of about 300°/40°, i.e., the maximum compressive stress came from WNW direction. The asymmetry of the fabrics in skeletal outlines and intensity indicates a non-coaxial deformation responsible for the mylonitization, while the angular relationship of the mode with the shear plane reveals the sense of shear, dextral along fault #6 and #5.

Figure 4.16 shows the c-axis fabrics for sample KMS-029 collected along fault #02, in which maxima III are displayed and a peak is near the position of maximum V, while the mode is located in northwest quadrant, suggesting a dextral sense of shear on the fault. Specimen KMS-026 (Figure 4.17) collected from fault #10 has peaks in maxima III and the mode in the northwest quadrant near the position of maximum V, confirming the dextral sense of shear detected from other kinematic indicators. Figure 4.18 shows the fabrics of sample KF-14 collected along a fault in Middle Bay which is located right beside the Main Site (see Figure 5.9); maxima II are presented in addition to maxima III, and the mode is also located in northwest quadrant, supporting the right-handed shear sense obtained by other independent means. Section KMS-051 (Figure

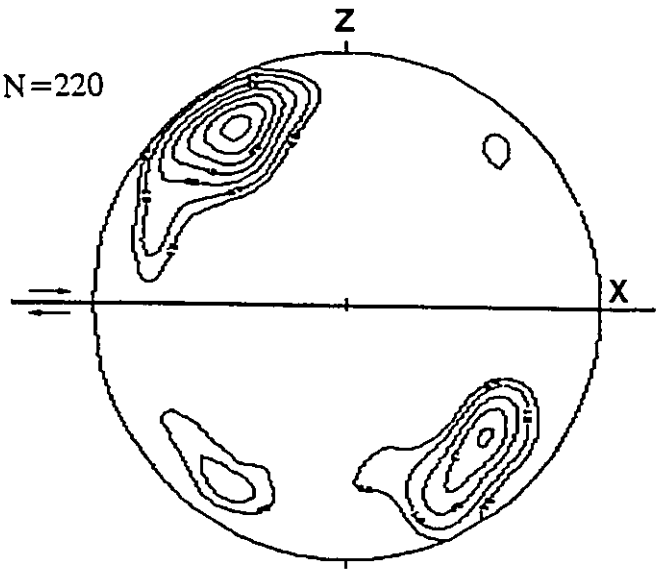

Figure 4.14, C-axis fabrics of KMS-043.
(contour: 1.0, 2.0, 3.0, 4.0, 5.0, 6.0, 7.0)

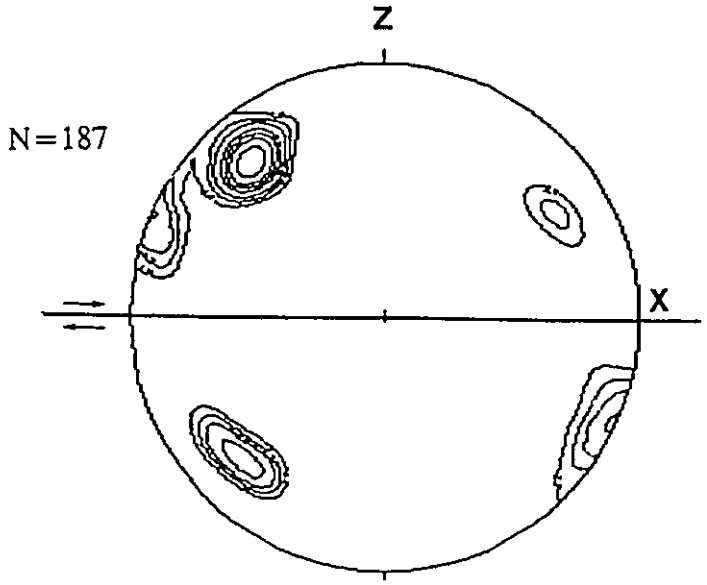

Figure 4.15, C-axis fabrics of KMS-028.
(contour: 1.0, 1.5, 2.0, 2.5, 3.0, 3.5, 4.0)

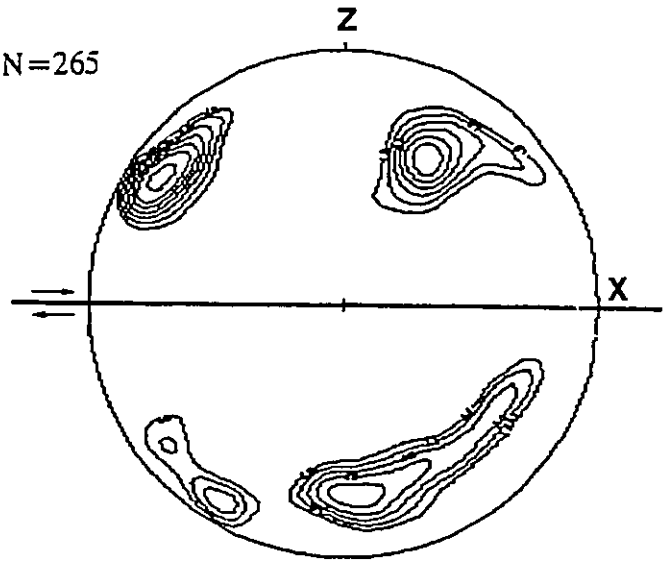

Figure 4.16, C-axis fabrics of KMS-029.
(contour: 1.0, 1.5, 2.0, 2.5, 3.0, 3.5, 4.0)

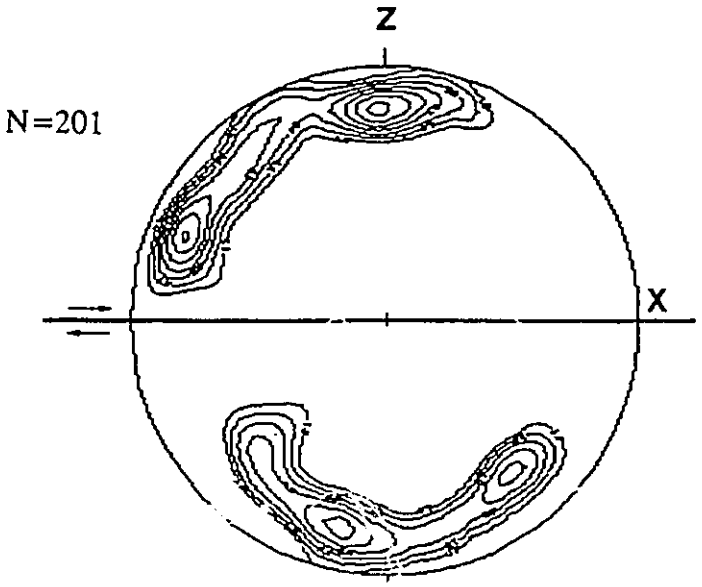

Figure 4.17, C-axis fabrics of KMS-026.
(contour: 1.0, 1.5, 2.0, 2.5, 3.0, 3.5, 4.0)

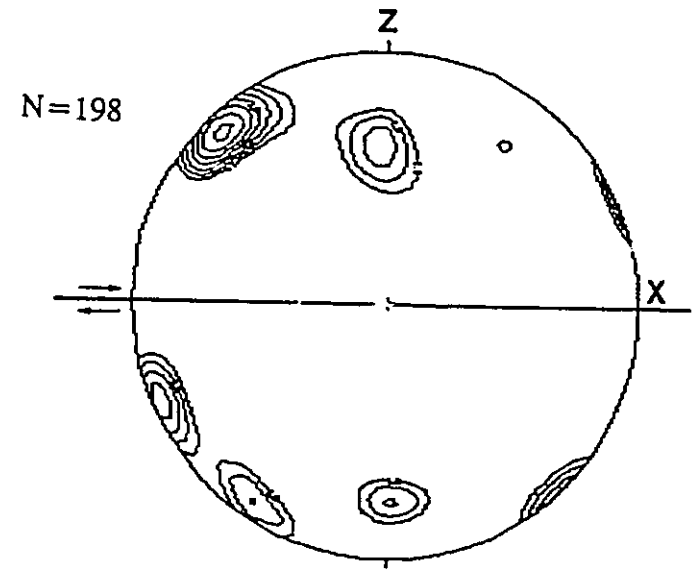

Figure 4.18, C-axis fabrics of KMS-014.
(contour: 1.5, 2.0, 2.5, 3.0, 3.5, 4.0, 4.5)

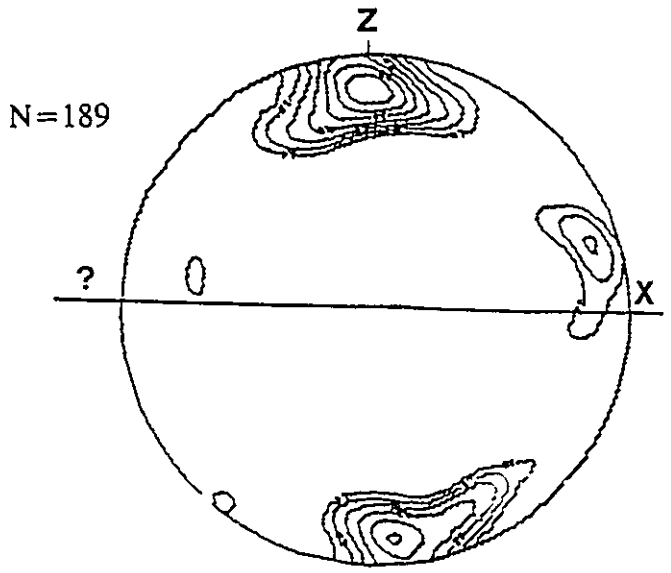

Figure 4.19, C-axis fabrics of KMS-051.
(contour: 1.0, 1.5, 2.0, 2.5, 3.0, 3.5, 4.0)

4.19) from fault rock in South Bay (see Figure 5.9) displays distinctive maxima V and incomplete maxima III, and the mode is almost perpendicular to the foliation and the shear plane. Therefore, in this case the sense of shear cannot be determined from c-axis fabrics alone.

In comparison, c-axis fabrics were analyzed in sample KF-7 collected from relatively undeformed granite in Killarney village. Figure 4.20 shows the fabrics in samples KF-7, in which there are no distinctive distribution patterns.

Experiments (Tullis et al, 1973) and numerical modelling (Lister, 1979; Lister and Paterson, 1979) of quartz deformation indicate that more than 10% of shortening or a shear strain of 1 or greater is required to produce a well-defined preferred crystallographic orientation in quartzite. The evidence of well developed c-axis fabrics in the mylonites suggests that the intercrystalline glide is an important deformation mechanism during faulting and the ductile shear strain should have been greater than 1 in the research area.

Optically measured c-axis orientations do not completely constrain the orientation of the crystal lattice, i.e., the orientation of <a> is not uniquely defined (Fueten, 1992). It is, however, possible to argue for the operation of certain glide systems for some distinctive fabrics. Starkey (1979) attributes the maxima I to slip on the prism <m> system, and maxima III to slip on rhombs <r> as well as the basal <a>. Lister and Dornsiepen (1982) propose that maxima III is the result of glide on the basal <a> and the prism <m> systems, which is supported by a detailed quartz analysis of

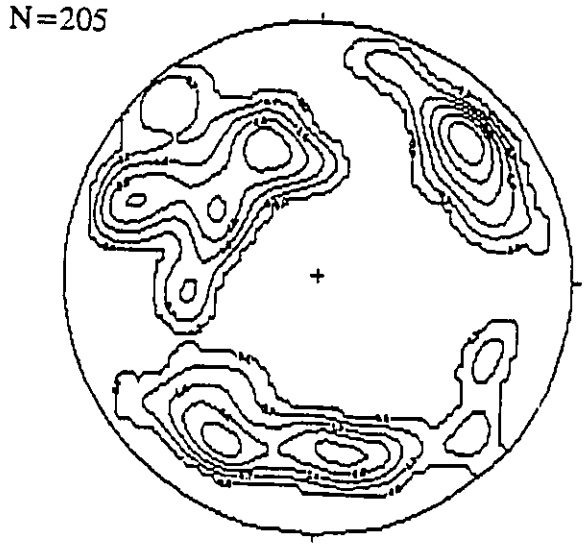

Figure 4.20, C-axis fabrics of KF-7.
(contour: 0.1, 0.5, 2.0, 2.5, 3.0, 3.5, 4.0)

Fueten and others (1991). The fabrics of maxima II are most likely formed by glide on positive or negative rhombs in the <a> direction, while maxima V are in positions where glide on the basal planes is maximized (Schmid et al, 1981). All quartz fabrics analyzed from mylonites in the research area posses peaks at maxima III, suggesting that glide on the basal <a> and the prism <m> was dominant during the deformation.

4.3.2.4 Displaced Broken Grains

Kinematic indicators discussed above are all related to quartz and its ductile deformation in mylonitic rocks. Meanwhile, feldspars, another common mineral in mylonitic rocks, usually remain brittle in a ductile matrix and are frequently broken and sheared in mylonites due to the relative movement in the shear zone. The resulting geometry can be used to deduce the over-all shear sense in the rock.

In determining the sense of shear for the over-all shear zone from displaced broken grains, it is important to know the angular relationship between the direction of the shear zone and the direction of the microfractures across the broken grains. If the microfractures are parallel to shear zone boundaries (Figure 4.21A), or have a small angle with shear zone boundaries (Figure 4.21B), i.e., in the position of synthetic Riedel shear (R) (see Figure 3.3), the sense of displacement along microfractures is the same as that of the over-all shear zone. If the microfractures are the antithetic Riedel shear (R'), the sense of displacement along microfractures is opposite to the over-all sense of

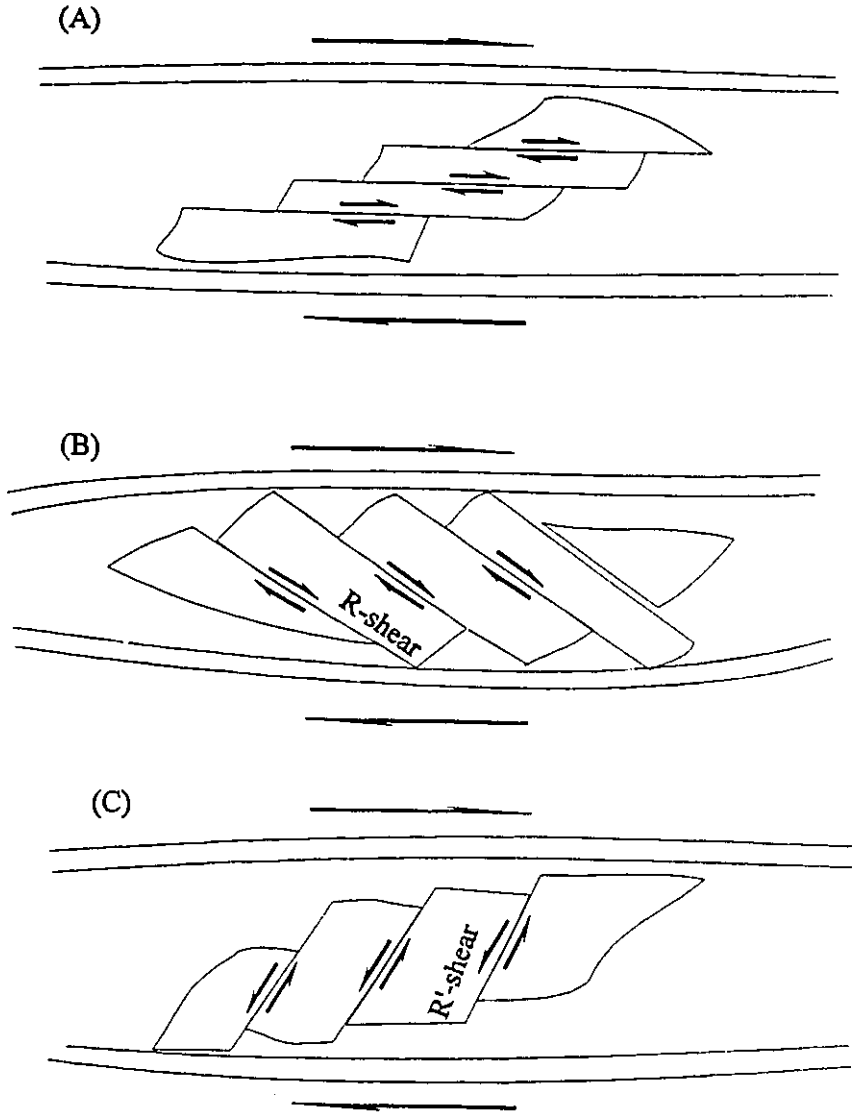

Figure 4.21, The use of displaced broken grains in a ductile matrix to deduce the sense of shear in a shear zone
(A) Microfractures within the broken grain are parallel to the shear zone
(B) Microfractures within the broken grain correspond to synthetic Riedel shear
(C) Microfractures within the broken grain correspond to antithetic Riedel shear

shear of the shear zone (Figure 4.21C).

Displaced broken grains of feldspar are observed in many thin sections, and they support the shear sense deduced from other kinematic indicators for the over-all shear zone. Figure 4.22 shows a displaced broken feldspar in which microfractures are parallel to the main shear zone, and have the same sense as the shear zone. Figure 4.23 shows microfractures of synthetic Riedel shear in a broken feldspar while Figure 4.24 shows microfractures of antithetic Riedel shear in another feldspar of the same thin section, all suggesting the dextral sense of shear on the main shear zone.

4.4 Paleopiezometry

When a rock undergoes deformation the crystal structure within minerals of the rock will "change" in response to the stresses acting locally within it and attempt to re-equilibrate with its thermodynamic environment. Equilibration may be achieved by breakdown and recrystallization of pre-existing minerals to form new minerals through grain growth (static annealing) or grain size reduction (dynamic recrystallization). Experimental studies of crystal systems show that equilibrium or steady state grain size is directly related to the differential stress under which the system was deformed (Twiss, 1977; Christie et al, 1980). Increasing differential stress decreases the recrystallized grain size (Figure 4.25). Through experimental calibration, the recrystallized grain size of quartz can be used to estimate the differential stress that was acting at the time of

Figure 4.22, Photomicrograph of mylonitic fabrics with displaced broken feldspar. The microfracture (mf) within the feldspar is parallel to the shear zone boundaries (E-W), and has the same sense of shear as the main shear zone.

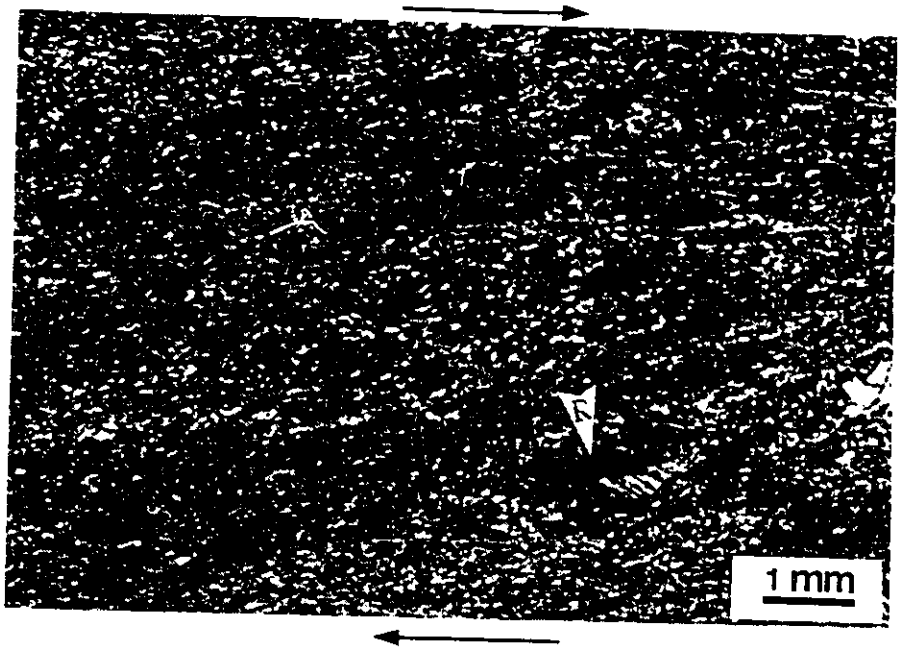

Figure 4.23, Photomicrograph of mylonitic fabrics with displaced broken feldspar. Microfractures within the feldspar correspond to the synthetic Riedel shear (R) and has the same sense of shear as the main shear zone.

Figure 4.24, Photomicrograph of mylonitic fabrics with displaced broken feldspar. Microfractures within the feldspar correspond to the antithetic Riedel shear (R') and has opposite sense of shear to the main shear zone.

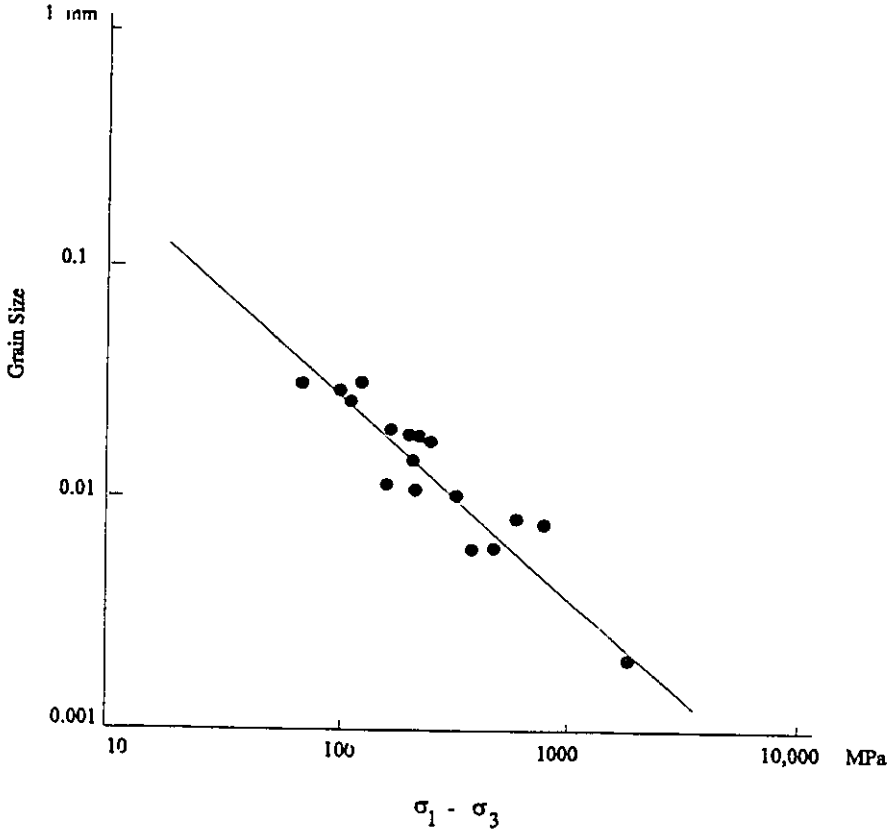

Figure 4.25, Experimentally determined relationships between grain size and differential stress for steady-state deformation in quartz (From Suppe, 1985).

recrystallization by the following equation:

$$\sigma_1-\sigma_3 \text{ (MPa)} = AD^{-n} \qquad \text{.....(4.1)}$$

where D is the diameter (μm) of recrystallized quartz grain, A and n are empirical constants (Table 4.1).

One should keep in mind that the above equation assumes that the recrystallized grain size measured is the equilibrium grain size for the desired stress state, which is, however, not always the case. An underestimate in differential stress results should grain growth not be taken into consideration during deformation. If the temperature is maintained after the stress has been relaxed, static annealing will proceed, thus increase the grain size. Unless the system is quenched in some way either during or immediately following the relaxation of the stress field, the grain size measured will be larger than the steady state grain size, so the use of this grain size will result in an underestimate of the differential stress. On the other hand, if the initial grain size is small and applied stress level is low enough that an unreasonable length of time will be necessary to allow the grain size to re-equilibrate; or if grain growth or recrystallization is inhibited by neighbouring minerals of a different composition, such as stronger feldspars (Twiss, 1977), an overestimate of differential stress will result from the use of this recrystallized grain size. Therefore, in the use of paleopiezometry of recrystallized quartz grains, it is necessary to determine if the observed grain size has resulted from an increase or decrease of the original grain size.

The paleopiezometry appears to be most useful when it is applied to the

Table 4.1, Empirical Constants of Paleopiezometry for Recrystallized Quartz Grain

A	n	Reference
381	0.71	Mercier et al, 1977
603	0.68	Twiss, 1977
4090	1.11	Christie and Ord, 1980
3902	1.43	Christie and Ord, 1980

recrystallization associated with major thrust faults (Twiss, 1977; Weathers et al, 1979; O'Donnell, 1986). If thrusting has occurred at, or proceeded to, a high crustal level, there is a good chance that the steady state grain size has been preserved because temperature could not be maintained at this level. Evidences of microstructures discussed above in the research area all indicate that the deformations responsible for the formation of penetrative fabrics and mylonitic fabrics, respectively, occurred at high crustal level, over time. Therefore, the use of paleopiezometry of recrystallized quartz grain should provide useful information regarding the stress field for these deformation events.

Mylonites were divided into two different regimes due to strain partitioning (Figure 4.26, see also Figure 3.16). In highly deformed regimes, quartz grains are fully recrystallized and grain sizes are much smaller than those recrystallized in poorly deformed regimes in which only some grains are recrystallized, and the majority of quartz grains remain unrecrystallized and show undulatory extinction, elongation and other deformation features. Samples collected far away from main faults, containing penetrative fabrics, present only low-deformed regime. Recrystallized quartz grains were measured and presented in Table 4.2 for samples from the research area. Calculation of differential stress were done by using the calibration of Christie et al (1980), since this calibration closely matches Suppe's (1985) conclusion shown in Figure 4.25.

Measurements of recrystallized quartz grains suggest differential stress of about 85-145 MPa to produce the high-grade mylonitic fabrics, and about 45-55 MPa for the penetrative fabrics, with a standard deviation of about 15 MPa and 3 MPa, respectively.

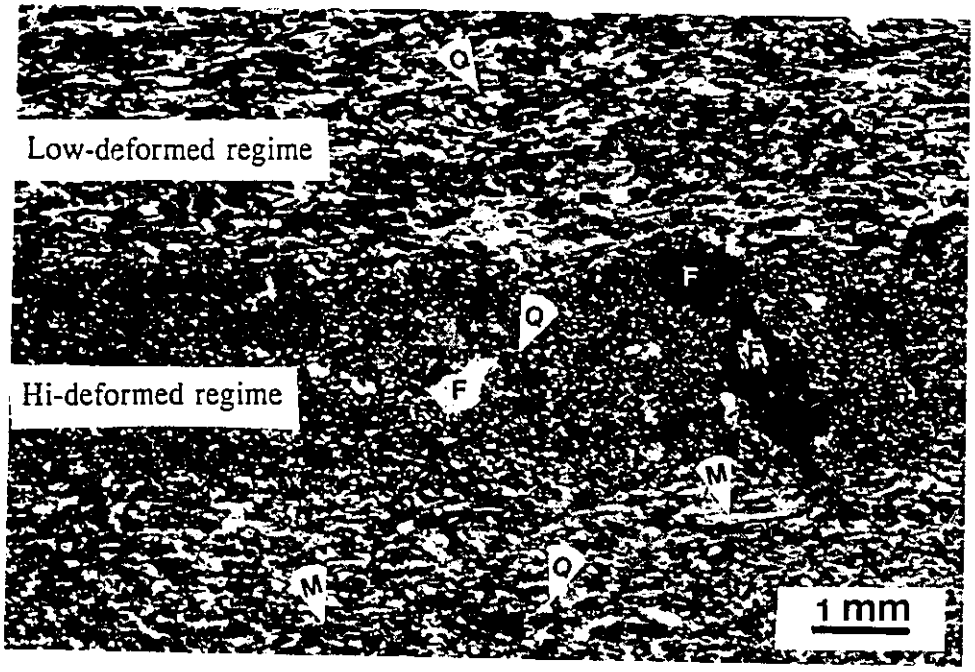

Figure 4.26. Photomicrograph of mylonitic fabrics, showing two distinctive deformation regimes. In high-deformed regime quartz grains are fully recrystallized and grain sizes are much finer than those in low-deformed regime.
Q-quartz F-feldspar M-mica

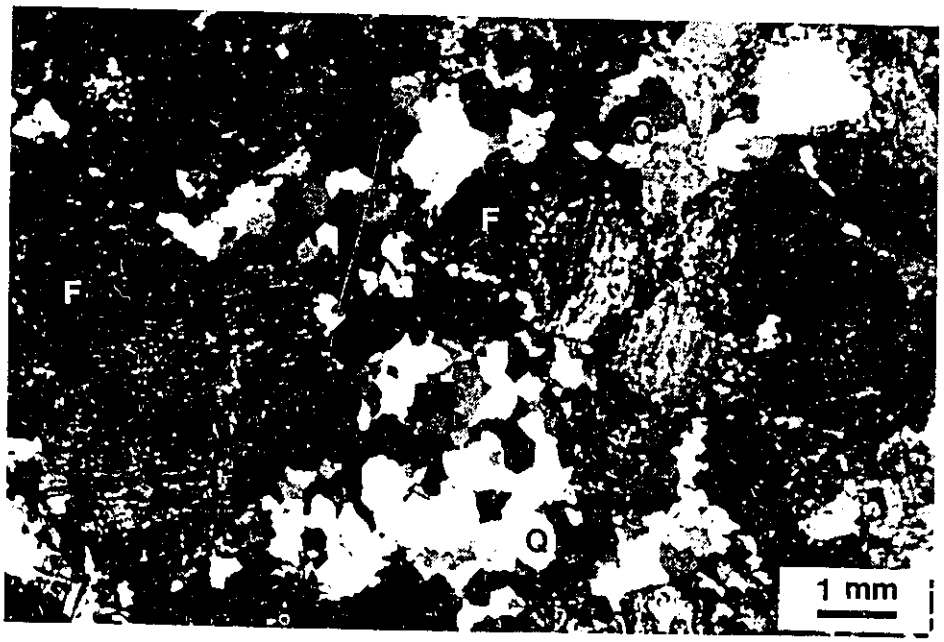

Figure 4.27. Photomicrograph of undeformed rock from Killarney village.

Table 4.2, Paleopiezometer for Recrystallized Quartz Grains

No.	Sample	Lo-Deformed Regime		Hi-Deformed Regime	
		G.Size	D.Stress	G.Size	D.Stress
1	KF-12	48.5	55		
2	KF-2	55.3	48		
3	KF-3	56.7	46		
4	KF-13	48.4	55	30.4	92
5	KF-14	55.3	48	30.7	91
6	KMS-063	55.5	47	30.4	92
7	KMS-061	60.6	43	31.1	90
8	KMS-064	63.8	41	29.5	96
9	KMS-066	59.5	44	29.8	95
10	KMS-014	54.9	48	32.4	86
11	KMS-030	51.6	51	30.3	93
12	KMS-012	57.9	45	26.9	106
13	KMS-013	57.7	45	30.9	91
14	KMS-037	53.9	49	32.6	86
15	KMS-004	50.9	52	31.6	88
16	KMS-022	56.5	46	32.3	86
17	KMS-010	53.9	49	25.9	110
18	KMS-009	53.9	49	32.1	87
19	KMS-011	53.9	49	33.1	84
20	KF-10	54.1	49	21.8	134
21	KMS-026	56.6	46	24.8	116
22	KMS-024	57.9	45	21.7	135
23	KMS-025	52.4	51	20.1	146
24	KMS-003	54.3	49	25.9	111
25	KMS-007	50.1	53	29.1	97
26	KMS-017	54.1	49	22.6	129
27	KMS-034	53.9	49	27.9	102
28	KMS-027	53.1	50	30.2	93
29	KMS-053	55.9	47	29.6	95
30	KMS-055	55.9	47	30.8	91
31	KMS-035	58.1	45	25.3	113
32	KMS-043	50.8	52	21.4	137
33	KMS-018	53.1	50	29.6	95
34	KMS-041	53.4	49	28.1	101
35	KMS-042	55.1	48	27.4	104
36	KMS-056	60.3	43	24.5	118
37	KMS-057	59.3	44	23.3	124
38	KMS-028	54.1	49	29.1	97
39	KMS-006	53.9	49	28.9	98
40	KMS-032	55.6	47	30.8	91
41	KMS-005	57.9	45	25.9	111
42	KMS-045	57.2	46	29.5	96
43	KMS-019	62.8	41	34.4	81
44	KMS-029	57.4	46	29.1	97
45	KF-9	53.9	49	29.9	94
46	KMS-046	54.7	48	31.3	89
47	KMS-047	56.5	46	31.1	90
48	KMS-048	51.9	51	30.9	91
49	KMS-060	58.1	45	25.4	113
50	KMS-051	51.9	51	32.4	86
51	KMS-052	54.2	49	30.1	94
52	KF-11	50.8	52	30.1	94
53	KF-8	57.9	45	29.9	94
54	KF-5	57.5	46	29.7	95
55	KF-6	55.9	47	31.4	89
MEAN		51.7 um	48 MPa	30.9 um	100 MPa
S.D.		3.2 um	3 MPa	0.5 um	15 MPa

Rock described as undeformed (Figure 4.27) from Killarney village has limited recrystallization, with a grain size corresponding to a differential stress of about 10 MPa (Figure 4.28). These differences imply variations in overall stress regimes, and therefore variations in conditions, over time.

Results of several studies of mylonites from major thrust belts indicate that the differential stresses involved in thrusting range from 20 MPa to 200 MPa, with average values of about 100 MPa (Twiss, 1977; Weathers et al, 1979; Kohlstedt and Weathers, 1980; Ord and Christie, 1984). Results of differential stress estimated in high-deformed regime from mylonites along main faults are right in line with those calculated by other authors, with average value of 100 MPa and standard deviation of 15 MPa (Table 4.2).

4.5 Discussion and Conclusion

On the basis of microstructural analysis, at least two major deformation events occurred after the emplacement of the KIC. The earlier tectonic event imposed a regional foliation and lineation on the porphyry and volcaniclastic rocks in the research area, while the latter event produced a zone of thrusting faults, with considerable dextral shear movement, and mylonite zones accompanying the faults.

Mineralogy and microstructural strain features of quartz and feldspar suggest the greenschist facies metamorphic condition was not exceeded during the formation of penetrative fabrics. Wanless and Loveridge (1972) obtained a whole rock Rb-Sr isochron

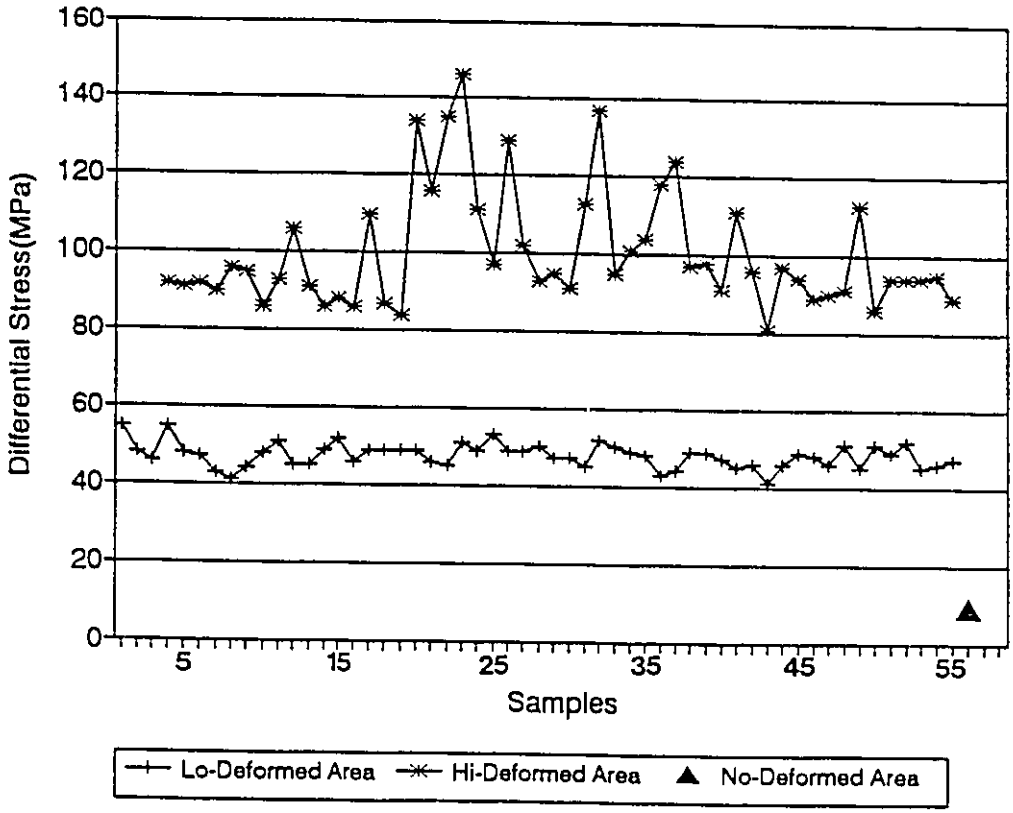

Figure 4.28, Differential stresses deduced from recrystallized quartz grains.

age of 1,623 Ma in the area, which is regarded as a reset date by van Breemen and Davidson (1988) and correlated with the flattening event responsible for the formation of these penetrative fabrics by Clifford (1990).

Mylonitic fabrics are observed in rocks along or close to main faults, and penetrative fabrics are still preserved in low-deformed regime of mylonites due to strain partitioning. Asymmetric porphyroclast system (σ-type), s-c fabric and displaced broken grain appear to be reliable kinematic indicators, confirming the dextral sense of shear accommodated by main faults deduced from other independent means. Although c-axis fabrics displayed strong asymmetries in terms of intensity and skeleton and also provided a tool for shear sense determination, the criteria of applying "skeletal outlines" may become problematic in some cases where a clear defined skeleton is not present or the angular relationship of skeleton with shear plane and foliation is indecisive in determining the sense of shear (e.g. Figure 4.19). As Garcia-Celma (1982) points out, local reversals of the shear sense are possible in cases in which rigid domains cause a highly inhomogeneous strain pattern, though these inconsistencies have not found in the research area. The over-all displacement sense of the shear zone can be determined with certainty if all lines of evidence agree.

Paleopiezometry of recrystallized quartz grain supports the determination that two major deformation events affected the region and also provides insight to the stress field associated with these events. The differential stress related to the flattening event ranged from 41 MPa to 55 MPa, with average value of 48 MPa and standard deviation of 3

MPa. The differential stress related to the thrusting ranged from 85 MPa to 146 MPa, with average value of 100 MPa and standard deviation of 15 MPa, which is right in line with results obtained from other major thrusting zones.

CHAPTER 5 KINKS

5.1 Introduction

Although the initiation and propagation of both microfractures and macrofractures have received considerable attention, the recognition and interpretation of the deformation processes involved in evolution of natural fault zones is far from complete. There is a growing awareness of the value of both fracture mechanics and damage mechanics approaches to the problem. Fracture mechanics attempts to define material parameters important to the fracture processes (Griffth, 1921; Irwin, 1957; Knott, 1973; Lawn, 1983) while damage mechanics emphasizes the various stages of fracture evolution and interaction during progressive deformation (Costin, 1987). Using these approaches together provides an important framework which can help the interpretation of experimental and natural faulting processes (Atkinson, 1987; Pollard and Aydin, 1988). However, the experimental determination of parameters crucial to fracture mechanics of rocks often remains difficult (Tullis and Tullis, 1986; Ferguson et al, 1987). In spite of this, we now have sufficient knowledge of fracture mechanics and damage mechanics to analyze and predict the possible path of fracture propagation for some simplified cases.

The fracture criteria in the macro-approach can be classified into three basic theories: (1) the Maximum Principal Stress Criterion, which states that a fracture tends

to propagate in a direction perpendicular to the maximum tensile stress in the region surrounding the fracture tip; (2) the Maximum Strain Energy Release Rate Criterion, which predicts that a fracture will propagate in the direction that maximizes the subsequent energy release rate; and (3) the Minimum Strain Energy Density Criterion, which indicates that a fracture will propagate in the direction along which the strain energy density is minimum. The first two theories are essentially equivalent (Cottrell, 1965) and widely accepted.

In this chapter, the first fracture criterion is applied to analyze and predict the propagation path of the increment of new crack at the tip of a existing fracture, a structure called "kink". "Kink" here refers to a secondary fracture that occurs at the end of a parent fracture and has an acute angle from the fracture. Figure 5.1 shows a secondary fracture which juts forth about 15 cm at an acute angle of 40° into the country rock from the tip of a parent fracture. The kink shown in Figure 5.2 is similar to that shown in Figure 5.1, but the kink angle is slightly different (34° here) and the kink contains 2 crack segments.

5.2 Theoretical Analysis

5.2.1 Stress Field near A Crack Tip

The general elastic theory is dealt with in great detail in many works, notably,

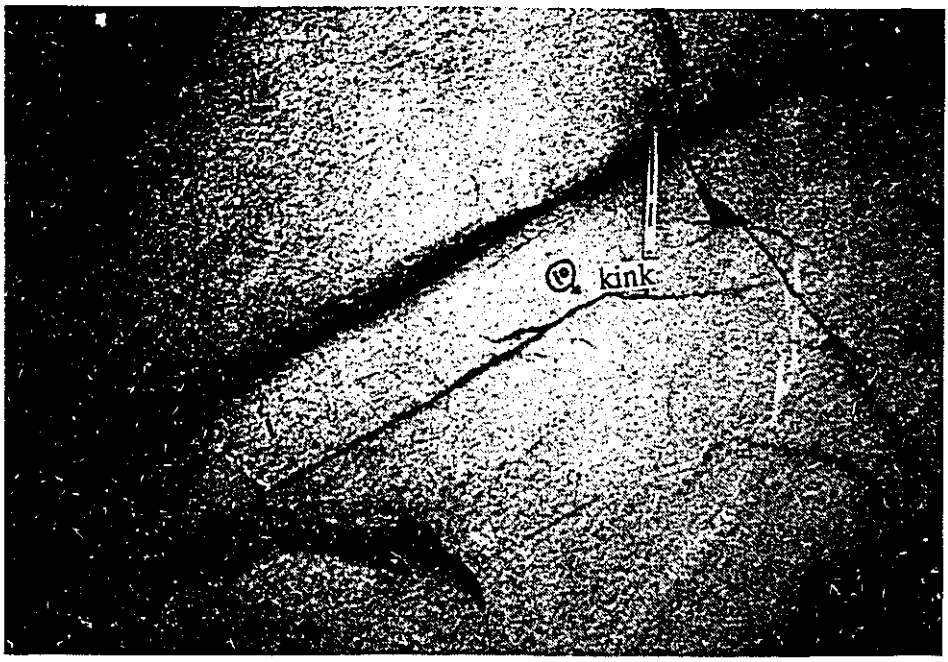

Figure 5.1, A kink with kink angle of about 40° in Main Site.

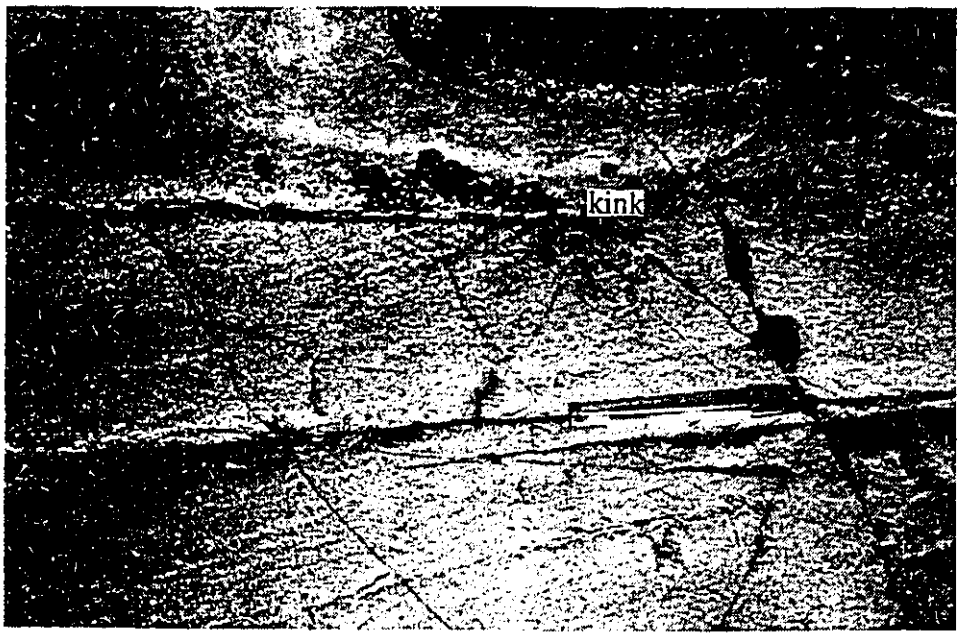

Figure 5.2, A kink with kink angle of about 35°, containing two crack segments in Main Site.

Timoshenko and Goodier (1951), Sokolnikoff (1956) and Jaeger and Cook (1976). The following specifications must be included in mechanical analyses of faulting: (1) the geometry of the region, (2) appropriate boundary and initial conditions, and (3) behaviour of all parts of the body (Segall and Pollard, 1980). Some general assumptions which facilitate the analyses mathematically, but do not void its application in geological field, will be made.

The following assumptions will be presumed in the mechanical analyses: (1) the far-field stress state is spatially uniform, (2) the fractures studied are in static equilibrium, (3) the rock body is homogeneous. And finally, by admitting no variation in geometry, material properties and boundary conditions in the x_3 direction (vertical direction), the problem becomes two dimensional (horizontal plane). This is appropriate for the study area, where fractures are approximately vertical, and there is substantial horizontal component of motion on faults. **The engineering usage for the sign coHxention of stresses is adopted for the following stress analysis, that is, normal stresses are positive if tensile.**

For an isolated crack shown in Figure 5.3, subjected to mode I and mode II loading, the three components of stress in the region near crack tip can be expressed as follows

$$\sigma_{11}=(\frac{2r}{a})^{-\frac{1}{2}}\{\Delta\sigma_I[\cos(\frac{\theta}{2})+\frac{1}{2}\sin\theta\sin(\frac{3\theta}{2})]+\Delta\sigma_{II}[\frac{1}{2}\sin\theta\cos(\frac{3\theta}{2})]\}...(5.1)$$

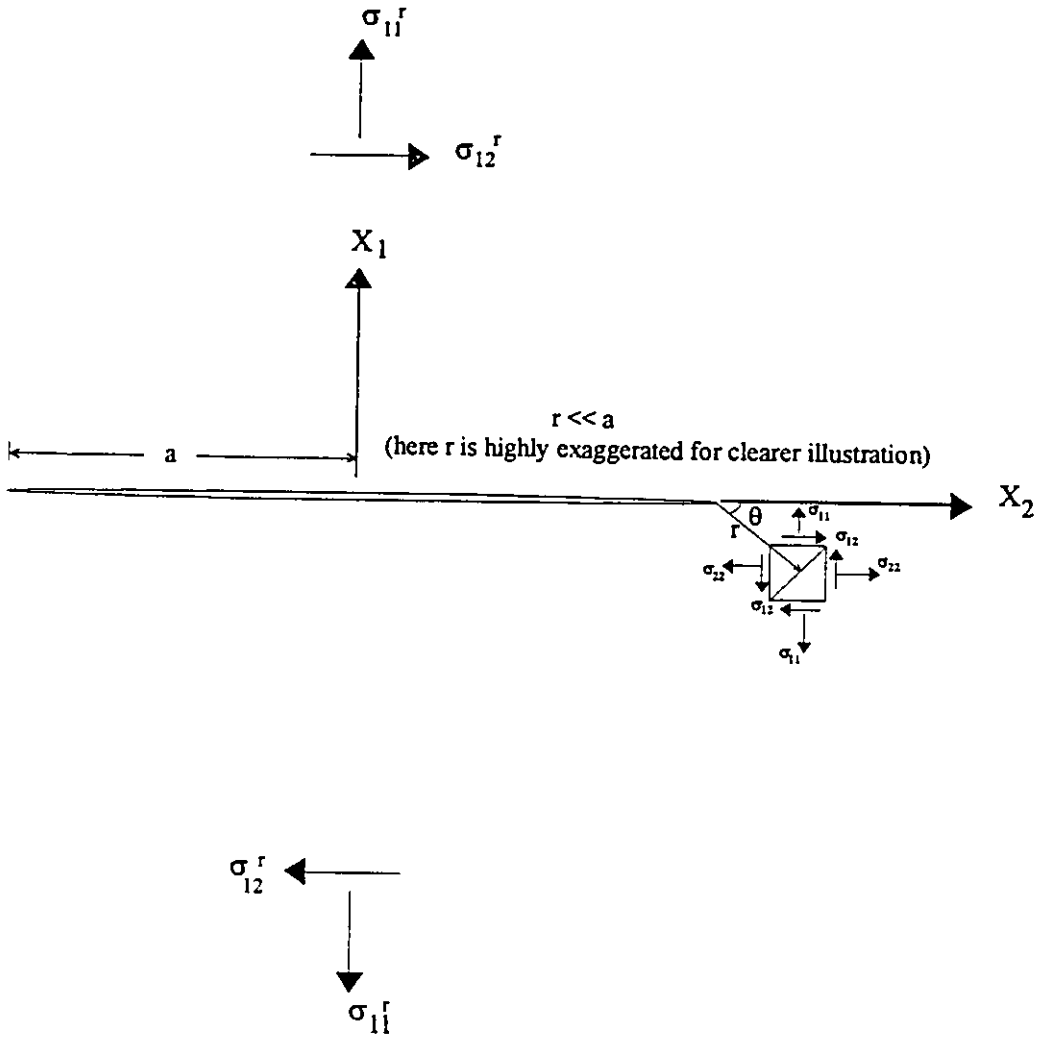

Figure 5.3, Illustration of a fracture, subjected to mode I and mode II loading.

$$\sigma_{12}=(\frac{2r}{a})^{-\frac{1}{2}}\{\Delta\sigma_I[\frac{1}{2}\sin\theta\cos(\frac{3\theta}{2})]+\Delta\sigma_{II}[\cos(\frac{\theta}{2})-\frac{1}{2}\sin\theta\sin(\frac{3\theta}{2})]\}...(5.2)$$

$$\sigma_{22}=(\frac{2r}{a})^{-\frac{1}{2}}\{\Delta\sigma_I[\cos(\frac{\theta}{2})-\frac{1}{2}\sin\theta\sin(\frac{3\theta}{2})]-\Delta\sigma_{II}[2\sin(\frac{\theta}{2})+\frac{1}{2}\sin\theta\cos(\frac{3\theta}{2})]\}...(5.3)$$

(Pollard and Segall, 1987) where a is the half length of the crack, $\Delta\sigma_I$, $\Delta\sigma_{II}$ are driving stresses, or effective stresses, i.e.

$$\Delta\sigma_I=\sigma_{11}^r-\sigma_{11}^c.....(5.4)$$

$$\Delta\sigma_{II}=\sigma_{12}^r-\sigma_{12}^c.....(5.5)$$

where σ_{11}^r and σ_{12}^r refer to the remote normal stress and remote shear stress, respectively; σ_{11}^c represents the normal stress on the crack, such as the fluid pressure inside the structure, and σ_{12}^c represents the frictional strength of the crack.

Roman subscripts in equations(5.1-5.5) refer to the different deformation modes. According to Irwin, three different deformation modes, corresponding to dilation or closing in x_1 direction (mode I), sliding in x_2 direction (mode II), and sliding in x_3 direction (mode III), are distinguished (Figure 5.4).

Equations (5.1-5.3) refer to two dimensional deformation. If the crack is also

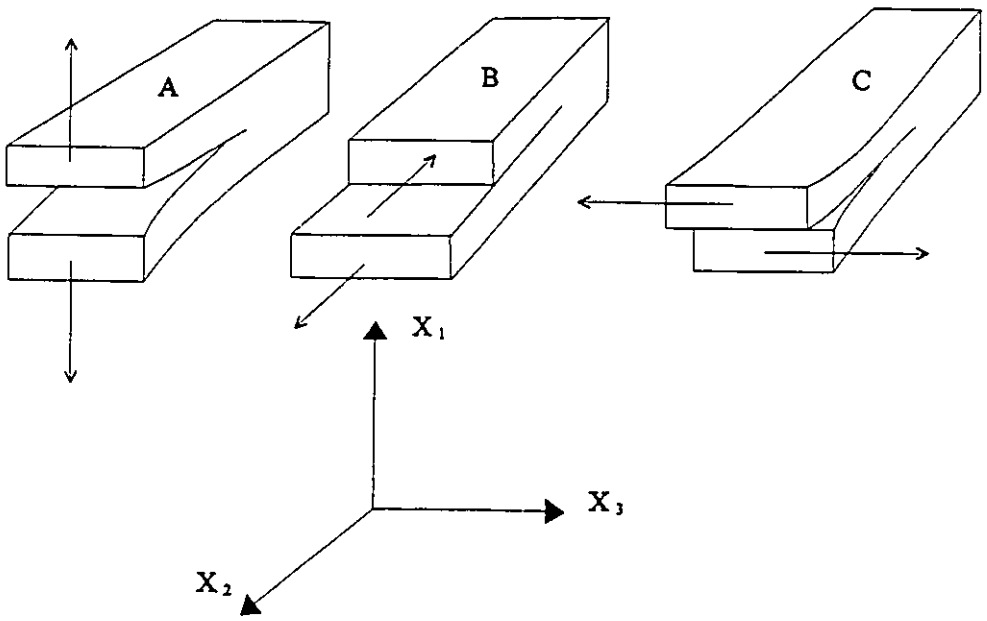

Figure 5.4, Illustration of three fundamental modes of faulting.
(A) mode I, opening or closing mode
(B) mode II, in-plane shear or sliding mode
(C) mode III, anti-plane shear or tearing mode

under mode III deformation, in addition to mode I and mode II, the other three stress components are,

$$\sigma_{13}=-\left(\frac{2r}{a}\right)^{-\frac{1}{2}}\Delta\sigma_{III}\cos\left(\frac{\theta}{2}\right).....(5.6)$$

$$\sigma_{23}=-\left(\frac{2r}{a}\right)^{-\frac{1}{2}}\Delta\sigma_{III}\sin\left(\frac{\theta}{2}\right).....(5.7)$$

$$\sigma_{33}=2\upsilon\left(\frac{2r}{a}\right)^{-\frac{1}{2}}\left[\Delta\sigma_{I}\cos\left(\frac{\theta}{2}\right)-\Delta\sigma_{II}\sin\left(\frac{\theta}{2}\right)\right].....(5.8)$$

These equations (5.1-5.8) play a prominent role in the field of fracture mechanics (Lawn and Wilshaw, 1975). The dependence of all stress components in these equations on $r^{-1/2}$ indicates the stress singularity at the crack tip.

5.2.2 Kink Angle

Kink angle is defined as the angle (θ) between the parent crack and the direction of the increment of new crack (e.g. Figure 5.3). The angle is positive if it is counter-clockwise from the parent crack.

For a crack under mode I and mode II deformation, the field of stress in the region near the crack tip is given by equations (5.1-5.3). The singularity in the stresses at the tip of the crack suggests that any secondary, stress-induced fractures should initiate

there, which is supported by previous studies (Pollard and Segall, 1987; Cruikshank et al, 1991) and my field observations.

According to the Maximum Principal Stress Criterion, the secondary fractures propagate away from the parent crack at an angle (θ) which maximizes the local tensile stress acting across the incipient crack path. In order to solve for θ from equations (5.1-5.3) the stresses are transformed into a cylindrical coordinate system centred on the crack tip (Figure 5.5). The circumferential stress $\sigma_{\theta\theta}$ is related to the Cartesian stress components by (Timoshenko and Goodier, 1951)

$$\sigma_{\theta\theta} = \sigma_{22}\sin^2\theta + \sigma_{11}\cos^2\theta - 2\sigma_{12}\sin\theta\cos\theta \quad \text{.....(5.9)}$$

Substituting equation (5.1-5.3) into equation (5.9), followed by algebraic manipulation, we get,

$$\sigma_{\theta\theta} = \left(\frac{a}{2r}\right)^{\frac{1}{2}}\left[\Delta\sigma_I \cos^3\left(\frac{\theta}{2}\right) - \frac{3}{2}\Delta\sigma_{II}\cos\left(\frac{\theta}{2}\right)\sin\theta\right] \quad \text{.....(5.10)}$$

To find the direction along which the circumferential stress is maximum, $\sigma_{\theta\theta}$ is differentiated with respect to θ, and the result is set to zero. This yields,

$$\Delta\sigma_I\left[\sin\left(\frac{\theta}{2}\right) + \sin\left(\frac{3\theta}{2}\right)\right] + \Delta\sigma_{II}\left[\cos\left(\frac{\theta}{2}\right) + 3\cos\left(\frac{3\theta}{2}\right)\right] = 0 \quad \text{....(5.11)}$$

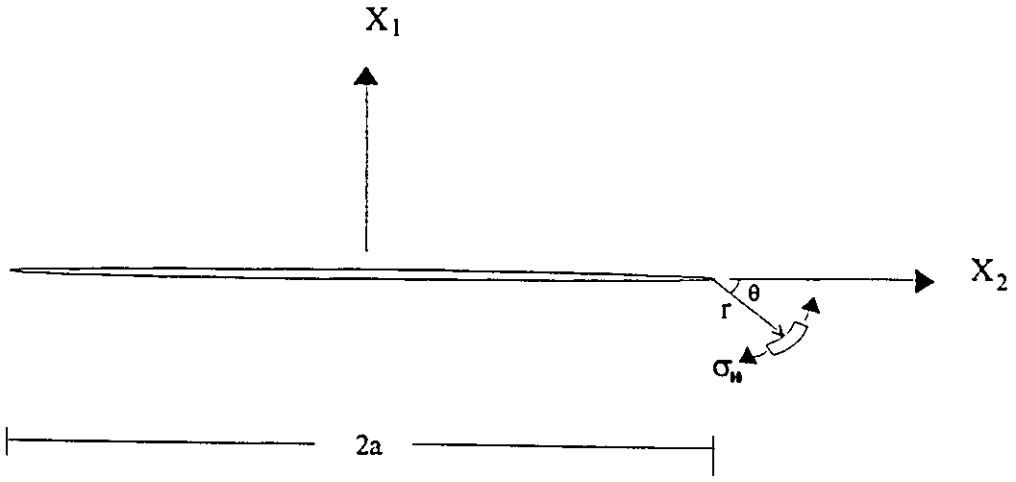

Figure 5.5, Illustration of circumferential stress $\sigma_{\theta\theta}$ actimg on an element near the crack tip.

or,

$$\frac{\Delta\sigma_{II}}{\Delta\sigma_{I}} = -\frac{\sin(\frac{\theta}{2})+\sin(\frac{3\theta}{2})}{\cos(\frac{\theta}{2})+3\cos(\frac{3\theta}{2})} \qquad .....(5.12)$$

This equation indicates that the kink angle (θ) is determined by the ratio of the effective stresses acting on the parent crack.

Cruikshank et al (1991) use a different approach to find out the kink angle. They follow the theoretical analysis presented by Cottrell and Rice (1980) and suggest that the direction of kinking is the direction that maximizes the mode I stress-intensity factor (k_I) and reduces the mode II stress-intensity factor (k_{II}) to zero at the tip of the increment of new crack.

According to Cottrell and Rice(1980), the stress-intensity factors, k_I and k_{II}, at the tip of the increment of new crack can be expressed in terms of stress-intensity factors for the parent cracks (K_I, K_{II}) as follows,

$$k_I = \frac{1}{4}K_I[3\cos(\frac{\theta}{2})+\cos(\frac{3\theta}{2})] - \frac{3}{4}K_{II}[\sin(\frac{\theta}{2})+\sin(\frac{3\theta}{2})] \quad ...(5.13)$$

$$k_{II} = \frac{1}{4}K_I[\sin(\frac{\theta}{2})+\sin(\frac{3\theta}{2})] + \frac{1}{4}K_{II}[\cos(\frac{\theta}{2})+3\cos(\frac{3\theta}{2})] \quad ...(5.14)$$

The orientation of the secondary fracture is determined by solving the equation (5.14), for $k_{II}=0$,

$$K_I[\sin(\frac{\theta}{2})+\sin(\frac{3\theta}{2})]+K_{II}[\cos(\frac{\theta}{2})+3\cos(\frac{3\theta}{2})]=0 \quad ...(5.15)$$

i.e.,

$$\frac{K_{II}}{K_I}=-\frac{\sin(\frac{\theta}{2})+\sin(\frac{3\theta}{2})}{\cos(\frac{\theta}{2})+3\cos(\frac{3\theta}{2})} \quad .....(5.16)$$

Solutions for stress-intensity factor K are tabulated by Paris and Sih (1965) and Tada et al (1973) for different conditions, which has the general form

$$K=\sigma\sqrt{l}f(geometry,loading) \quad .....(5.17)$$

where σ is a generalized loading stress, l is a characteristic length in the geometry of the body (usually the half length of crack, a) and the non-dimensional function f depends on the details of geometry and loading. For instance, for an isolated crack as shown in Figure 5.3, it yields

$$K_I=(\sigma_{11}^r-\sigma_{11}^c)\sqrt{a\pi}=\Delta\sigma_I\sqrt{a\pi} \quad .....(5.18)$$

$$K_{II}=(\sigma_{12}^{r}-\sigma_{12}^{c})\sqrt{a\pi}=\Delta\sigma_{II}\sqrt{a\pi}\text{.....(5.19)}$$

Therefore, substituting equations (5.18) and (5.19) into equation (5.16) yields the equation (5.12). Meanwhile, Cruikshank et al (1991) ignore the frictional strength (σ_{12}^{c}) of the crack and regard the fluid pressure (P) in the crack as the normal stress acting on the crack(σ_{11}^{c}). The fluid pressure is positive if compressive. Thus,

$$\Delta\sigma_{II}=\sigma_{12}^{r}\text{.....(5.20)}$$

$$\Delta\sigma_{I}=\sigma_{11}^{r}+P\text{.....(5.21)}$$

and

$$\frac{\sigma_{12}^{r}}{\sigma_{11}^{r}+P}=-\frac{\sin(\frac{\theta}{2})+\sin(\frac{3\theta}{2})}{\cos(\frac{\theta}{2})+3\cos(\frac{3\theta}{2})}\text{...(5.22)}$$

Therefore, they come to a conclusion that kink angle (θ) is defined by the ratio of the far-field stresses.

The solution to equation (5.12) is given in Table 5.1 for clockwise kink angle (negative). For counter-clockwise angle (positive), one needs simply multiply all

numbers in the table by -1. Surely the absolute value of the stress ratio is the same for the same $|\theta|$; the sign is merely a matter of definition for the mathematics. Table 5.1 is also diagrammatically presented in Figure 5.6.

5.2.3 Special Features of Kink Angle

There are two extremes for equation (5.12), which are worth particular attention.

First, when the effective shear stress becomes very large compared to the effective normal stress ($\Delta\sigma_{II} \gg \Delta\sigma_I$), the kink angle is approaching its upper limit of 70.5° according to equation (5.12). Pollard and Segall (1987) studied a case of pure mode II sliding on a crack, and found that an incipient crack would be expected to form at about 70.5° from the parent crack and propagate along a path which traces the trajectory of the maximum compressive stress.

Second, when the effective shear stress becomes very small compared to the effective normal stress ($\Delta\sigma_{II}/\Delta\sigma_I \ll 1$), equation (5.12) can be simplified as

$$\theta \sim -\frac{2\Delta\sigma_{II}}{\Delta\sigma_I} \sim -\frac{2K_{II}}{K_I} \quad \text{.....(5.23)}$$

TABLE 5.1 Relationship between Kink angles and Ratio of Effective Stresses

Kink Angle (°)	Ratio of Effective stresses ($\Delta\sigma_{II}/\Delta\sigma_{I}$)	Kink Angle (°)	Ratio of Effective stresses ($\Delta\sigma_{II}/\Delta\sigma_{I}$)
-1	0.0087	-36	0.4119
-2	0.0175	-37	0.4311
-3	0.0262	-38	0.4514
-4	0.0350	-39	0.4727
-5	0.0438	-40	0.4952
-6	0.0527	-41	0.5190
-7	0.0616	-42	0.5443
-8	0.0706	-43	0.5712
-9	0.0797	-44	0.5999
-10	0.0888	-45	0.6306
-11	0.0981	-46	0.6636
-12	0.1075	-47	0.6992
-13	0.1170	-48	0.7377
-14	0.1266	-49	0.7795
-15	0.1364	-50	0.8256
-16	0.1463	-51	0.8752
-17	0.1564	-52	0.9304
-18	0.1668	-53	0.9915
-19	0.1773	-54	1.0560
-20	0.1880	-55	1.1366
-21	0.1990	-56	1.2235
-22	0.2103	-57	1.3230
-23	0.2218	-58	1.4380
-24	0.2337	-59	1.5725
-25	0.2459	-60	1.7321
-26	0.2584	-61	1.9247
-27	0.2714	-62	2.1619
-28	0.2847	-63	2.4615
-29	0.2986	-64	2.8523
-30	0.3129	-65	3.3836
-31	0.3277	-66	4.1485
-32	0.3431	-67	5.3458
-33	0.3592	-68	7.4882
-34	0.3760	-69	12.4305
-35	0.3935	-70	36.0580

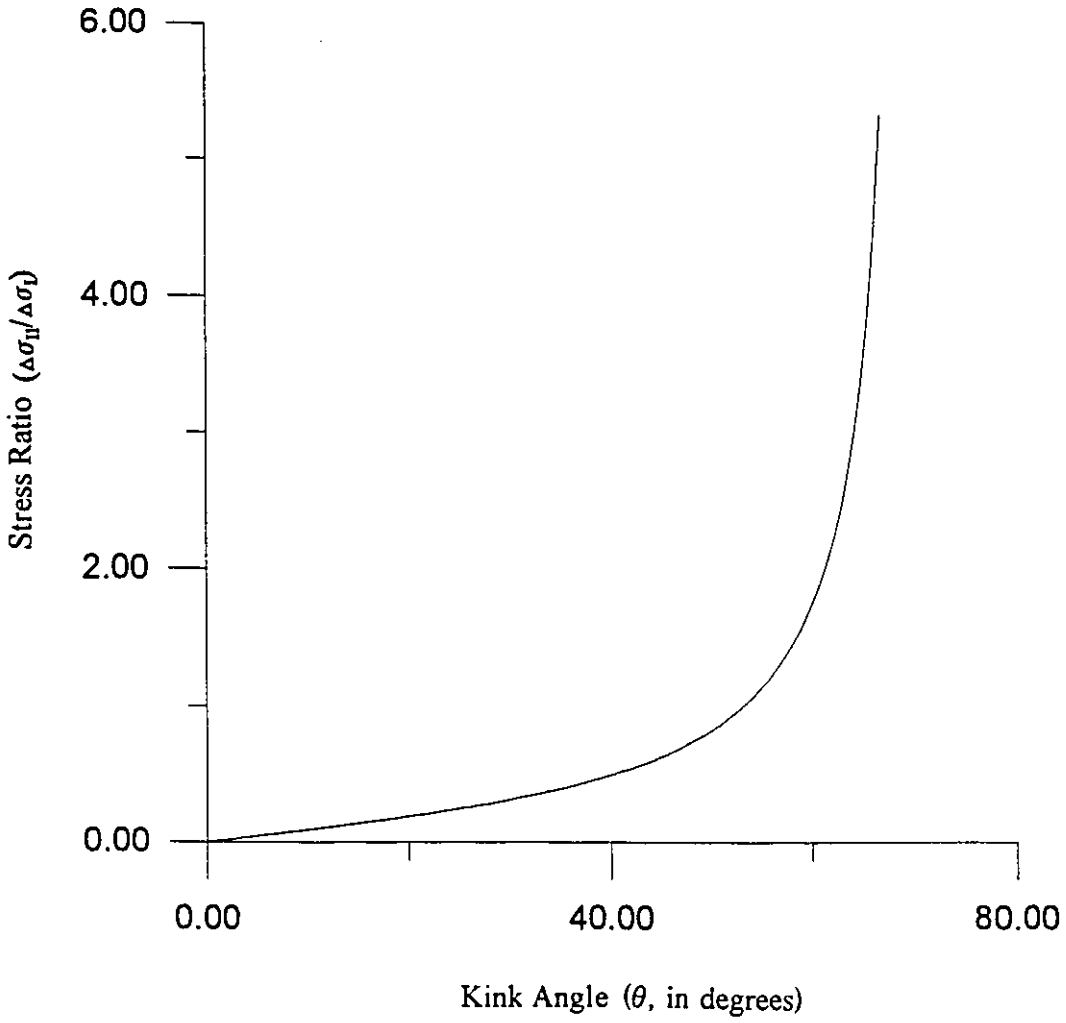

Figure 5.6, Relationship between kink angle and the ratio of effective stresses.

Meanwhile, from equation (5.13) and (5.14), we can obtain

$$k_I \sim K_I[1+\frac{3}{2}(\frac{K_{II}}{K_I})^2] \sim K_I[1+\frac{3}{8}\theta^2] \qquad (|\frac{K_{II}}{K_I}|<1,\ |\theta|<1).....(5.24)$$

It becomes clear that regardless of other elements of the stress state, if a straight crack begins to propagate when the loading is a combination of mode I and mode II, the resulting fracture will kink. The reason why the crack kinks if there is shear is revealed in equation (5.24): the mode I stress-intensity factor for the extension, k_I, is larger if the crack kinks($\theta \neq 0$) than it is if the crack remains straight and propagates in its own plane($\theta = 0$). If there is no shear, the kink angle, of course, will remain zero, which represents the pure mode I loading.

5.2.4 Kinematic Significance

The simplified equation (5.23) shows more clearly how the stress state is related to the angle of kinking.

According to equation (5.23), the direction of kinking is determined by the sense of shear (Figure 5.7). If the shear is dextral (positive), the kink angle is clockwise (negative); and if the shear is sinistral (negative), the kink angle is counter-clockwise (positive). Therefore, in turn, the sense of shear can be deduced if the direction of kinking is known, which can be easily distinguished as clockwise or counter-clockwise

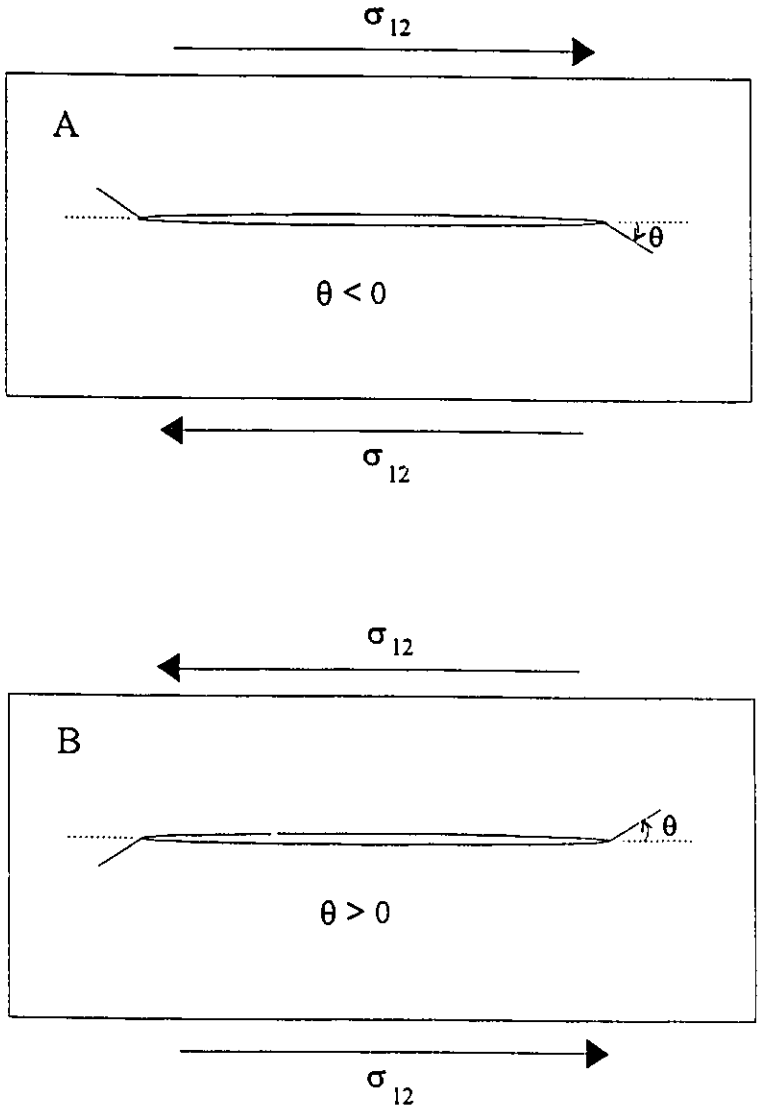

Figure 5.7, Kinematic significance of kink angles.
(A) For dextral shear, the kink angle is clockwise (negative);
(B) For sinistral shear, the kink angle is counter-clockwise (positive).

from the parent crack on outcrops. Thus, the kink angle presents a useful kinematic indicator to determine the shear sense on the parent fracture, in addition to determining the ratio of the driving stresses.

5.2.5 Relative Displacement

Kinking at a crack tip is due to the shear on the crack. The relative displacement on the crack walls due to the shear movement can be determined as follows.

Consider the crack surfaces (Figure 5.8) where

$$x_1 = 0^{\pm} \qquad \text{and} \qquad |x_2| \le a$$

the shear displacement on the crack surfaces is

$$u = \pm \Delta\sigma_{II} \frac{(1-\upsilon)}{\mu} (a^2 - x^{*2})^{\frac{1}{2}} - \Delta\sigma_{I} \frac{(1-2\upsilon)x^{*}}{2\mu} \qquad \text{.....(5.25)}$$

(Pollard and Segall, 1987) in which υ is Poisson's ratio, μ is shear modulus, and a is the half length of the crack.

The $\pm$ signs in the first term of equation (5.25) refer to the upper wall ($x_1 = 0^+$) and the lower wall ($x_1 = 0^-$) of the crack, respectively.

Practically, measurements along geological discontinuities give the relative displacement of linear markers or the separation of planar structures that have been cut by the crack and displaced to non-adjacent positions. The second term in equation (5.25)

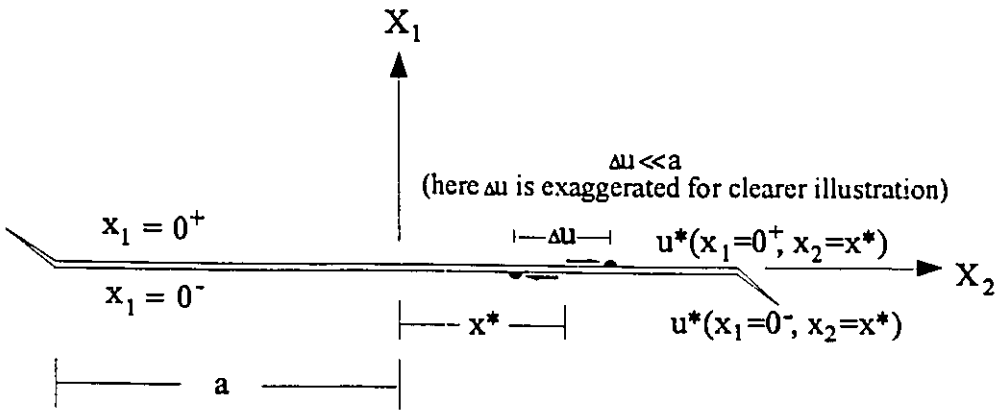

Figure 5.8, Illustration of displacement on fracture walls

does not contribute to the relative displacement Δu which is the difference between particular displacement components at adjacent points across the crack,

i.e.,

$$\Delta u = u(x_1=0^+,\ x_2=x^*) - u(x_1=0^-,\ x_2=x^*)$$

Therefore, the relative displacement across the crack is

$$\Delta u = 2\Delta\sigma_{II}\frac{(1-\upsilon)}{\mu}(a^2-x^{*2})^{\frac{1}{2}} \quad \text{.....(5.26)}$$

Obviously, the maximum value of relative displacement occurs at the crack centre, $x^*=0$, and the relative displacement falls to zero at $x^*=a$, thereby defining the crack periphery.

Equation (5.26) provides a method to estimate the effective stress $\Delta\sigma_{II}$ or the ratio of elastic moduli $(1-\upsilon)/\mu$ from field and laboratory data. The relative displacement Δu, the position (x^*) and the length (2a) of the crack may be measured if the outcrop is well exposed in the field. The elastic moduli may be measured in the laboratory or estimated from tests on similar rocks if the conditions of temperature and pressure are known. This leaves only the effective stress as unknown in the equation. Alternatively, if the effective stress can be estimated by some other independent means, the ratio of elastic moduli may be calculated.

It is necessary to point out that the effective stress is a combination of remote and crack stresses (σ_{ij}^r-σ_{ij}^c). Equation (5.26) does not indicate how to separate these two stresses once the effective stress has been determined. Some independent methods are

required. For example, in the case of a dry joint formed by tectonic tension (mode I), and later subjected to in-plane shear (mode II), the crack normal stress(σ_{11}^c) would be negligible. Similarly, knowledge of frictional strength of the material from rock mechanics experiments in a fault zone would put a bound on the crack shear stress.

5.3 Field Observation

5.3 1 Introduction

The Killarney area provides a good opportunity to study secondary fractures because of the excellent exposure of rocks. More than forty kinks have been identified and measured in the research area. In order to distinguish the different parts of the mapping area, some tentative names have been given to different outcrops, namely, Main Site, Lighthouse Shore, Middle Bay, South Bay and Killarney Village (Figure 5.9).

5.3.2 Distribution of Kinks

5.3.2.1 Main Site (MS)

There are two different groups of kinks in MS. Group one includes kinks whose parent fractures are either parallel to main faults or are actually the segments of main

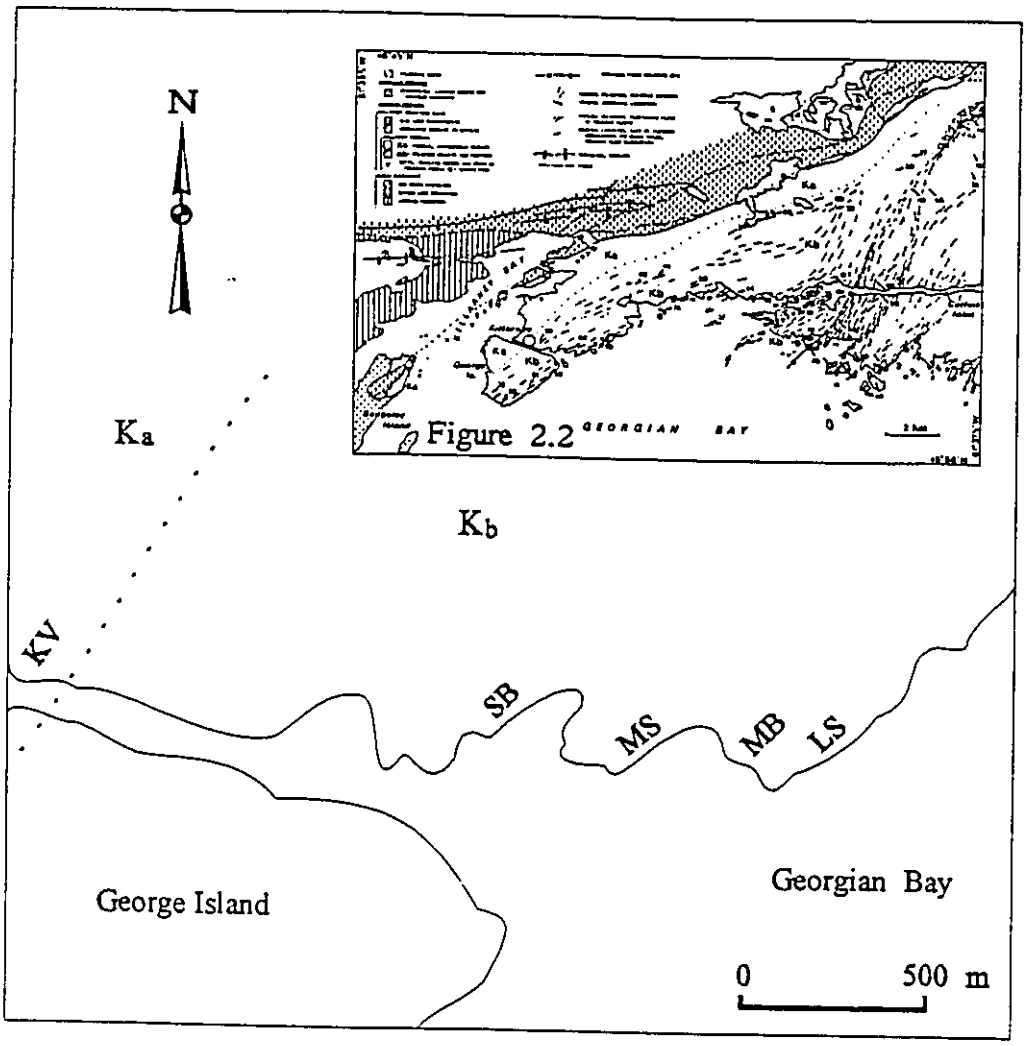

Figure 5.9, Illustration of different outcrops in the research area.
MS: Main Site; SB: South Bay; MB: Middle Bay
LS: Lighthouse Shore; KV: Killarney Village
K_a: Non-Foliated Area; K_b: Foliated Area

faults themselves. In contrast, group two includes kinks whose parent fractures are oblique to main faults, and are usually cut by main faults.

A typical example of kinks in group one is shown in Figure 5.1, whose parent fracture is actually a part of main fault #10. The attitude of the main fault is 240°/80° and the attitude of the secondary fracture is 280°/80°. The kink angle can be easily obtained from these attitudes of the main fault and the secondary fracture.

Figure 5.2 shows another kink whose parent fracture is another segment of fault #10. Here the attitude of the fault is 238°/80°, while the attitude of the secondary fracture is 272°/70°.

Figure 5.10 shows a kink whose parent fracture is parallel to main faults, but it is not a main fault itself, with total length of about 8 m. The attitudes of the parent fracture and the secondary fracture are 240°/80° and 90°/70°, respectively.

There are six kinks identified in group one. The common features of kinks in this group are that their parent fractures all have approximately the same attitude, about 240°/80°, and are relatively large, commonly with length of at least 8 metres.

Kinks in group two are usually smaller; parent fractures are usually less than 3 metres long, and have various attitudes.

Figure 5.11 shows several different kinks of group two. The attitudes of the parent fractures and the secondary fractures are presented in Table 5.2

Rose diagram (Figure 5.12) shows orientation distribution of the kinks in MS. Obviously, there is a trend that the parent fractures of kinks are parallel or subparallel

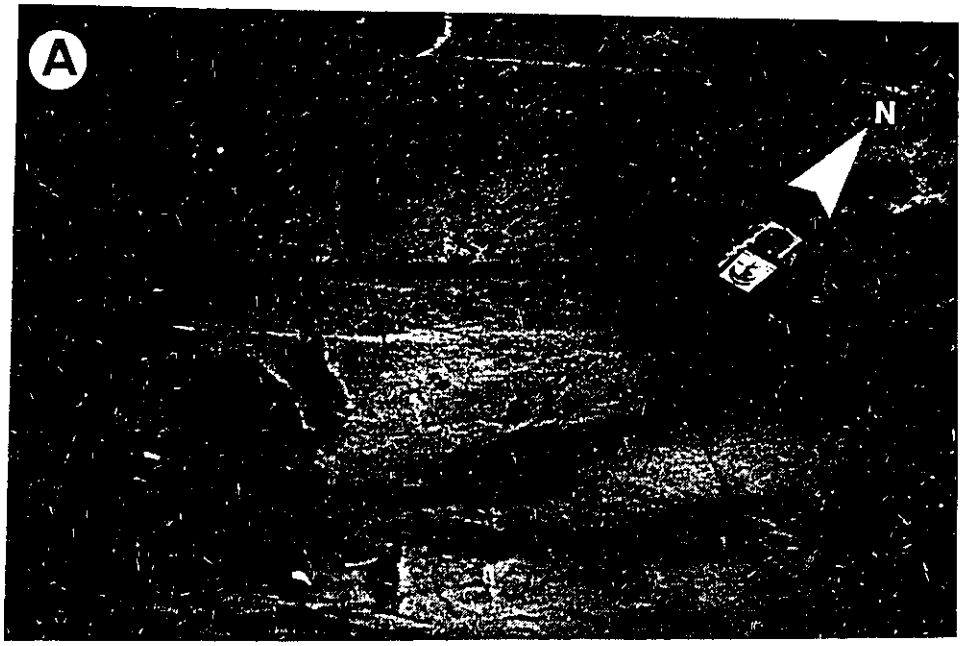

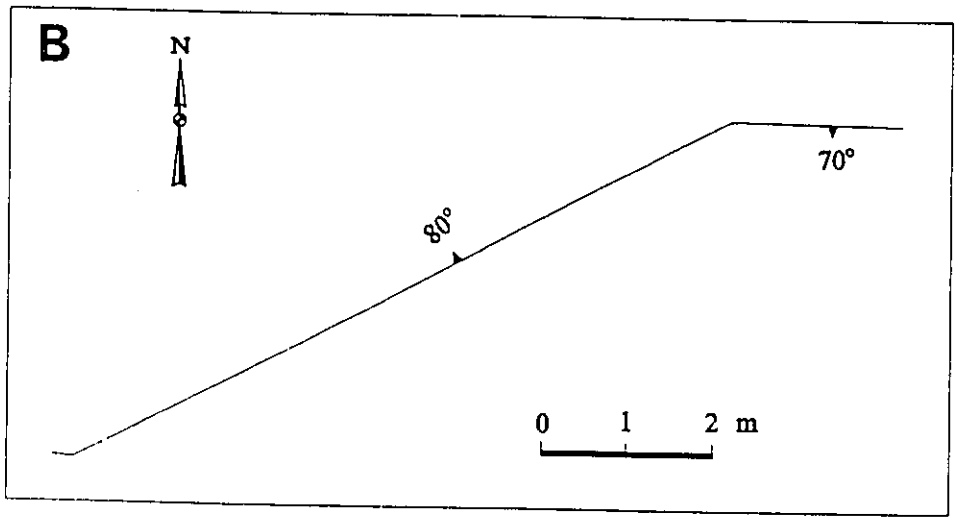

Figure 5.10, Showing a kink whose parent fracture parallel to main faults, but not a main fault itself in Main Site.
(A) Photo of the outcrop
(B) Outline of the kink

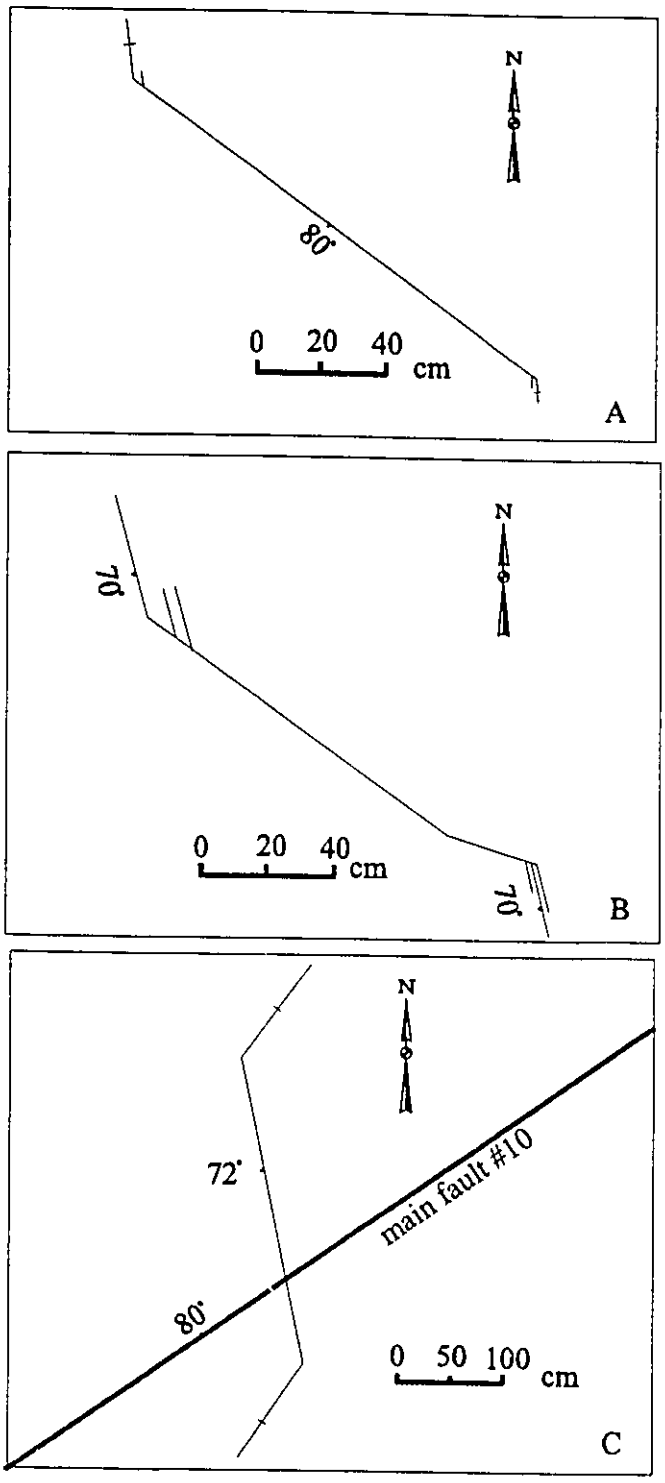

Figure 5.11, Illustration of kinks whose parent freactures are oblique to main faults in MS.

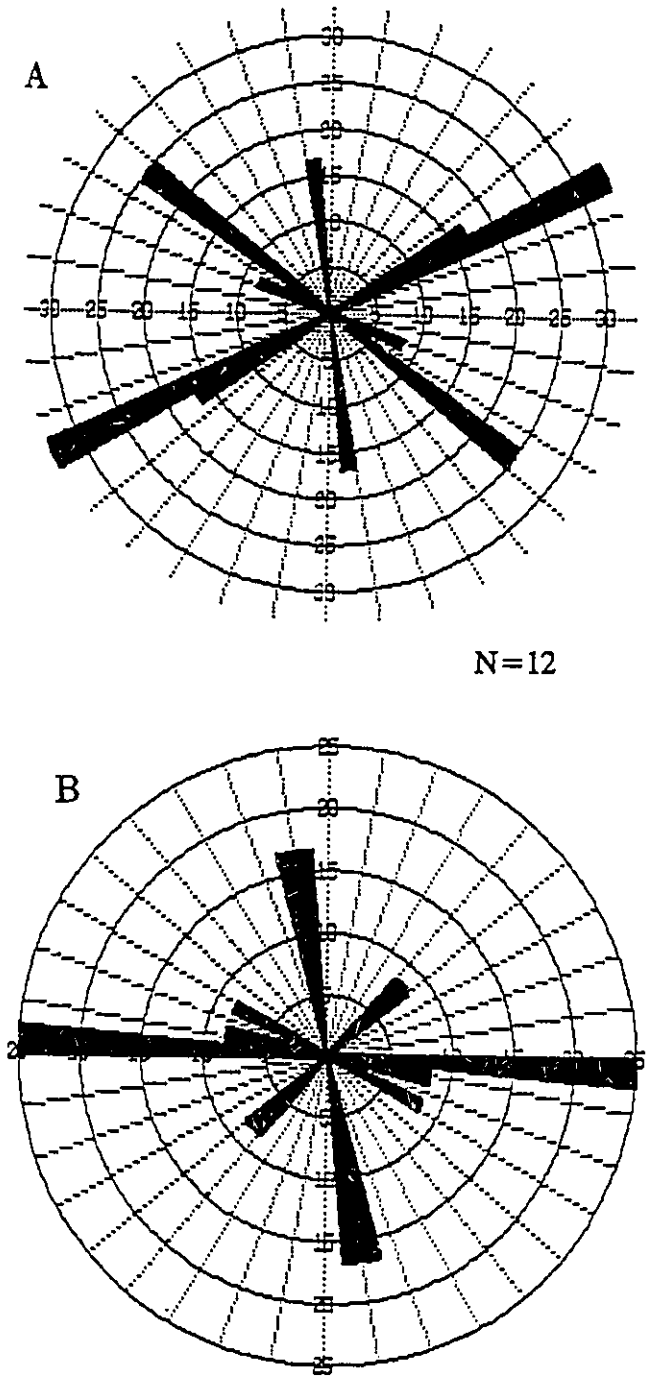

Figure 5.12, Orientation distribution of kinks in MS.
(A) Orientation of kink's parent fractures
(B) Orientation of kinks

TABLE 5.2, Attitudes of Kinks and Kink Angles in the Research Area

LOCATION	NO.	ATTITUDE OF PARENT FRACTURE	ATTITUDE OF SECONDARY FRACTUR	KINK ANGLE
MAIN SITE	1	240/80 (#10)	280/80	-40
	2	242/80 (#19)	295/80	-54
	3	240/80 (#08)	272/68	-33
	4	238/80 (#10)	272/70	-34
	5	237/80	275/90	-39
	6	240/80	090/70	-42
	7	170/72	220/90	-52
	8	170/72	220/90	-52
	9	125/80	170/80	-45
	10	125/80	170/90	-46
	11	125/90	165/70	-44
	12	110/90	165/70	-57
MIDDLE BAY	13	038/82	250/90	-33
	14	038/82	252/80	-38
	15	105/85	330/75	-49
	16	105/85	322/90	-37
	17	107/80	145/90	-39
	18	248/75	290/90	-44
	19	242/80	286/80	-43
	20	245/80	282/78	-36
SOUTH BAY	21	045/90	080/90	-35
	22	045/90	080/90	-35
	23	100/80	145/90	-46
	24	120/90	160/90	-40
	25	125/90	160/90	-35
	26	126/85	190/90	-64
	27	230/90	285/90	-55
	28	280/75	145/90	-47
	29	280/75	145/90	-47
	30	280/75	150/90	-52
	31	280/75	155/90	-56
	32	280/75	150/90	-52
	33	350/90	295/52	+63
LIGHTHOUSE SHORE	34	355/90	320/90	+35
	35	355/90	302/90	+53
	36	352/90	292/90	+60
KILLARNEY VILLAGE	37	036/90	090/90	-54
	38	100/90	046/90	-54
	39	065/90	115/90	-50
	40	055/90	115/90	-60
	41	058/90	120/90	-62
	42	120/90	150/90	-30
	43	130/90	160/90	-30

to main faults, striking 240°.

5.3.2.2 Lighthouse Shore and Middle Bay

Lighthouse Shore is located at about 250 m NE of the Main Site (MS). Middle Bay is a relatively small outcrop, located between Lighthouse Shore and the MS.

Structures in Lighthouse Shore and Middle Bay are not as systematic as those in MS. Deformation intensity decreases from MS, easterly towards Middle Bay and Lighthouse Shore, westerly towards South Bay.

There are not many kinks found along Lighthouse Shore. Figure 5.13 presents three kinks which are the only ones found there. The attitudes of these kinks are also shown in Table 5.2. The lengths of the parent fractures are about 2 metres. Two kinks occur at two ends of the same parent fracture. The other kink occurs at one tip of another parent fracture which is subparallel to the previous parent fracture and is only about 0.5 metre apart from the previous one.

There are eight kinks found in Middle Bay, some of which are shown in Figure 5.14. Middle Bay contacts MS immediately, so fracture patterns here are similar to those in MS, but not as strongly developed as in MS. As in MS, kinks here can be divided into two groups. Group one contains three kinks whose parent fractures are subparallel to main faults. Group two contains five kinks whose parent fractures are oblique to main faults. Again, the parent fractures subparallel to main faults are larger

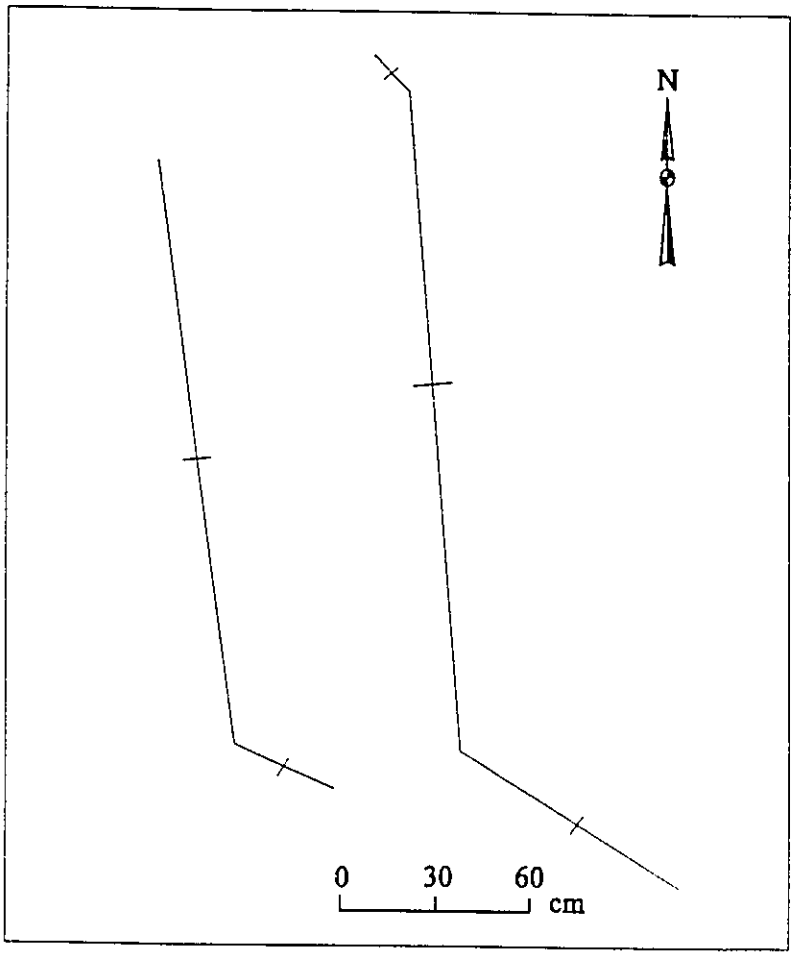

Figure 5.13, Kinks in Lighthouse Shore

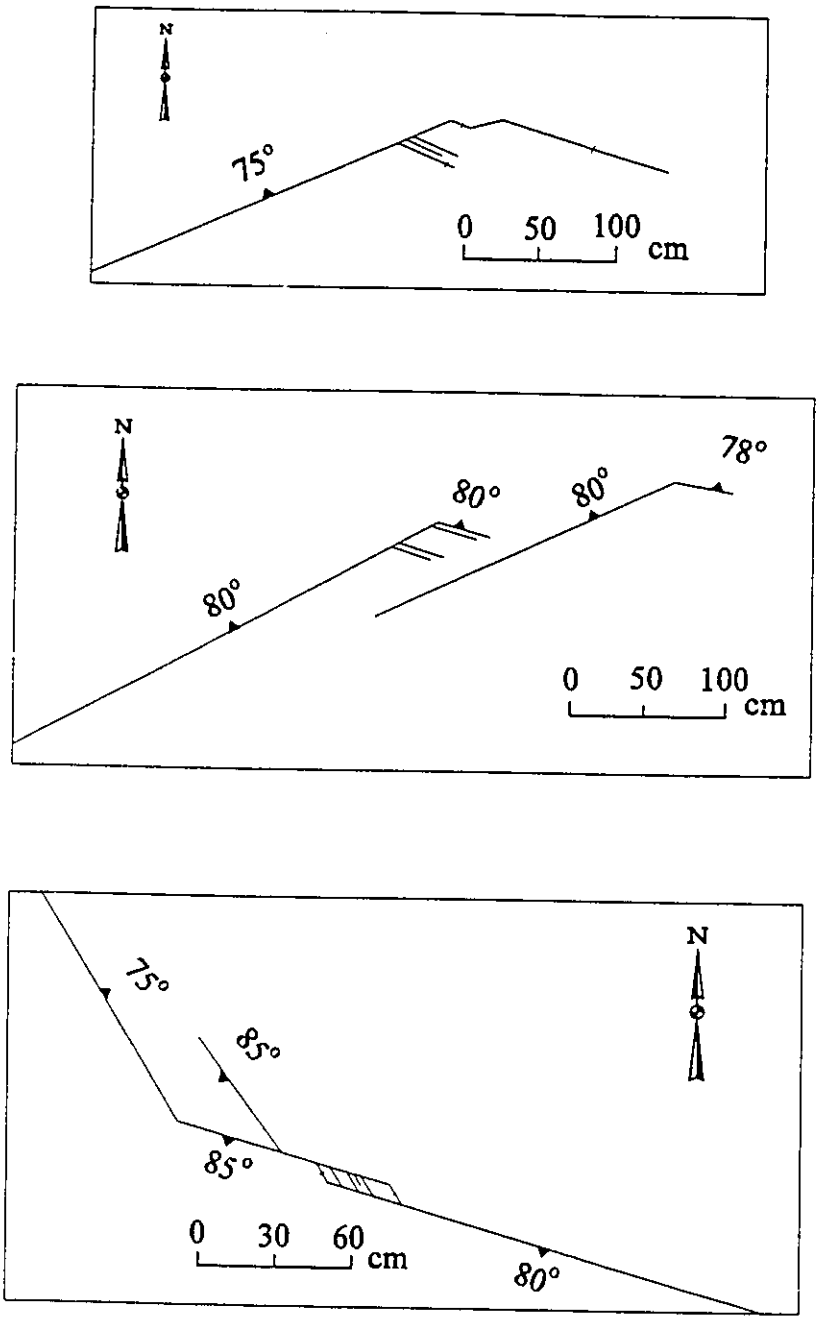

Figure 5.14, Kinks in Middle Bay

than those oblique to main faults.

The rose diagram (Figure 5.15) shows the orientation distribution of the parent fractures and the secondary fractures. Clearly, the preference of parallel or subparallel to main faults is not as strong as that in MS.

5.3.2.3 South Bay

South Bay is located at about 500 metres SW from MS. The trace of main faults is not very clear in the area, though we can still see a few faults which have similar orientation as main faults.

Kinks found in South Bay are all oblique to main faults. Thirteen kinks are identified, and some of them are shown in Figure 5.16.

Rose diagram (Figure 5.17) shows the orientation distribution of the parent fractures and the secondary fractures.

5.3.2.4 Killarney Village

Killarney village is about 2 km west of MS, and is situated in a relatively undeformed region (Ka in Figure 2.2). In order to compare fracture patterns between deformed and undeformed regions, several outcrops in Killarney village were investigated, and some kinks were found there as well.

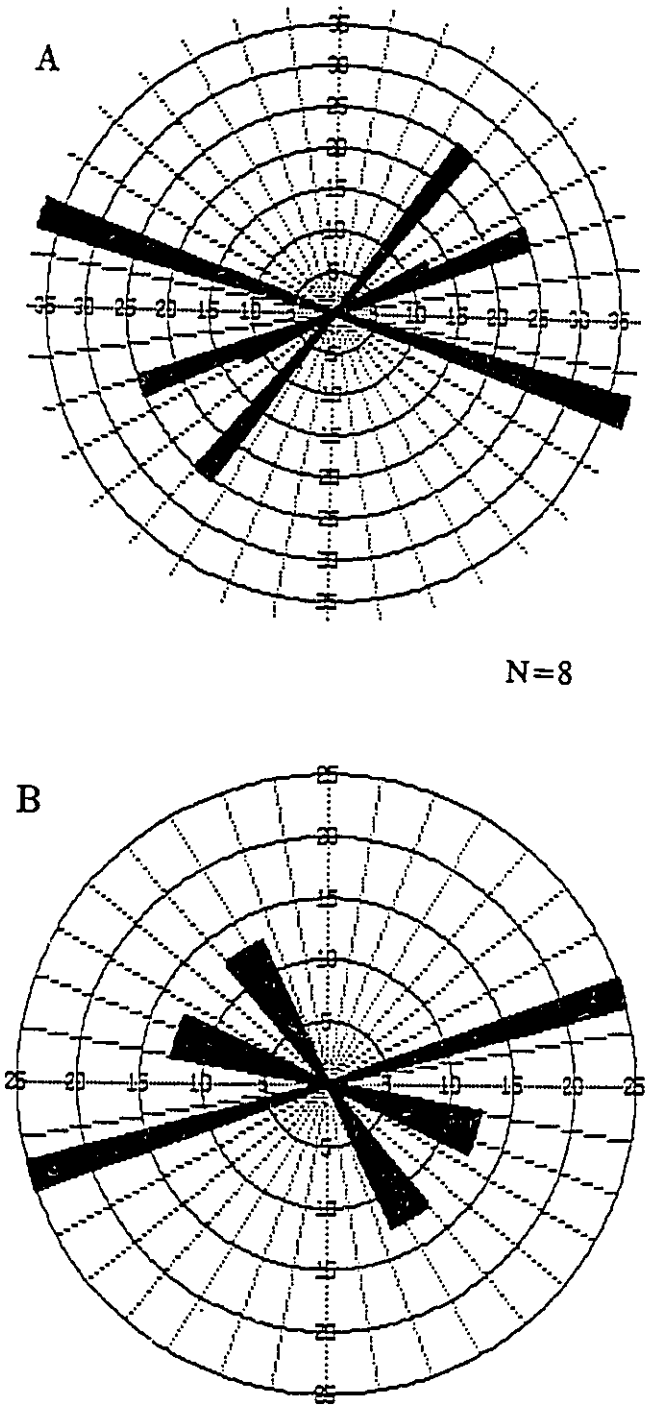

Figure 5.15, Orientation distribution of kinks in Middle Bay.
(A) Orientation of kink's parent fractures
(B) Orientation of kinks

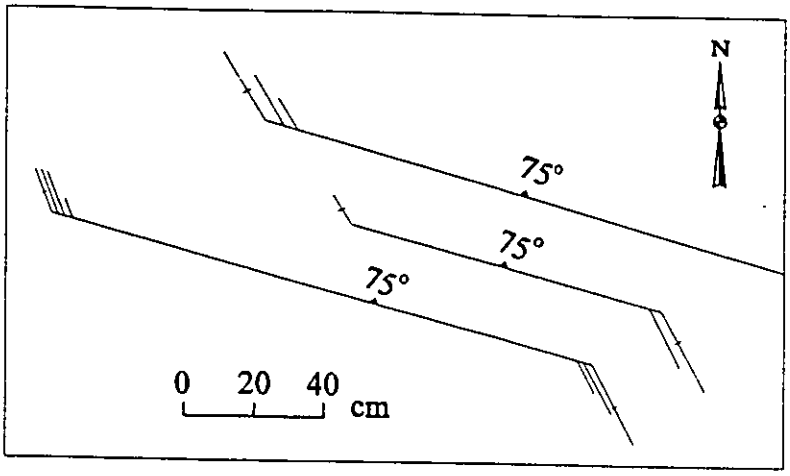

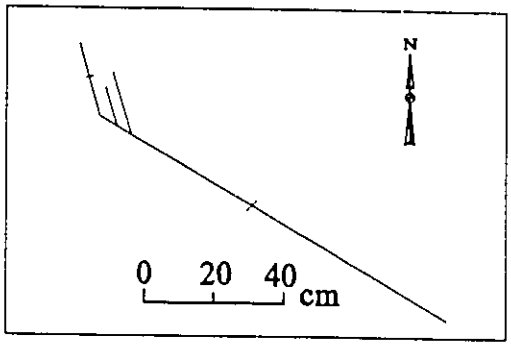

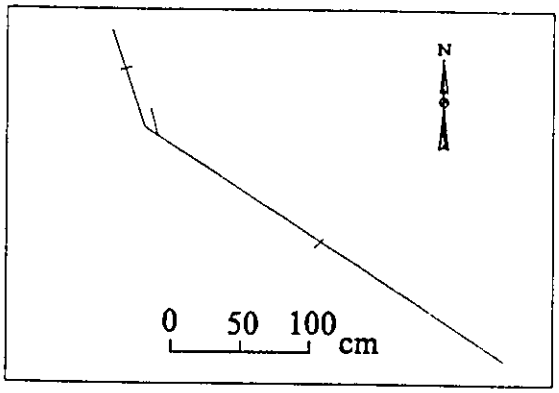

Figure 5.16, Kinks in South Bay

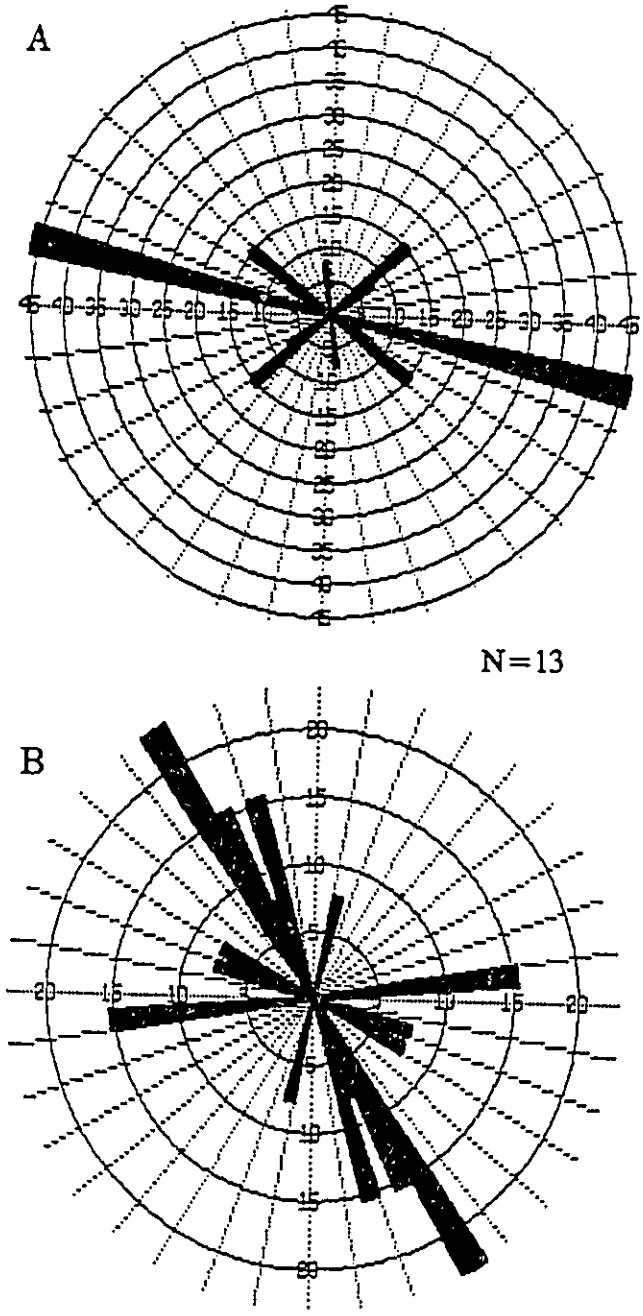

Figure 5.17, Orientation distribution of kinks in South Bay.
(A) Orientation of kink's parent fractures
(B) Orientation of kinks

Some common structural features in this region are: (1) there is no systematic fracture pattern; (2) fractures are very short, usually no more than 5 metres long; (3) fractures are almost all vertical.

Figure 5.18 shows some kinks found in the village.

Rose diagram (Figure 5.19) shows the orientation distribution of the kinks.

5.3.3 Range of Kink Angles

Table 5.2 shows all kink angles measured for this study. The range of kink angles is summarized in Figure 5.20(A-D) for different localities, and in Figure 5.21 for the whole region except Lighthouse Shore where the kink angles have different sign (positive) and Killarney Village where rocks are generally undeformed.

There are 32 clockwise kinks identified in the deformed region (including MS, MB, SB), the minimum absolute value of whose angles is 33°, maximum 64°, mean 45°, and standard deviation 8°.

Seven kinks found in Killarney Village are all clockwise. The minimum absolute value of the kink angles is 30°, maximum 62°, mean 50°, and standard deviation 13°. Apparently, the orientations of kinks in this undeformed region are less consistent and the standard deviation of kink angles is larger than those in deformed region.

There are only four counter-clockwise kinks identified in the region, three of which are found in Lighthouse Shore, and one in South Bay. The orientation of these

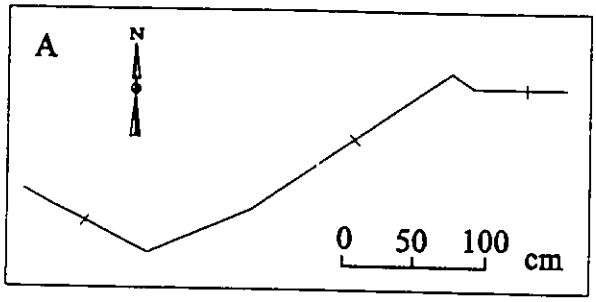

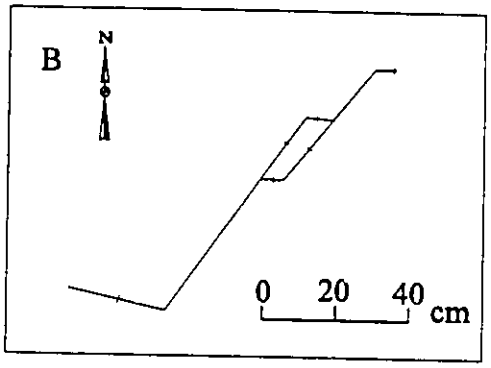

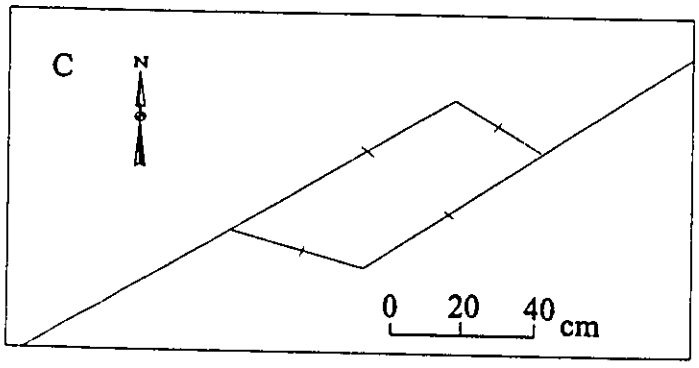

Figure 5.18, Kinks in Killarney Village.
(A) and (B) reveal a bridge structure each.

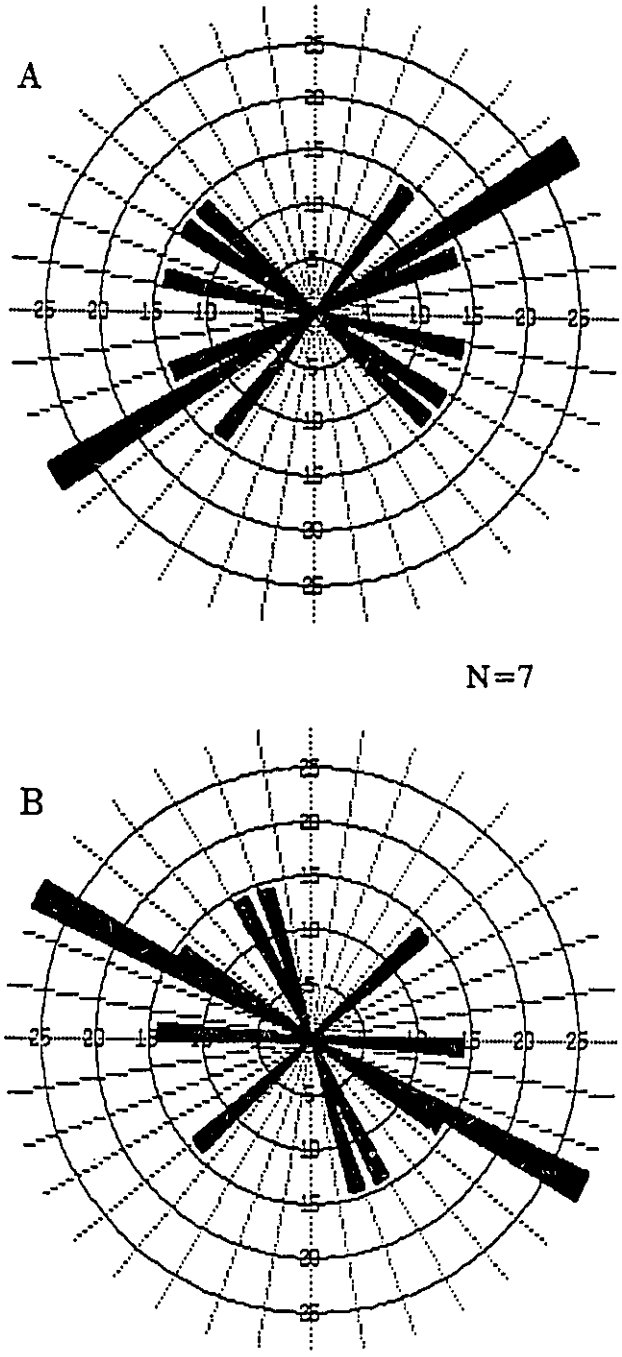

Figure 5.19, Orientation distribution of kinks in Killarney village.
(A) Orientation of kink's parent fractures
(B) Orientation of kinks

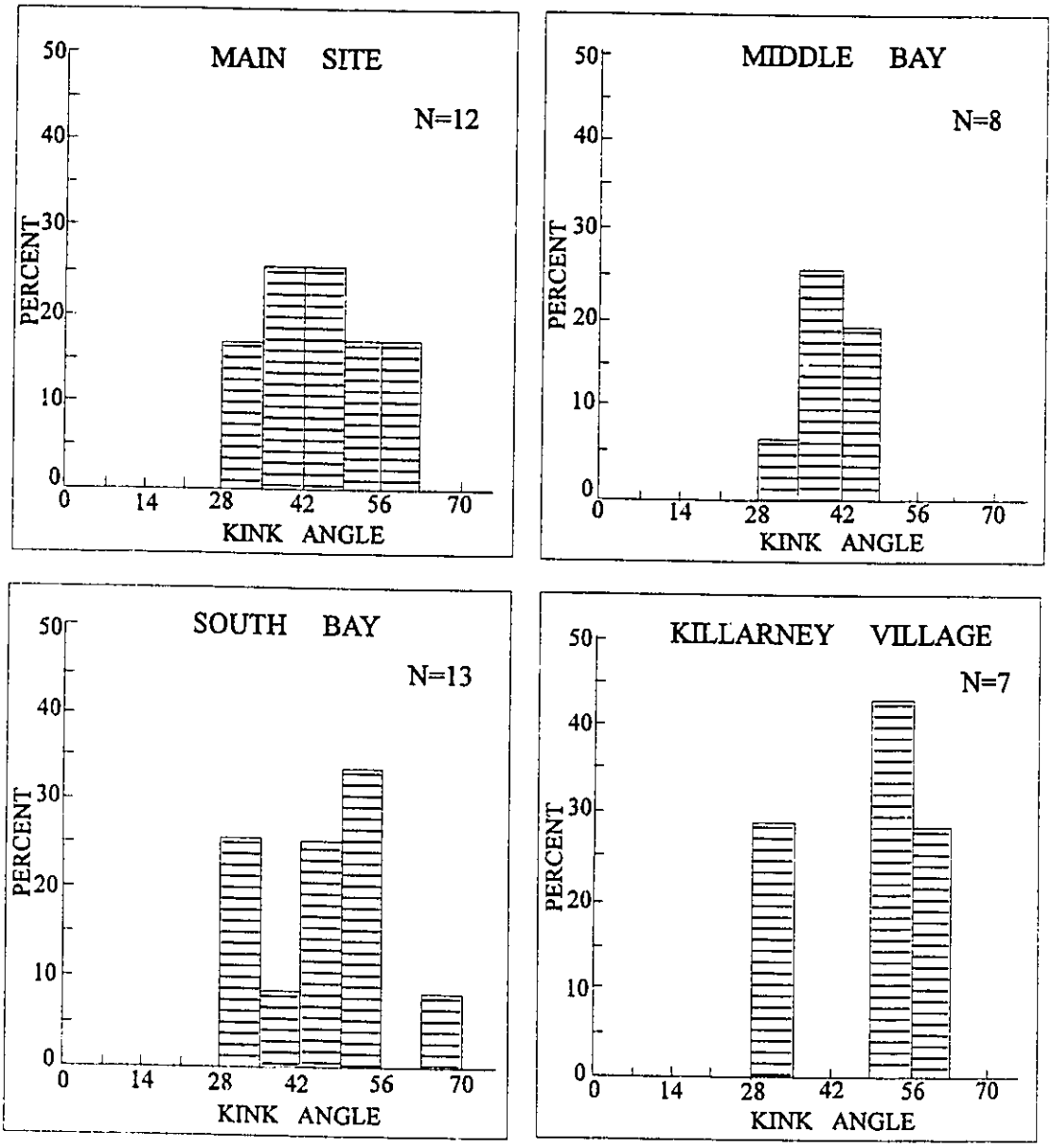

Figure 5.20, Distribution of kink angles (in degrees) of individual localities.

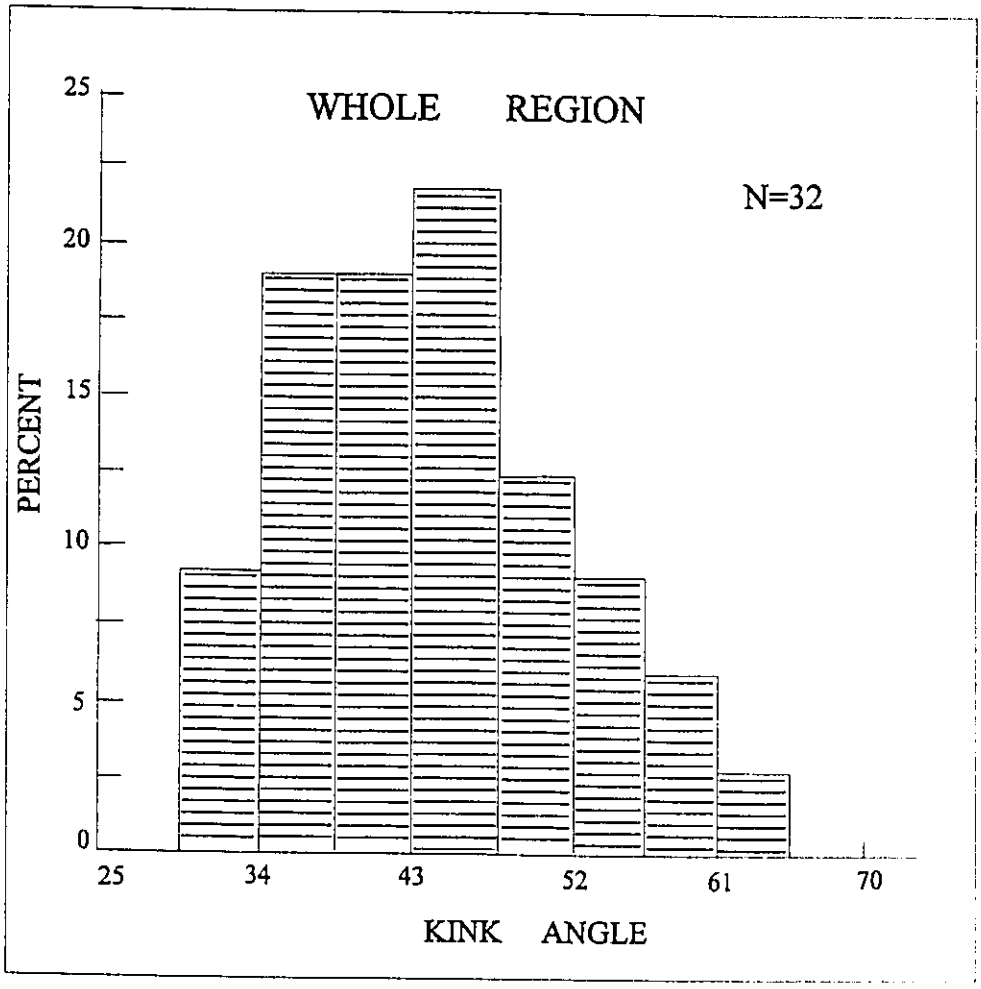

Figure 5.21, Distribution of kink angles (in degrees) of the whole region.

kinks are very consistent (Figure 5.22), and the value of kink angles is relative bigger.

5.3.4 Shear Sense and the Ratio of Effective Stresses

As discussed in previous paragraphs, kinks provide a useful tool to determine the shear sense and the ratio of effective stresses.

There are only 4 kinks which have counter-clockwise kink angle, indicating sinistral shear sense along their parent fractures, in the region.

All other kinks identified in the region, 32 in deformed area and 7 in undeformed area, have clockwise kink angles, indicating a dextral shear sense on their parent fractures. This confirms the general scenario that the region is cut by a set of parallel faults which have dextral sense of shear determined by other independent means (see Chapter 3 & 4).

The ratio of the effective stresses responsible for the formation of kinks is determined by the kink angle,

$$\frac{\Delta\sigma_{II}}{\Delta\sigma_{I}} = -\frac{\sin(\frac{\theta}{2})+\sin(\frac{3\theta}{2})}{\cos(\frac{\theta}{2})+3\cos(\frac{3\theta}{2})} \quad \text{.....(5.27)}$$

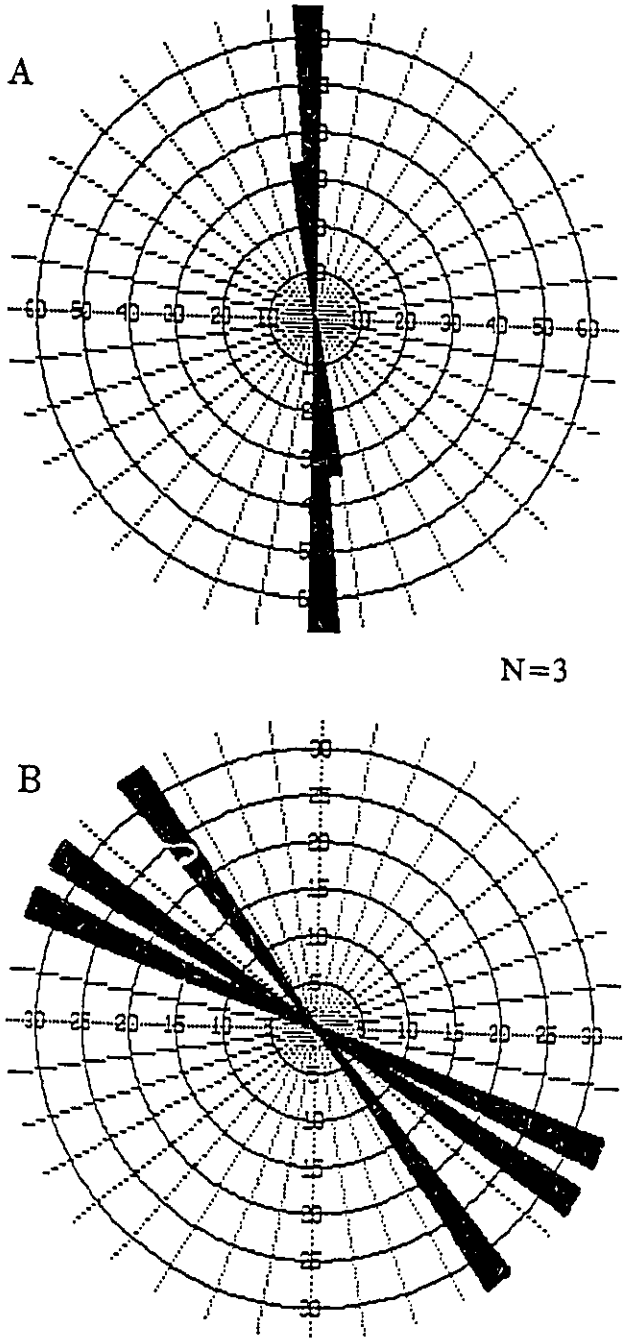

Figure 5.22, Orientation distribution of kinks in Lighthouse Shore.
(A) Orientation of kink's parent fractures
(B) Orientation of kinks

where θ is the kink angle, $\Delta\sigma_{II}$ is the effective mode II loading (shear stress) and $\Delta\sigma_{I}$ is the effective mode I loading (normal stress).

By making use of Table 5.1 and Table 5.2, the stress ratio can be estimated for the different localities in the region (Table 5.3).

It is shown in Table 5.3 that the effective shear stress was roughly smaller than the effective normal stress in deformed region, and the effective shear stress was roughly equal to the effective normal stress in undeformed region while both shear stress and normal stress in undeformed region were smaller than those in deformed region, although there were a few other factors that might affect the deformation grade.

5.4 Conclusions

From the theoretical and practical analysis of one type of secondary fractures, namely kinks, the following conclusions can be drawn,

(a) if a straight fracture, subjected to mode I and mode II loading, begins to propagate, the resulting fracture will kink;

(b) the kink angle is a reliable kinematic indicator: a clockwise kink angle indicates dextral sense of shear on the parent fracture while a counter-clockwise kink angle indicates sinistral sense of shear;

(c) the value of kink angle is determined by the ratio of the effective shear stress and the effective normal stress;

TABLE 5.3 Kink Angles and Stress Ratio in the Research Area

Location	NO.	Kink Angle (0)	Stress Ratio
MAIN SITE	1	-40	0.5
	2	-54	1.1
	3	-33	0.4
	4	-42	0.5
	5	-34	0.4
	6	-39	0.5
	7	-52	0.9
	8	-52	0.9
	9	-45	0.6
	10	-46	0.7
	11	-44	0.6
	12	-57	1.3
	MEAN	-45	0.7
	S.D.	8	0.3
MIDDLE BAY	13	-33	0.4
	14	-38	0.5
	15	-49	0.8
	16	-37	0.4
	17	-39	0.5
	18	-44	0.6
	19	-43	0.6
	20	-36	0.4
	MEAN	-40	0.5
	S.D.	5	0.1
SOUTH BAY	21	-35	0.4
	22	-35	0.4
	23	-46	0.7
	24	-40	0.5
	25	-35	0.4
	26	-64	2.9
	27	-55	1.1
	28	-47	0.7
	29	-47	0.7
	30	-52	0.9
	31	-56	1.2
	32	-52	0.9
	MEAN	-47	0.9
	S.D.	9	0.7
LIGHTHOUSE SHORE	33	35	-0.4
	34	53	-1.0
	35	60	-1.7
	MEAN	49	-1.0
	S.D.	13	0.7
KILLARNEY VILLAGE	36	-54	1.1
	37	-54	1.1
	38	-50	0.8
	39	-60	1.7
	40	-62	2.2
	41	-30	0.3
	42	-30	0.3
	MEAN	-50	1.1
	S.D.	13	0.7

(Negative value of kink angles refers to clockwise;
negative value of the stress ratio refers to sinistral shear sense.)

(d) the kink angles in the research area suggest most parent fractures have had dextral sense of shear;

(e) the effective shear stress was generally smaller than the effective normal stress in the deformed region during the formation of kinks.

CHAPTER 6 WEDGES

6.1 Introduction

In the last decade, considerable work has been done to understand the mechanics of accretionary thrust wedges (e.g. Dahlem, 1984; Platt, 1986; Yin, 1986, 1993). These studies provide valuable insights into the relationships among stress distribution, boundary conditions, wedge geometry and rock rheology for the development of thrust wedges. A typical thrust wedge is a wedge-shaped block bounded by a basal thrust at the bottom of the block with a stress-free upper surface. Both elastic models and plastic models have been introduced to investigate the initiation of faults within thrust wedges (Yin, 1993; Stockmal, 1983). It is a consensus in both models that the geometric pattern of faults corresponds to slip lines in thrust wedges.

Many wedge structures exist in the research area. A wedge structure here, however, is bounded by two fractures, within which secondary fractures have been intensively developed while the country rocks are relatively clean, and the fracture patterns inside and outside of wedges are different. Usually, the closer to the vertex of a wedge, the more intensely the minor fractures were developed. Mechanically, the major differences between wedges here and the previously studied thrust wedges are boundary conditions and body forces. Because a thrust wedge is defined in a cross-

section, body forces due to gravity in the wedge must be taken into consideration when trying to develop a two-dimensional mechanical model for the formation of the faults within the wedge (Yin, 1993). A wedge in the research area is defined in an approximately horizontal plane (ground surface), so the body force due to gravity can be ignored as we try to establish a two-dimensional mechanical model to evaluate the stress distribution within the wedge.

In this chapter, the wedges in the research area are examined, and then an elastic model is developed to account for the initiation of secondary fractures within them; further, the possible process of their formation is discussed. The basis for an elastic model is that the elastic deformation, although small, is important for the initiation of Coulomb-type fractures (Jaeger and Cook, 1976). Coulomb-type fracturing, in turn, has long been considered to be the mechanism for initiation of natural fractures (e.g. Anderson, 1942; Yin, 1993). Furthermore, wedges observed in the research area are all brittly-deformed structures.

6.2 Field Observations

6.2.1 General Feature of Wedges

6.2.1.1 Wedge Boundaries

As observed in the field, a typical wedge is generally bounded by a joint and a fault which truncates the joint (Figure 6.1). The fault is usually one of the main faults or parallel to them, revealing dextral shear movement.

6.2.1.2 Wedge Angle

The wedge angle, designated α, is defined as the acute angle on the ground surface between two non-parallel fractures, one of which usually truncates the other (Figure 6.1). The magnitude of wedge angles observed in the field ranges from 10° to 75°, though most of them are less than 45°.

6.2.1.3 Wedge Length

The wedge length is another wedge parameter which, together with the wedge angle, determines the size of a wedge, and is the distance measured on one of wedge's boundaries-the truncating fault from the wedge apex to where the secondary fractures are barely developed beyond it (Figure 6.1).

6.2.1.4 Secondary Fractures within Wedges

Fracture patterns are sharply different between inside and outside of wedges

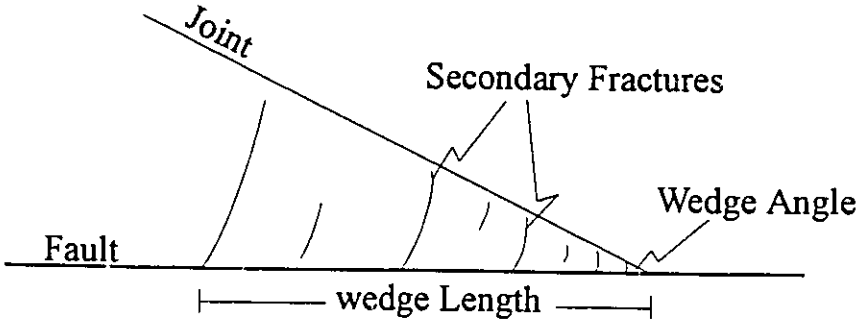

Figure 6.1, Showing the configuration of a wedge

throughout the field observations. The fracture pattern inside a wedge is much more consistent than that outside a wedge. From field observations, secondary fractures inside wedges are inferred to be generally tensile fractures and are gently curved in most cases. The spacing of fractures usually decreases toward the wedge apex.

6.2.2 Examples

6.2.2.1 Small Wedge Angles (<45°)

Figure 6.2 shows a pair of adjacent wedges, having wedge angles of about 20°. The secondary fractures were more intensely developed in the lower wedge than in the upper one. The tensile fractures within wedges are gently curved. The tape in the photograph is 20 cm long.

Figure 6.3 shows a wedge with a wedge angle of about 22°. The boundary beside the compass is one of the main faults #14z, and it truncates the other boundary. The secondary fractures, though not very intensely developed, are distinct from those outside the wedge, and also show gentle curves toward the wedge apex. The wedge length is about 2 m.

Figure 6.4 shows another pair of adjacent wedges. The common boundary of the wedges is a main fault, striking 240° and dipping 80° NW. The other boundary of the wedges is a joint which was cut and displaced by the main fault. The process of cutting

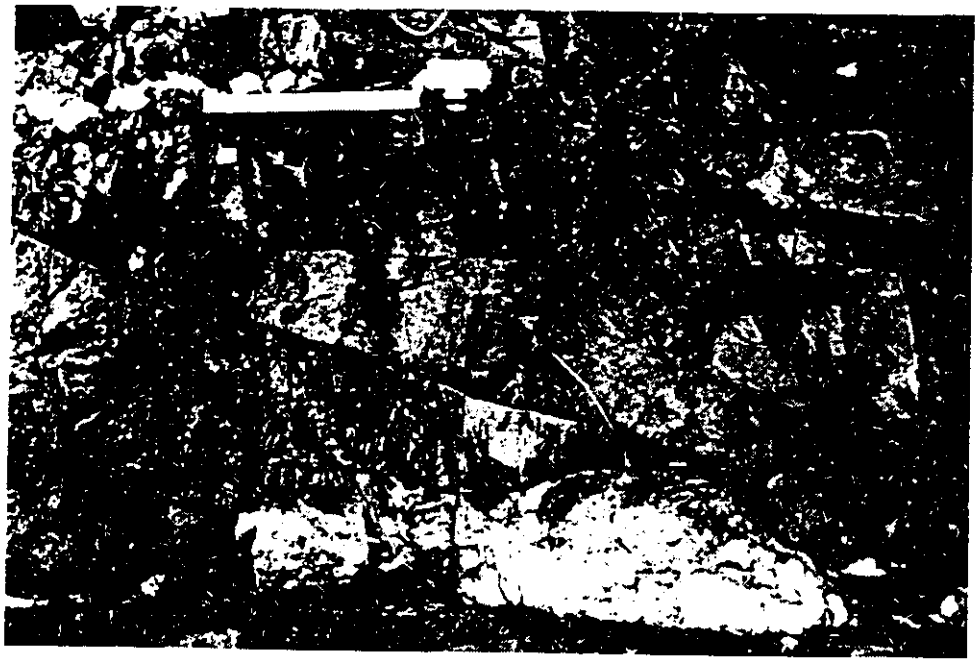

Figure 6.2, Examples of wedges with wedge angle of about 20°.
(The tape measurement is 20 cm)

Figure 6.3, Example of a wedge with wedge angle of about 22°.
(The compass is about 15 cm long)

Figure 6.4, Example of wedges with wedge angle of about 35°.
(The geological hammer is about 35 cm long)

Figure 6.5, Example of a wedge with wedge angle of about 40°.
(The tape measurement is 50 cm)

and displacing the existing joint was probably the cause of the formation of wedges, which is the mechanical basis for selecting the boundary conditions when we set up an elastic model to evaluate the stress distribution within wedges in next paragraph. The wedge angles here are about 35°, and the wedge length is about 1.5 m for the one on left and 1 m for the one on right. The secondary fractures within these wedges are gently curved and the convex of the curves is toward the apex of their own wedge.

Figure 6.5 shows a wedge, with a wedge angle of about 40°. The boundary beside the tape is the main fault #10, with right-handed movement. The wedge length is about 1.5 m. The secondary fractures inside the wedge are gently curved, and the convex of the curves is toward the wedge apex as revealed by the fractures near the apex.

6.2.2.2 Intermediate Wedge Angles ($\sim 45°$)

Figure 6.6 and Figure 6.7 show two different wedges with one thing in common, a wedge angle of approximately 45°. The secondary fracture patterns are similar within these wedges, but are quite different from those described previously. There are two sets of secondary fractures, though not evenly developed, in each wedge, and they are conjugate shear fractures rather than tensile fractures.

6.2.2.3 Large Wedge Angles ($> 45°$)

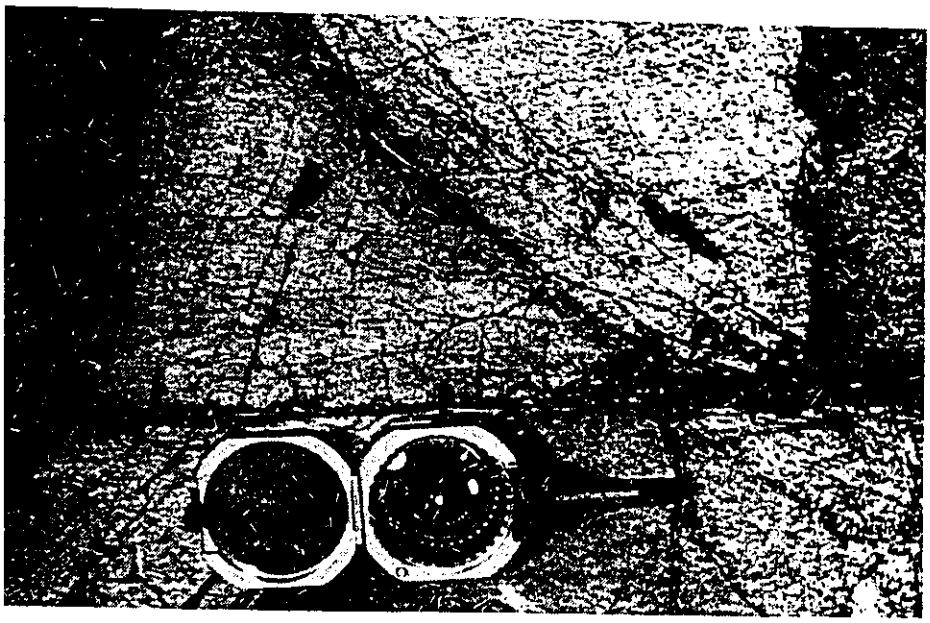

Figure 6.6, Example of a wedge with wedge angle of about 45°.
(The compass is about 15 cm long)

Figure 6.7, Example of a wedge with wedge angle of about 45°.
(The tape measurement is 20 cm)

Wedges with wedge angle larger than 45° are rare in the research area. Figure 6.8c shows one example of a wedge with wedge angle of about 65°. The secondary fractures inside these wedges are curved tensile fractures, but the convex of the curves is toward the wedge rear unlike that inside wedges with small wedge angles.

Figure 6.8 also shows some other examples of wedges observed in the field. There is a general feature worth to point out, that is, the convex of the curved tensile fractures in wedges with a wedge angle less than 45° is toward the wedge apex, whereas the convex is toward the wedge rear if the wedge angle is more than 45°.

6.3 Theoretical Analysis

6.3.1 Elastic Model

Clearly, the wedge structures are not uncommon, and they all show similar features. Thus, some questions arise: what is the mechanism of their formation? can the fracture patterns developed within these wedges be explained in terms of such parameters as boundary conditions and material properties? To explore solutions to these questions, an elastic wedge model is set up to evaluate the stress distributions within wedges in this section.

To simplify the problem, two assumptions are made: (1) the two fractures bounding the wedge are vertical; and (2) the stress, strain and the wedge geometry do

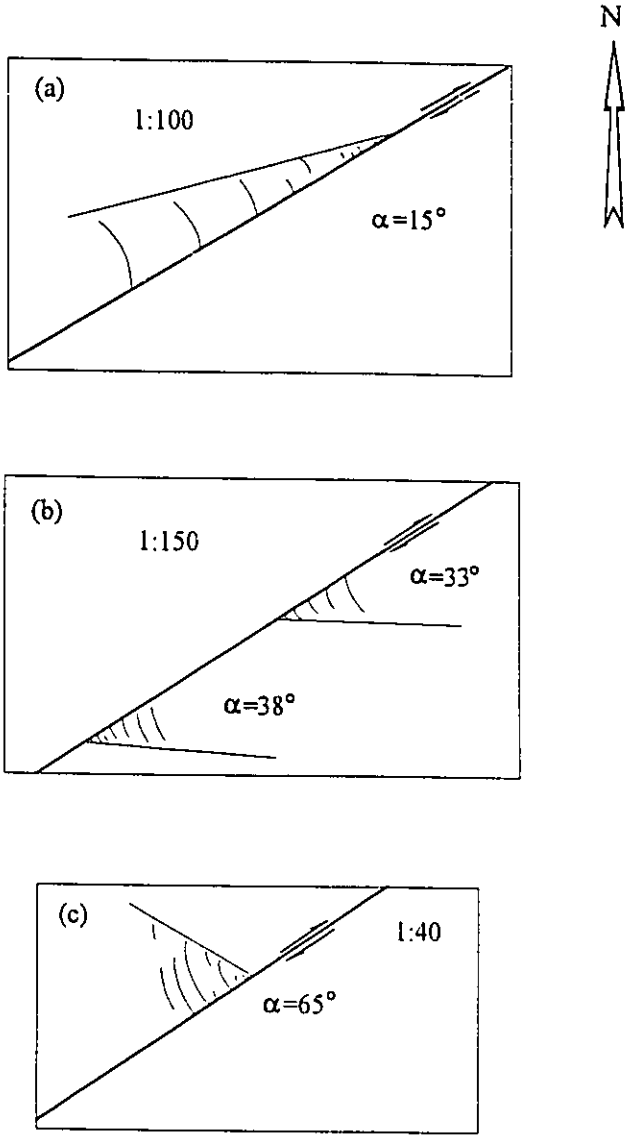

Figure 6.8, Examples of some other wedges observed in the research area

not change along the direction perpendicular to the ground surface (plane stress, plane strain). The first assumption is a good approximation to the field observations since most bounding fractures in the area dip at about 80° or more. The second assumption is reasonable if the bounding fractures are vertical and the wedges were not deeply buried.

Based on the above assumptions, the problem can be treated as two-dimensional. Therefore, the framework of reference for the wedge is chosen as shown in Figure 6.9. The wedge is regarded as lying on the ground surface, and the x axis is set to parallel to one of the wedge's boundary. **The sign convention used for the stress analysis below follows that of engineering usage, i.e., the stress is positive if tensile.**

6.3.2 Boundary Conditions

From the field observations, wedges are found to be bounded by a joint and a fault which truncated the joint. Therefore, if the coordinates are chosen so that the x axis is parallel to the fault and points to the apex of the wedge as shown in Figure 6.9, the two boundaries can be expressed as

(1) the fault boundary: $y=0$

(2) the joint boundary: $y=(x_o-x)\tan\alpha$

where α is the wedge angle , x_o is the wedge length.

The joints bounding the wedges are found to be small (no more than 3 metres long), dry (no fillings inside) and non-systematic, suggesting that they are of superficial

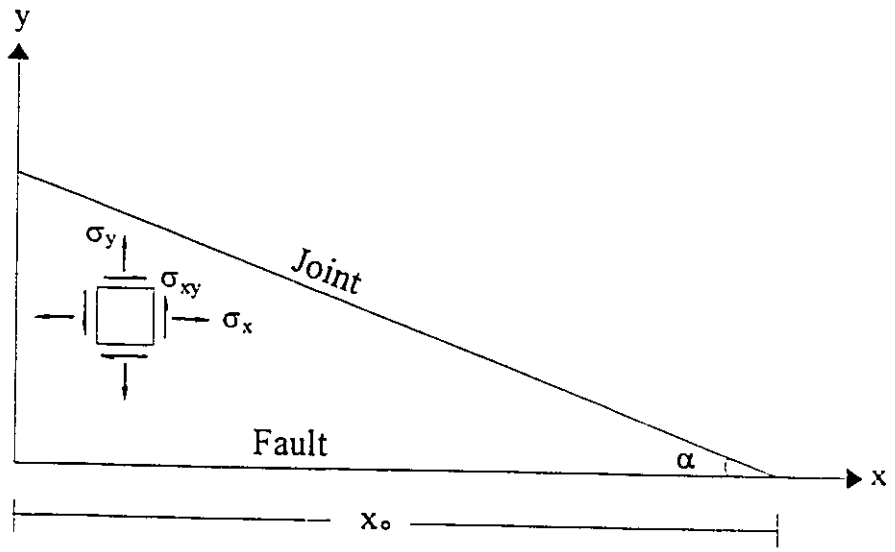

Figure 6.9, The framework of reference chosen for the stress analysis

origin (Dunne and Hancock, 1994). Therefore, the boundary condition along the joint is assumed to be stress free, i.e.,

$$\sigma_b=\tau_b=0 \qquad \text{.....(6.1)}$$

in which σ_b and τ_b are the normal and shear stress components across the wedge boundary where $y=(x_o-x)\tan\alpha$.

σ_b and τ_b are related to stress components σ_x, σ_y and σ_{xy} along the boundary by

$$\sigma_b=l^2\sigma_x+m^2\sigma_y+2lm\sigma_{xy} \qquad \text{.....(6.2)}$$

$$\tau_b=(l^2-m^2)\sigma_{xy}+lm(\sigma_y-\sigma_x) \qquad \text{.....(6.3)}$$

(Jaeger and Cook, 1976; Yin, 1993) where $l=\sin\alpha$ and $m=\cos\alpha$; σ_x, σ_y and σ_{xy} are normal and shear stress components in the x and y directions.

The boundary condition along the fault is assumed to follow Amonton's law (Jaeger and Cook, 1976)

$$\sigma_{xy}(x,0)=-\mu(1-\lambda)\sigma_y(x,0) \qquad \text{.....(6.4)}$$

where μ and λ are the coefficient of friction and the pore fluid pressure ratio (the ratio of the pore fluid and lithostatic pressures) along the fault, respectively.

6.3.3 Stress Distribution in Wedges

6.3.3.1 Theory

Neglecting body forces, the stress equilibrium equations for a plane stress

condition, which must be satisfied throughout the wedge, are

$$\frac{\partial \sigma_x}{\partial x}+\frac{\partial \sigma_{xy}}{\partial y}=0 \quad \text{.....(6.5)}$$

$$\frac{\partial \sigma_{xy}}{\partial x}+\frac{\partial \sigma_y}{\partial y}=0 \quad \text{.....(6.6)}$$

The stress-strain relations are expressed by Hooke's law,

$$\varepsilon_x=\frac{1}{E}(\sigma_x-\upsilon\sigma_y) \quad \text{.....(6.7)}$$

$$\varepsilon_y=\frac{1}{E}(\sigma_y-\upsilon\sigma_x) \quad \text{.....(6.8)}$$

$$\varepsilon_{xy}=\frac{2(1+\upsilon)}{E}\sigma_{xy} \qquad or \qquad \varepsilon_{xy}=\frac{1}{G}\sigma_{xy} \quad \text{.....(6.9)}$$

in which ϵ_x, ϵ_y and ϵ_{xy} are three components of strain, E is Young's modulus, υ is Poisson's ratio and G is called shear modulus. Apparently, $G=E/2(1+\upsilon)$.

Throughout the wedge, the strain components are also connected by the compatibility condition, i.e.

$$\frac{\partial^2 \varepsilon_x}{\partial y^2}+\frac{\partial^2 \varepsilon_y}{\partial x^2}-2\frac{\partial^2 \varepsilon_{xy}}{\partial x \partial y} \quad \text{.....(6.10)}$$

By using both Hooke's law and the strain compatibility condition, a harmonic equation can be derived,

$$(\frac{\partial^2}{\partial x^2}+\frac{\partial^2}{\partial y^2})(\sigma_x+\sigma_y)=0 \quad or \quad \nabla^2(\sigma_x+\sigma_y)=0 \quad \text{.....(6.11)}$$

which is called Laplace's equation.

From the above discussion, it is clear that the three stress components must, throughout the wedge, satisfy three fundamental equations, namely, the stress equilibrium equations (6.5 and 6.6) and the Laplace's equation (6.11).

Now suppose that there is a function Φ such that

$$\sigma_x=\frac{\partial^2 \Phi}{\partial y^2} \quad \text{.....(6.12)}$$

$$\sigma_y=\frac{\partial^2 \Phi}{\partial x^2} \quad \text{.....(6.13)}$$

$$\sigma_{xy} = -\frac{\partial^2 \Phi}{\partial x \partial y} \quad \text{.....(6.14)}$$

so that the stress equilibrium equations (6.5 and 6.6) are satisfied automatically. Substitution of equations (6.12-6.14) into the Laplace's equation (6.11) results

$$\frac{\partial^4 \Phi}{\partial x^4} + 2\frac{\partial^4 \Phi}{\partial x^2 \partial y^2} + \frac{\partial^4 \Phi}{\partial y^4} = 0 \quad or \quad \nabla^4 \Phi = 0 \quad \text{.....(6.15)}$$

This is the so-called biharmonic equation, and any solution of it will automatically satisfy the three fundamental equations. The function Φ is called Airy's stress function (see Hafner, 1951; Fung, 1965).

One of the solving methods for this type of problems is to introduce a suitable Airy's stress function containing certain unknown constants, and then determine those constants from the boundary conditions.

After a few trials, a solution is obtained by choosing the Airy's stress function as

$$\Phi = \frac{1}{6}k_1 x^3 + \frac{1}{2}k_2 x^2 y + \frac{1}{2}k_3 x^2 + k_4 xy + \frac{1}{2}k_5 y^2 + \frac{1}{2}k_6 xy^2 + \frac{1}{6}k_7 y^3 \quad \text{.....(6.16)}$$

Obviously, the biharmonic equation is satisfied. k_1 to k_7 are constants to be determined by the boundary conditions.

Using equations (6.12-6.14), we obtain

$$\sigma_x = k_5 + k_6 x + k_7 y \qquad \text{.....(6.17)}$$

$$\sigma_y = k_3 + k_1 x + k_2 y \qquad \text{.....(6.18)}$$

$$\sigma_{xy} = -k_4 - k_2 x - k_6 y \qquad \text{.....(6.19)}$$

From boundary condition (6.4), it yields

$$k_2 = \mu(1-\lambda)k_1 \qquad \text{.....(6.20)}$$

$$k_4 = \mu(1-\lambda)k_3 \qquad \text{.....(6.21)}$$

Making use of boundary condition (6.1) and equations (6.20 and 6.21), followed by algebraic manipulation, we get

$$k_2 = \mu(1-\lambda)k_1 \qquad \text{.....(6.22)}$$

$$k_3 = -x_o k_1 \qquad \text{.....(6.23)}$$

$$k_4 = -\mu(1-\lambda)x_o k_1 \qquad \text{.....(6.24)}$$

$$k_5 = -c\tan^2\alpha x_o k_1 \qquad \text{.....(6.25)}$$

$$k_6 = c\tan^2\alpha k_1 \qquad \text{.....(6.26)}$$

$$k_7 = \mu(1-\lambda)c\tan^2\alpha k_1 \qquad \text{.....(6.27)}$$

The stress distribution within the wedge can now be rewritten as

$$\sigma_x = -c\tan^2\alpha x_o k_1 + c\tan^2\alpha k_1 x + \mu(1-\lambda)c\tan^2\alpha k_1 y \qquad \text{.....(6.28)}$$

$$\sigma_y = -x_o k_1 + k_1 x + \mu(1-\lambda)k_1 y \qquad \text{.....(6.29)}$$

$$\sigma_{xy} = \mu(1-\lambda)x_o k_1 - \mu(1-\lambda)k_1 x - c\tan^2\alpha k_1 y \qquad \text{.....(6.30)}$$

From σ_x, σ_y and σ_{xy}, the value and the direction of the principal stresses, and the maximum shear stress can be determined:

$$\sigma_1 = \frac{\sigma_x + \sigma_y}{2} + \sqrt[2]{(\frac{\sigma_x - \sigma_y}{2})^2 + \sigma_{xy}^2} \qquad .....(6.31)$$

$$\sigma_2 = \frac{\sigma_x + \sigma_y}{2} - \sqrt[2]{(\frac{\sigma_x - \sigma_y}{2})^2 + \sigma_{xy}^2} \qquad .....(6.32)$$

$$\tau_{max} = \sqrt[2]{\frac{1}{4}(\sigma_x - \sigma_y)^2 + \sigma_{xy}^2} \qquad .....(6.33)$$

$$tan2\varphi = \frac{2\sigma_{xy}}{\sigma_x - \sigma_y} \qquad .....(6.34)$$

where φ is the angle between the direction of the greatest principal stress σ_1 and the x axis.

Substituting equations (6.28-6.30) into equation (6.34), we get

$$tan2\varphi = \frac{2[\mu(1-\lambda)x_o - \mu(1-\lambda)x - ctan^2\alpha y]}{(1-ctan^2\alpha)x_o + (ctan^2\alpha - 1)x + \mu(1-\lambda)(ctan^2\alpha - 1)y} \qquad .....(6.35)$$

By using the above equation, the stress trajectories within a wedge can be plotted, and further the slip lines can be plotted as well.

6.3.3.2 Results

Based on the previous analysis, the stress distribution in wedges can be determined and the role of parameters μ, λ and the wedge configuration in controlling the stress distributions can be evaluated.

Figure 6.10a shows the stress distribution in a wedge, in which the coefficient of friction $\mu=0.7$, the pore fluid pressure ratio $\lambda=0.1$, wedge length $x_o=15$ units (e.g. cm, dm, m or ft, etc.), and the wedge angle $\alpha=15°$. The dashed-lines represent the trajectories of the least principal stress (σ_2) and the continuous lines represent the trajectories of the greatest principal stress (σ_1). As mentioned earlier, **the sign convention of stresses used here follows that of the engineering usage, i. e., σ_1 is the maximum tensile stress (or the minimum compressive stress) and σ_2 is the maximum compressive stress (or the minimum tensile stress).** Obviously, the tensile fractures developed in the wedge should trace the trajectories of σ_2 if the rock is homogeneous. The trajectories of σ_2 are curved and the convex of the curves is toward the wedge apex. Figure 6.10b and Figure 6.10c show the stress distributions in wedges with similar parameters as that in Figure 6.10a except λ is different, $\lambda=0.5$ for Figure 6.10b and $\lambda=0,9$ for Figure 6.10c. Apparently, the pattern of the stress distributions in Figure

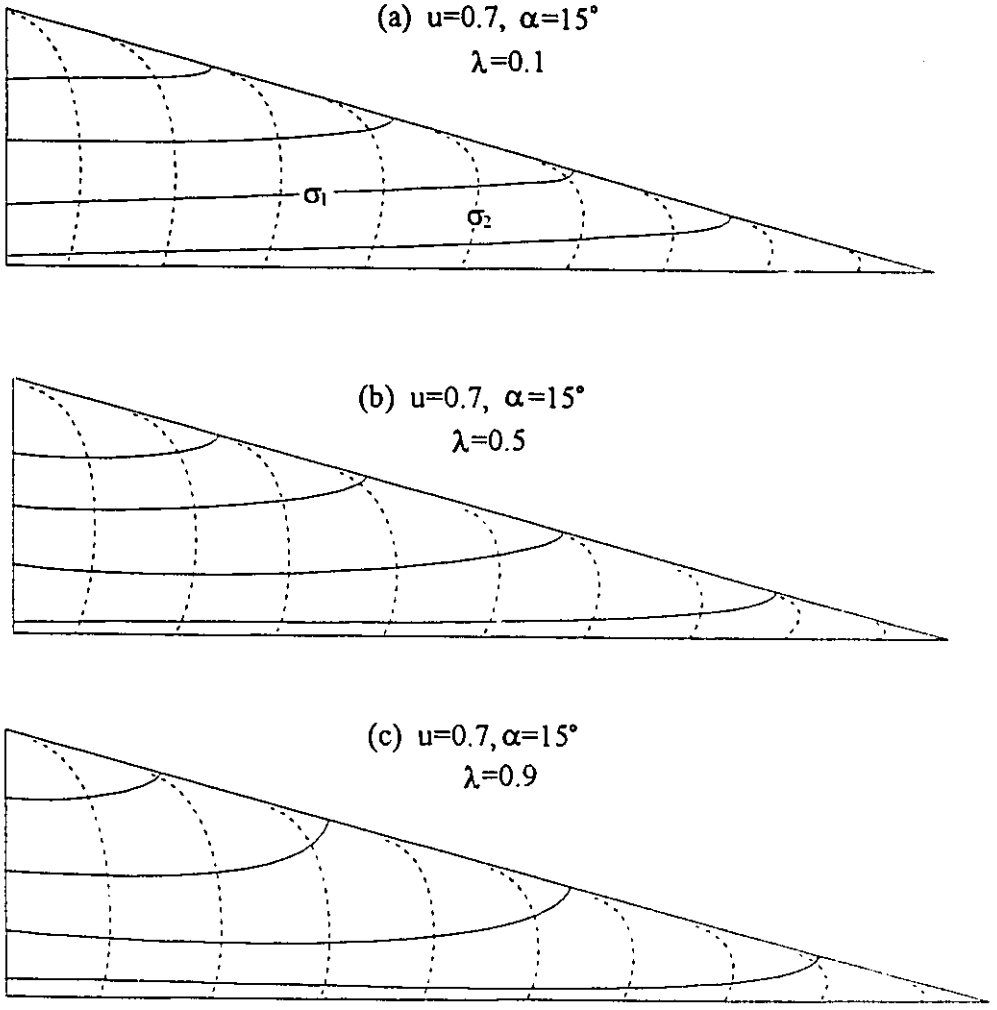

σ_1: the maximum tensile stress σ_2: the maximum compressive stress

Figure 6.10, Stress distribution in wedges with wedge angle of 15°.

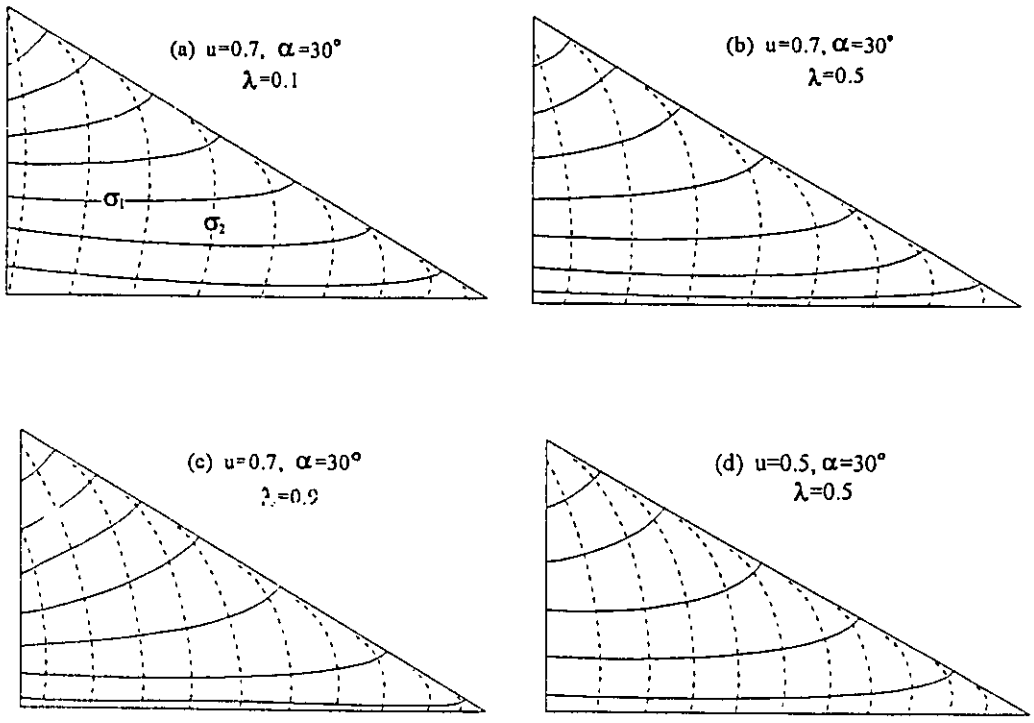

Figure 6.11, Stress distribution in wedges with wedge angle of 30°.

6.10a, b and c is almost identical, i.e., the stress distribution in wedges with wedge angle of 15° is not sensitive to the pore fluid pressure ratio(λ).

Figure 6.11a-d shows the stress distributions in wedges with wedge angle of 30°. The boundary parameters of the wedges are indicated in the figure as well. The trajectories of the maximum compressive stress (σ_2) are curved and the convex of the curves is toward the wedge apex, and any potential tensile fractures developed in the wedges should follow the track of these trajectories. It is also revealed that the stress distributions have no significant difference among Figure 6.11a-Figure 6.11d, although the pore fluid pressure ratio(λ) varies from as low as 0.1 (Figure 6.11a) to as high as 0.9 (Figure 6.11c); the coefficient of friction(μ) varies from 0.7 (Figure 6.11a-c) to 0.5 (Figure 6.11d)

Figure 6.12 shows the stress distributions in wedges with wedge angle of 60°. Obviously, the stress trajectories are quite different in Figure 6.12a from those in Figure 6.12b,c,d. In Figure 6.12a, where λ=0.1 and other parameters of the wedge are the same as those in Figure 6.12b (λ=0.5) and in Figure 6.12c (λ=0.9), the stress trajectories are almost straight lines, σ_2 in particular, while in Figure 6.12b,c the stress trajectories are curves and the convex of σ_2 is toward the rear of the wedge which is opposite to that in wedges with wedge angle of 15° or 30°. The stress distributions in Figure 6.12d are similar to those in Figure 6.12 b-c, although the coefficient of friction (μ) are changed from 0.7 to 0.5. Apparently, the stress distribution in wedges with wedge angle of 60° is only sensitive to the pore fluid pressure ratio(λ), and the stress

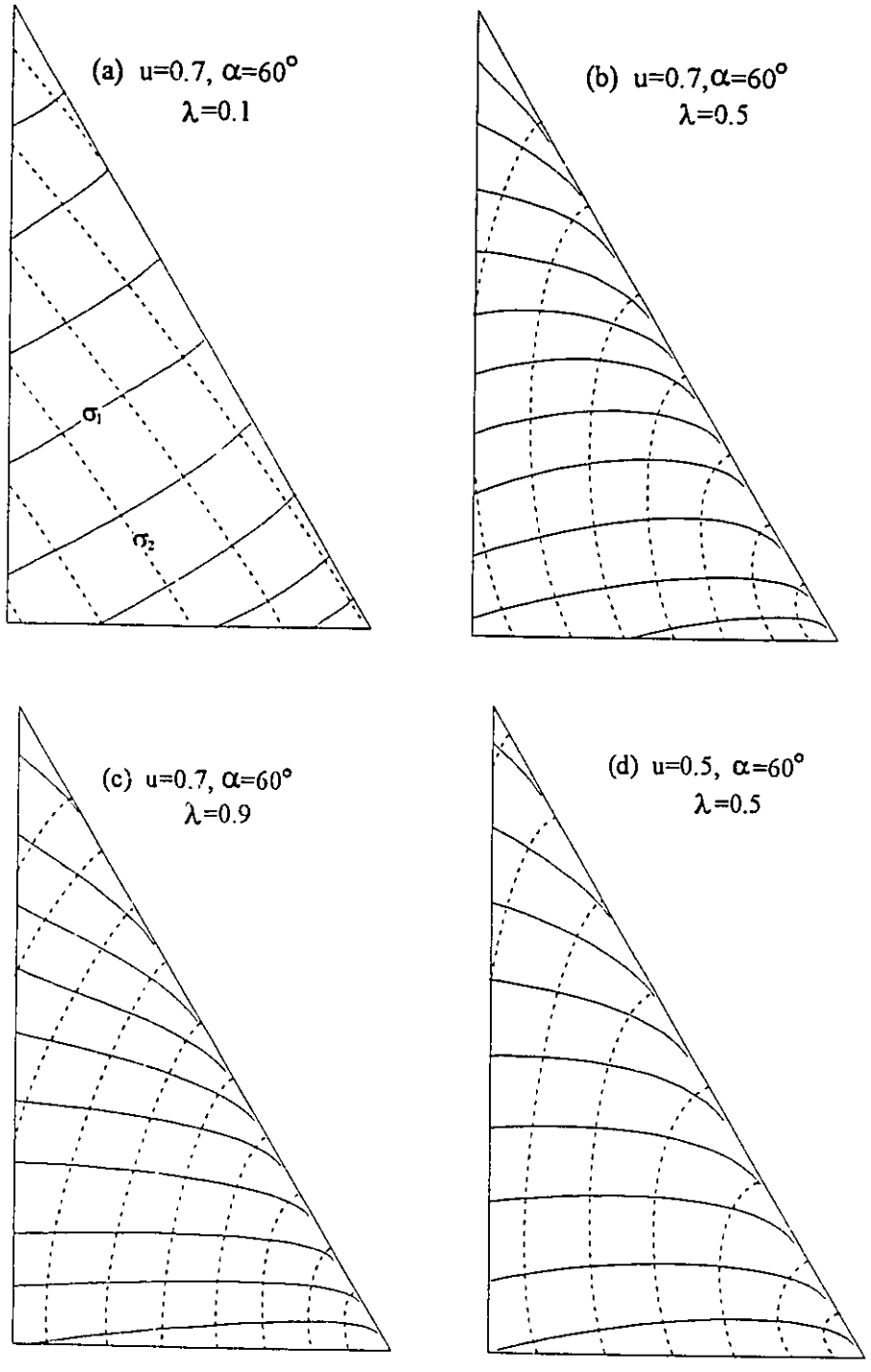

Figure 6.12, Stress distribution in wedges with wedge angle of 60°.

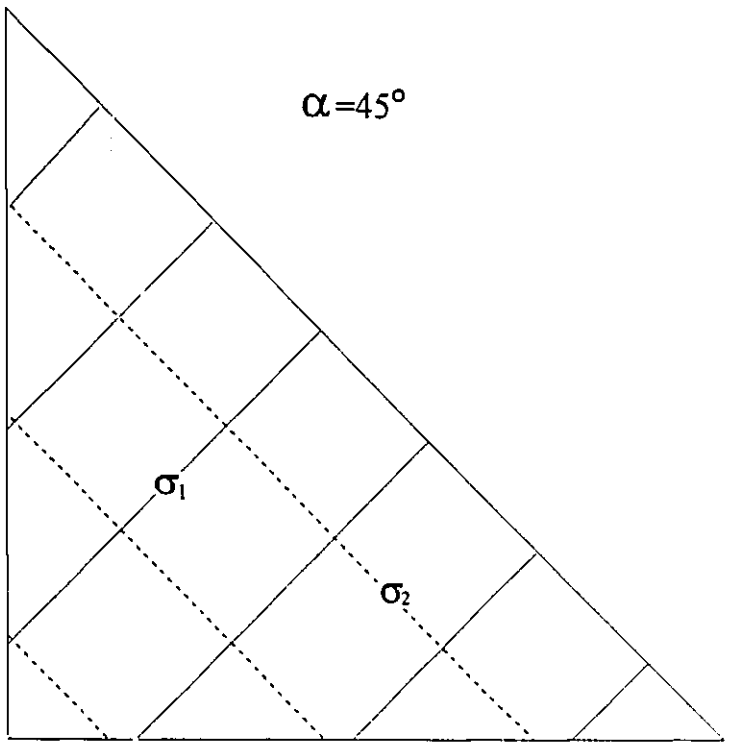

Figure 6.13, Stress Distribution in wedge with wedge angle of 45°.

trajectories are almost straight when the λ is low (e.g., 0.1) whereas the stress trajectories are curved when the λ is high (e.g., 0.5 or higher).

Figure 6.13 shows a special case where the wedge angle equals to 45°. In this case, no matter how the μ and λ are changed, the stress trajectories within the wedge are the same and are straight lines.

From the plot of stress trajectories, it is a simple task to draw slip-lines within a wedge as the direction of maximum shear stress (or any preferred direction of active slip) at any point bisects the angles between the directions of the principal stresses at that point. The secondary shear fractures developed within wedges, such as in Figure 6.6 and Figure 6.7, correspond to the slip-lines in the wedges.

In summary, according to the elastic model derived in earlier paragraphs, the stress trajectories are curves within wedges except those with a wedge angle of 45°. When the wedge angle is smaller than 45°, the stress distributions are not markedly sensitive to the parameters μ and λ though curvature increases as α increases, and the convex of σ_2 trajectories is toward the wedge apex. When the wedge angle is bigger than 45°, the stress distributions are sensitive to λ but not to μ, and the convex of σ_2 trajectories is toward the wedge rear. In short, the stress distribution within the wedge is controlled mainly by the wedge angle (α), and secondly by the pore fluid pressure ratio (λ) when the wedge angle is relatively big (e.g., 60°).

6.3.4 Application

By comparing the field observations with the stress trajectories derived from the elastic model, excellent correspondence between real examples and the predicted fracture patterns within wedges exists. Tensile fractures developed in wedges with wedge angle less than 45° (e.g., Figure 6.2, Figure 6.3, Figure 6.4, etc.) are curved toward the wedge apex, and match the trajectories of the maximum compressive stress in wedges with similar wedge angle (e.g., Figure 6.10 and Figure 6.11). Tensile fractures developed in wedges with wedge angle more than 45° (e.g., Figure 6.8c) are curved toward the wedge rear, and match the trajectories of the maximum compressive stress in wedges with corresponding wedge angle (e.g., Figure 6.12b,c,d). In the special cases of wedge angle of 45° (e.g., Figure 6.6), conjugate shear fractures were developed, and match the slip-lines predicted by the model (Figure 6.14).

Therefore, the process of the formation of the wedges observed in the research area may be extrapolated. At first, there were some non-systematic joints existed in the area (Figure 6.15a). A later tectonic event affected the region, and produced or more likely reactivated some faults. These faults cut and displaced the joints, which caused the stress disturbance around their conjunctions and developed the secondary fractures within them (Figure 6.15b).

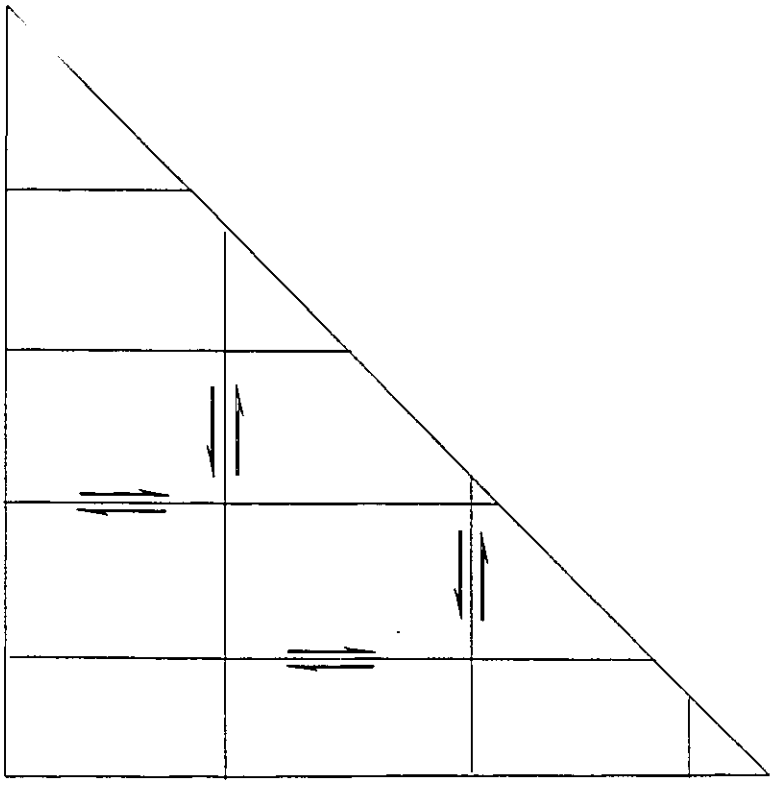

Figure 6.14, Slip lines in the wedge with wedge angle of 45°

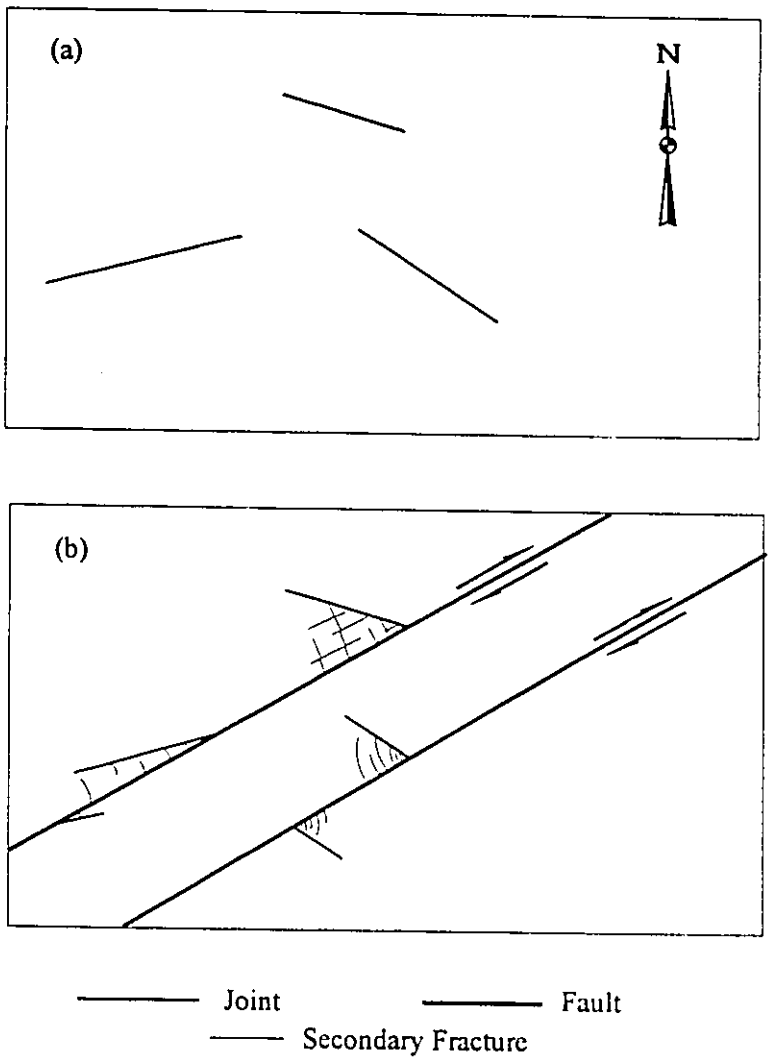

Figure 6.15, Illustration of the formation of wedges.

6.4 Conclusions

Based upon field observations, an elastic model is developed to evaluate the stress distribution in wedges. The model, in turn, can be used to explain the field observations and to predict the fracture patterns developed in wedges.

The model predicts that (1) when the wedge angle is less than 45°, the tensile fractures developed in the wedge are curved, and the convex of the curves is toward the wedge apex; the fracture pattern is not sensitive to other parameters, such as μ and λ; (2) when the wedge angle is 45°, the fractures developed in the wedge will be straight no matter how other parameters vary and no matter whether the fractures are tensile or shear; (3) when the wedge angle is more than 45°, the fracture pattern becomes dependent on the magnitude of λ; the tensile fractures developed in the wedge will be almost straight should λ be small (e.g., 0.1); otherwise the tensile fractures will be curved and the convex of the curves will be toward the wedge rear should λ be large (e.g., 0.5 or larger). It can be inferred that λ was relatively large when the wedges were formed in the research area because the secondary fractures developed in the wedges with wedge angle of more than 45° are curved (e.g., Figure 6.8c). The model also indicates that the wedge angle is the prime factor controlling the fracture patterns within wedges; the formation of wedges in the area is related to the development of main faults.

CHAPTER 7, SYNTHESIS

7.1, Introduction

The Killarney Magmatic Belt (KMB) consists of a set of northeast-trending granitoid rocks; and includes the Chief Lake Batholith (CLB), the Bell Lake Granite (BLG) and the Killarney Igneous Complex (KIC). The belt is bounded to the northwest by Huronian Supergroup rocks of the Southern Province, and to the southeast by the GFTZ of the Grenville Province (Figure 7.1). Both CLB and KIC intrusive events have been dated at about 1.7 Ga (Krogh and Davis, 1969, 1970; van Breemen and Davidson, 1988) while the BLG intrusive event has been dated at about 1.5 Ga (van Breemen and Davidson, 1988). Two well-known tectonic events in the region have been dated at about 1.85 Ga (Penokean Orogeny)(Card et al, 1972; van Schmus, 1976) and 1.0-1.2 Ga (Grenville Orogeny)(Krogh and Wardle, 1984), respectively. Although the KMB has long been a subject of studies by many workers (e.g., Quirke and Collins, 1930; Brooks, 1967, 1976; Clifford, 1986, 1990; Davidson, 1986), the cause of its formation is still not clear. Davidson(1986) suggested the sequence as a high-level volcano-plutonic complex. Clifford (1990) classified the KIC as an anorogenic granite with volcanic facies from the geochemical studies, and suggested that it was formed in a place without any compression during emplacement.

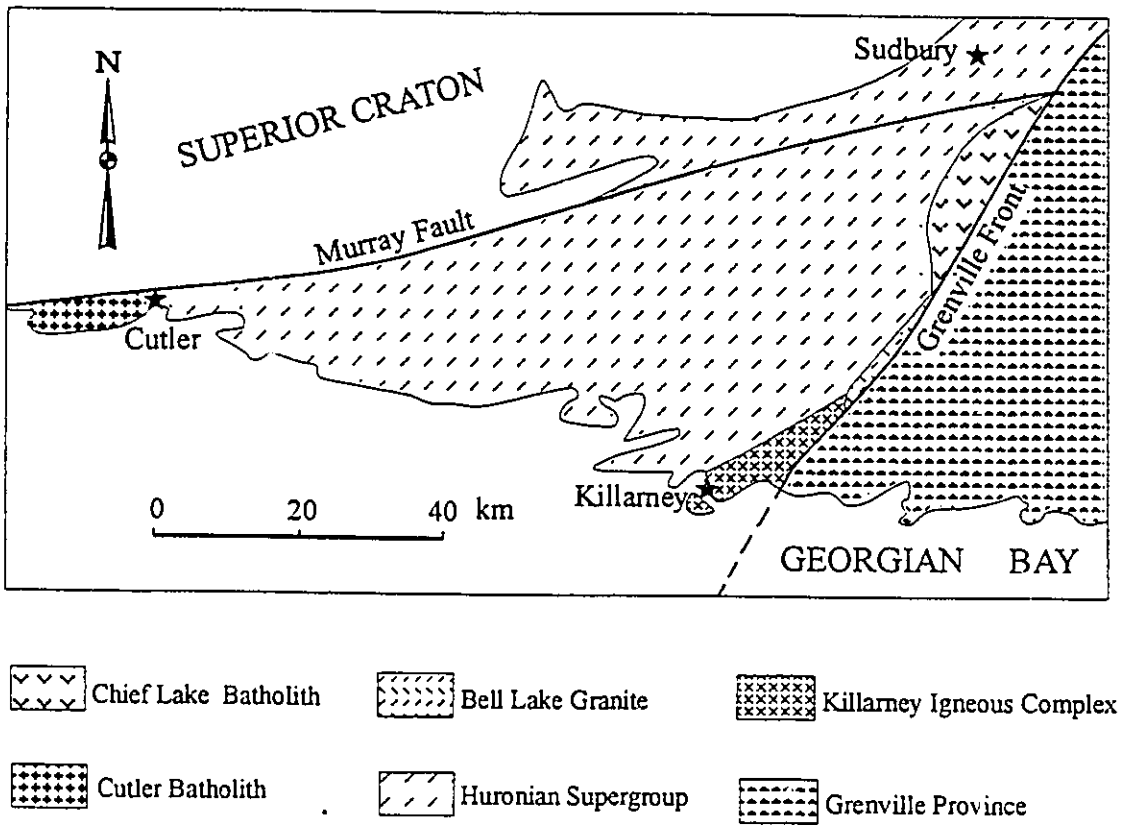

Figure 7.1, Simplified tectonic map of the Killarney Magmatic Belt and the surrounding areas.

Based upon the structural studies and geochronological evidences, a tectonic model is proposed for the geological history of the KIC and the surrounding area in this chapter, suggesting the KMB was emplaced in a transtensional environment due to the tectonic escape of the Huronian Supergroup.

7.2, Geochronology and Structural Development

7.2.1, Grenville Province

The Grenville Province was subdivided, from northwest to southeast, into the Grenville Front Tectonic Zone (GFTZ), the Central Gneiss Belt (CGB) and the Central Metasedimentary Belt (CMB) (Wynne-Edwards, 1972). These subdivisions can be further divided into terranes and domains (Figure 7.2)(see summaries by Easton, 1992).

The CGB consists mainly of upper amphibolite face gneisses, and locally granulite face, quartzo-feldspathic gneisses. It contains various Archean to Mesoproterozoic crustal segments (Easton, 1986; Dickin and McNutt, 1989). Granitic and monzonitic plutons have been dated at about 1.7 Ga in Nipissing terrane (Lumbers, 1978; Lumbers and Vertolli, 1991), and at about 1.5 Ga in Algonquin and Tomiko terranes (Bickford et al, 1986). Culshaw et al (1991) report that metamorphism was associated with this magmatic event in the Britt domain. In Parry Sound terrane, mafic to intermediate rocks were extracted from the mantle at about 1.4-1.5 Ga (Dickin and McNutt, 1989). All

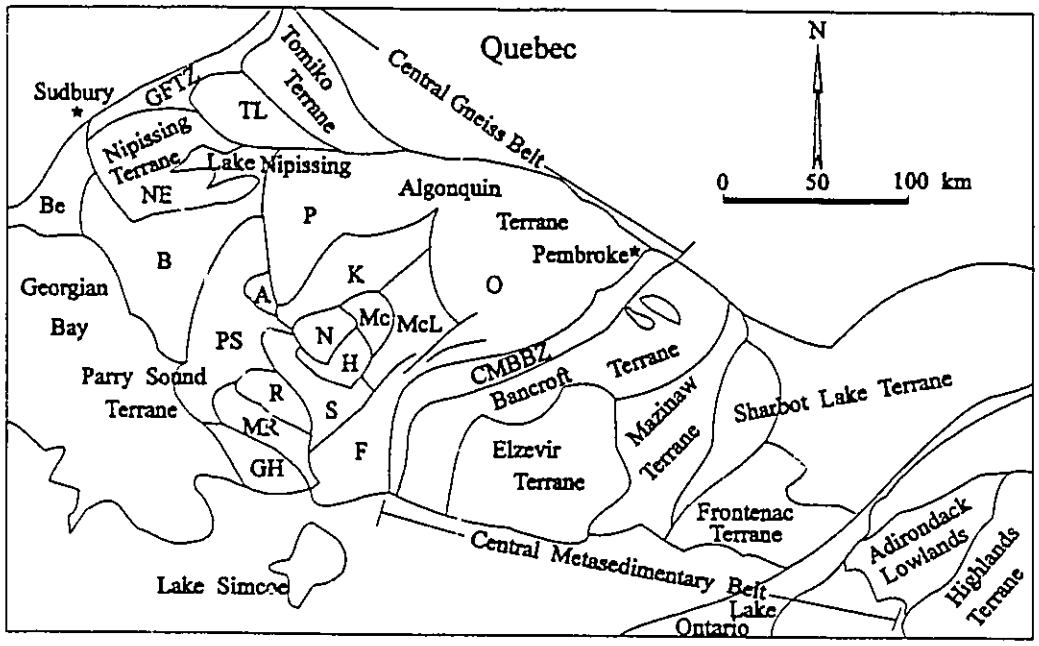

Figure 7.2, Subdivisions of Grenville Province (after Easton, 1992).

Abbreviations

A	Ahmic Domain	GH	Go Home Domain	NE	Nepewassi Domain
B	Britt Domain	H	Huntsville Domain	O	Opeongo Domain
Be	Beaverstone Domain	K	Kiask Domain	P	Powassan Domain
CMBBZ	Central Metasedimentary Belt Boundary Zone	Mc	McCraney Domain	PS	Parry Sound Domain
		McL	McClintock Domain	R	Rosseau Domain
F	Fishog Domain	MR	Moon River Domain	S	Seguin Domain
GFTZ	Grenville Front Tectonic Zone	N	Novar Domain	TL	Tilden Lake Domain

terranes and domains have been affected by the Grenville Orogeny.

The CMB is separated from CGB by the Central Metasedimentary Belt Boundary Zone (CMBBZ) which is a major shear zone characterized by strongly deformed rocks with northeasterly striking, southeasterly dipping tectonic layering and southeast-plunging mineral lineations. The CMB consists mainly of Mesoproterozoic volcanic rocks, marble and clastic metasedimentary rocks, and has been divided into several lithotectonic terranes based on differences in lithology, geochronology and structural history (see summaries by Easton, 1992). Volcanism and plutonism in the belt have been dated at about 1.2-1.3 Ga (Miller, 1983).

The GFTZ forms a belt 15 to 80 KM wide, trending northeasterly for about 2000 KM in Canada. The dominant rock type in the zone is mylonite, with a strong and persistent northeasterly trending foliation and southeasterly plunging lineation. Detrital zircon populations dated at about 1.7 Ga were found in the zone, which might suggest a period of sedimentation following the formation of the Killarney Magmatic Belt (Krogh, 1989). The Grenville Front is the northwest limit of the GFTZ and has long been recognized as a major tectonic feature of the Canadian Shield. Various kinematic indicators (e.g., asymmetric porphyroclasts, S-C fabrics, etc.) all indicate northwest-directed thrusting on the Grenville Front, with a sinistral horizontal component of motion. There are no reliable markers which can be used to calculate the displacement on the shear surfaces at the Grenville Front by using classical structural methods. However, uplift of the Grenville Province side relative to the Southern Province side be

estimated at up to 10-20 km based on the metamorphic assemblages (O'Donnell, 1986; Wynne-Edwards, 1972). There has been considerable debate on whether the Grenville Front is a long-lived structural feature extending back to the Neoarchean (Stockwell, 1982) or the Paleoproterozoic (Lumbers, 1978), or whether it is solely related to the Grenville Orogeny. Based on previous studies and current work, the Grenville Front is believed to be a long-lived shear zone, and the model presented below will show that the GF has been intermittently active for at least 700 Ma (1750-1050 Ma).

7.2.2, Southern Province

At the southern margin of the Superior craton, the Southern Province consists of the Paleoproterozoic Huronian Supergroup of 2.2-2.5 Ga, dominantly siliceous, continental margin metasedimentary rocks. Main structural features in Huronian Supergroup are a series of east-trending, north-verging anticlines and synclines and associated south-dipping thrust faults, and some conjugate sets of northeast- and northwest-trending strike-slip faults (Bennett et al 1991). These features all indicate that there was a northward compression across the Huronian Supergroup during the Penokean Orogeny (1.85 Ga) (Card et al, 1972; van Schmus, 1976) in which the rocks of the Huronian Supergroup were subjected to metamorphism of subgreenschist to amphibolite facies. In the area north of the Murray Fault, rocks are subgreenschist to lower greenschist facies assemblages while in the area south of the Murray Fault, rocks have

been metamorphosed from middle greenschist to amphibolite facies and have been subjected to a higher degree of deformation.

The Murray Fault has long been recognized to be an important structural feature in the Southern Province. Card et al (1972) provide evidence to suggest that the Murray Fault system was initially part of a graben system forming depositional basins for Huronian sediments. It subsequently became a steeply south-dipping thrust fault with considerable dextral shear displacement during later deformation (ca. 1.85 Ga and later, Zolnai et al, 1984). Furthermore, Sudbury diabase dykes (1.22-1.25 Ga, Fahrig and West, 1986) have been found to have suffered dextral displacement across the Murray Fault (Davidson, 1992), which further suggest that the Murray Fault has had late movements with a dextral component.

7.2.3, Killarney Magmatic Belt

The Chief Lake Batholith is the largest granitoid body of KMB, and has been dated at about 1.71-1.67 Ga (Krogh and Davis, 1969, 1970). It has recognizable intrusive contacts on both sides. On the northwestern side, the granite intruded into the Huronian Supergroup along both bedding and cleavage (Spaven, 1966), and trapped large enclaves of the Lorrain Quartzite (two over 500m long), whose long axes are generally parallel to the flow fabric in the host granite. Similar intrusive features are found on the southeastern side of the batholith (Hsu, 1968), which imply that the batholith was

emplaced at this structural level in absence of any substantial compression. Flow foliation is developed throughout much of the granite, accentuated by mylonization, and there is also a southeasterly plunging lineation developed near the Grenville Front.

The Bell Lake Granite is a coarse grained reddish porphyritic granite to granodiorite, and has been dated at about 1.47 Ga (van Breemen and Davidson, 1988), 1.52 Ga (Krogh and Davis, 1970). The granite intruded Huronian metasediments on its northwest side, wedging apart bedding planes and enclosing numerous quartzite enclaves in the vicinity of the contact. The granite has been strongly sheared on its southeast boundary, producing a black mylonite (O'Donnell, 1986). A regional foliation, striking between 20° to 70° and dipping 40° or greater to southeast, has been developed throughout the granite. A regional lineation generally plunges to the southeast. There are also numerous shear zones developed within the granite, marked by mylonites. These shear zones are parallel to the regional foliation, and kinematic indicators within the zones are in agreement with northwest-directed overthrusting.

The KIC consists of granite, porphyry and fragmental volcanic rocks, and has been dated at about 1.71-1.73 Ga for the volcanic rocks, 1.74 Ga for the granite (van Breemen and Davidson, 1988). It shows evidence that it has been subjected to several deformation events after its formation. A hydrothermal alteration has resulted in local, restricted silicification of the volcaniclastic assemblages (Clifford, 1986). An episode of flattening and stretching followed the hydrothermal activity and imposed a regional foliation and lineation in the porphyry-volcaniclastic assemblages. This flattening event

is perhaps related to the activity at about 1.62 Ga (Wanless and Loveridge, 1972). Both the nature and degree of these foliation and lineation are different from the foliation and lineation developed in the mylonite zone of the Grenville Front. A set of subparallel faults, striking about 240° and dipping about 80° to the NNW, have been superimposed on the regional foliation along the lakeshore east of Killarney village. Mesoscopic and microscopic kinematic indicators all suggest that the faults are oblique reverse faults, with a substantial dextral horizontal component of motion (Fan and Clifford, 1993). The faults are cut by a set of Sudbury diabase dikes which show no sign of deformation here.

Geochemical studies of KMB granitoids (Clifford, 1990; Lumbers and Vertolli, 1991) indicate that they possess the chemical signature of anorogenic granites. Clifford(1990) further suggests that the KIC was emplaced in a non-compressional environment. The model presented below extends this idea.

7.3, Geological History of the KIC and the Surrounding Area

On the basis of current knowledge of structural studies and geochronology, the tectonic evolution, during the interval of the Penokean Orogeny and the Grenville Orogeny, of the proto-Grenville Front and the formation of the Killarney Magmatic Belt can be discussed. A tectonic model is proposed, and suggests the CLB, KIC and BLG were emplaced in a transtensional environment due to the tectonic escape of the Huronian block (Figure 7.3B), and later the tectonic escape of the KIC (Figure 7.3C)

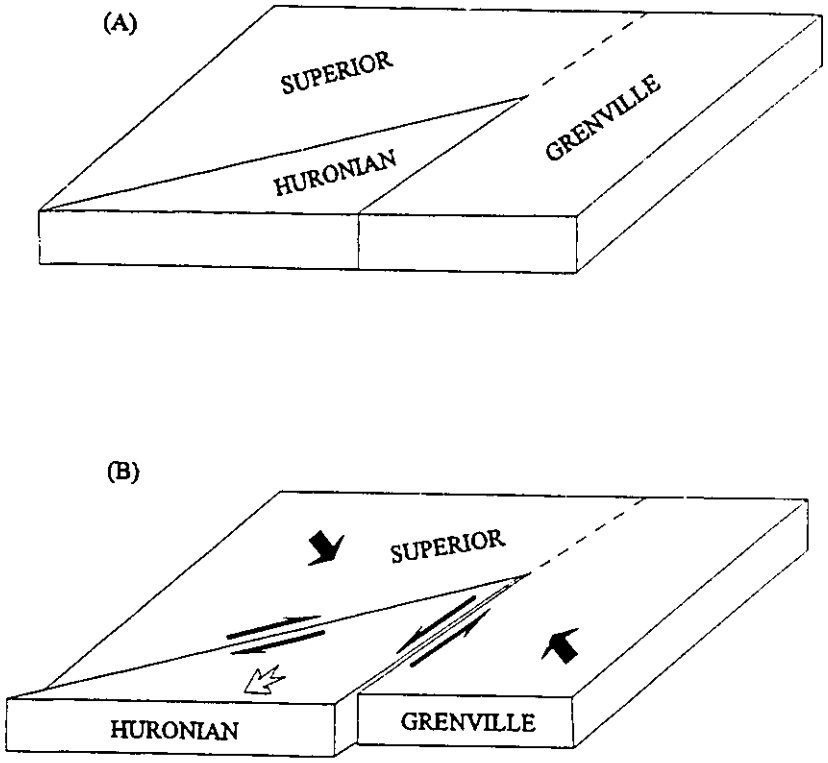

Figure 7.3 (continued...)

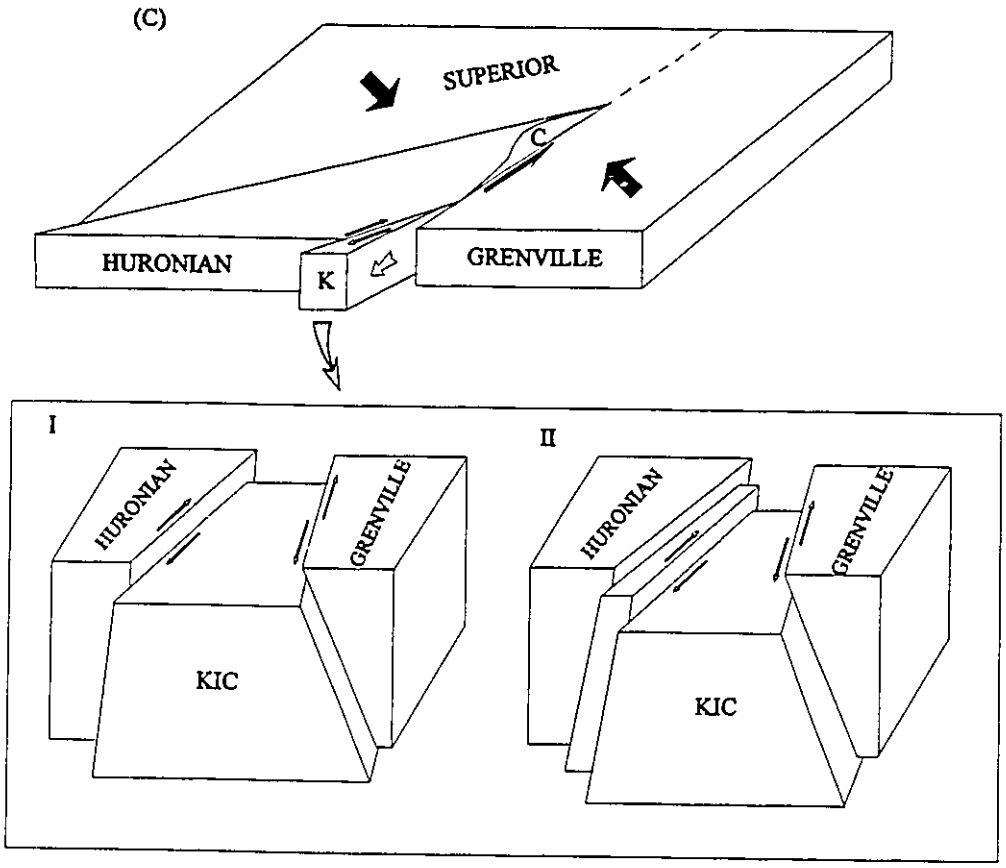

Figure 7.3, Illustration of the simplified indentation model.
(A) ca. 1.85-1.75 Ga
(B) ca. 1.75-1.65 Ga
(C) ca. 1.55-1.45 Ga (see text for details)
K-Killarney Igneous Complex (KIC); C-Chief Lake Batholith (CLB)

7.3.1, 1.85-1.75 Ga

There are no significant tectonic events reported in the region during the period of 1.85-1.75 Ga. Figure 7.3A shows the wedge of Huronian Supergroup bounded to the northwest by the Superior Craton, and to the southeast by elements of the Grenville Province for this repose period after the Penokean Orogeny.

7.3.2, 1.75-1.65 Ga

During the period of 1.75-1.65 Ga, either Grenville block started (or restarted) its northwesterly encroachment upon Huronian block or Superior craton started (or restarted) its southeasterly indentation. The Huronian block was squeezed out along a dextral shear zone (the Murray Fault) on its northwest boundary and a postulated sinistral shear zone (the proto-Grenville Front) on its southeast boundary. Rotation of these blocks (Superior block, Huronian block and Grenville Block) might also be involved in this process. The tectonic escape of the Huronian block towards the SW left some "free space" at its apex and a transtension zone appeared along the contact between Grenville block and the Huronian block (Figure 7.3B). The Chief Lake Batholith and the Killarney Igneous Complex were then emplaced relatively resistance-free into the transtension zone. They wedged in along bedding planes and cleavages to pry apart and rip off large pieces

of quartzite and other metamorphosed rocks on both sides of the transtension zone (e.g. NW side of KIC; NW side and SE side of CLB).

Meanwhile, granitic and monzonitic plutons dated at about 1.7 Ga were emplaced in the Central Gneiss Belt of Grenville Province (Lumbers, 1978; Lumbers and Vertolli, 1991). Detrital zircon population in a muscovite quartzite of unquestionable sedimentary origin dated at about 1.7 Ga have been found in the GFTZ (Krogh, 1989), which might imply that a basin whose long axis was parallel to the transtension zone had existed and a period of sedimentation had occurred after the formation of the KIC and CLB plutons.

7.3.3, 1.65-1.55 Ga

After the emplacement of CLB and KIC, a local flattening and stretching event affected KIC and imposed a regional foliation and lineation in the porphyry-volcaniclastic assemblages at about 1.62 Ga. The whole region then re-entered a relative repose period (1.62-1.55 Ga).

7.3.4, 1.55-1.45 Ga

During the period of 1.55-1.45 Ga, Grenville block renewed its northwesterly encroachment toward Huronian block or Superior craton renewed its southeasterly indentation (Figure 7.3C). The Huronian block as a whole might have been squeezed

out from between the Superior block and the Grenville block; alternatively, the KIC alone was squeezed out a little from between the Huronian block and the Grenville block, so developing some free space (a transtension zone) at its triangular apex. This tectonism imposed a set of subparallel faults with accompanying mylonites upon the earlier regional foliation (ca. 1.62 Ga) in the KIC along the lakeshore east of Killarney village. These faults, now trending about 240° and dipping about 80° NNW, are thrusting faults with substantial dextral horizontal movements. Figure 7.3C(I)-(II) present the model in more detail for the vicinity of the KIC, especially Figure 7.3C(II) which shows a thrusting zone with dextral shear developed within the KIC. This explains the structural features observed in the vicinity of the Killarney village.

In the meantime, the Bell Lake Granite was then emplaced into the transtension zone, wedging apart bedding planes and enclosing numerous quartzite enclaves in the vicinity of the contact between the Huronian block and the Grenville block (O'Donnell, 1986). Granitic and monzonitic plutons dated at about 1.5 Ga have been found in Algonquin and Tomiko terranes of the Central Gneiss Belt, and the associated metamorphism has been reported in the Britt Domain of the CGB (Culshaw et al, 1991; Ketchum et al, 1994). Krogh (1989) reported a metamorphic event dated at about 1.45 Ga from the leucosome pods in the Killarney area. After 1.45 Ga, the region reentered another relative repose period (1.45-1.25 Ga).

Thereafter, the region was cut by the Sudbury swarm of northwest-trending diabase dikes at about 1.24 Ga. And finally, the Grenville Orogeny (1.0-1.2 Ga)

deformed and obliterated most previous structural features within Grenville Province and the southeast side of the KMB close to the Grenville Front, and imposed a mylonitic foliation and lineation in the vicinity of the Grenville Front.

7.4, Conclusions

The northwesterly encroachment of the Grenville Province or the southeasterly indentation of the Superior craton forced the wedge of the Huronian Supergroup to move toward the southwest on the Grenville Front and the Murray Fault, and produced a transtension zone between the Huronian Supergroup and the Grenville Province, which provided the space and the thermal environment for the emplacement of the Chief Lake Batholith and the Killarney Igneous Complex at about 1.75-1.65 Ga. A second episode of encroachment or indentation occurred during the period of 1.55-1.45 Ga, and provided the space and the thermal environment for the emplacement of the Bell Lake Granite. Both Grenville Front and the Murray Fault appear to be long-lived shear zones, intermittently active for more than 700 Ma.

The model presented here implies that there might be a transpression environment along the contact between the Superior craton and the Huronian Supergroup during the encroachment or the indentation. This may explain the intrusion of the Cutler Pluton, located along the boundary between Superior craton and the Huronian Supergroup (see Figure 7.1). The composite pluton dated at about 1.7 Ga (Wetherill et al, 1960) consists

of medium- to coarse-grained, foliated quartz monzonite, granodiorite and tonalite, and has S-type granite characteristics, suggesting the tectonic environment on northwest boundary of the Huronian Supergroup was different from that on southeast boundary of the Huronian Supergroup during its emplacement.

CHAPTER 8, CONCLUSIONS AND SUGGESTIONS FOR FUTURE RESEARCH

8.1, Conclusions

The Killarney Magmatic Belt (KMB), consisting of the Killarney Igneous Complex (1.74-1.71 Ga), the Chief Lake Batholith (1.71-1.67 Ga) and the Bell Lake Granite (1.52-1.47 Ga), lies along the Grenville Front Tectonic Zone (GFTZ); its constituents posses the characteristics of anorogenic granite. The intrusive features of the KMB suggest that it was emplaced in a non-compressional environment, even though the GFTZ is overwhelmingly a zone of compressional structures. It is proposed that the Killarney Igneous Complex (KIC) and the Chief Lake Batholith (CLB) were emplaced in a transtension zone due to the tectonic escape of the Huronian Supergroup caused by the southeasterly indentation of the Superior craton or the northwesterly encroachment of the Grenville Province, during 1.75-1.65 Ga.

After its emplacement, the KIC underwent two major compressional deformation, in addition to some minor, local events, for example, a hydrothermal alteration resulted in silicification of the volcaniclastic rocks. The first major compressional deformation imposed a regional foliation and lineation in the porphyry-volcaniclastic assemblages, at about 1.623 Ga of age. These foliation and lineation are quite different in nature from those of the GFTZ produced by a much later tectonic event, the Grenville Orogeny (ca.

1.10 Ga). The second major event affected the KIC was due to the renewed indentation of the Superior craton or encroachment of the Grenville Province, during the period of 1.55-1.45 Ga. This event effectively produced a transtension zone between the KIC and the Grenville Province, so providing the space and the thermal environment for the emplacement of the Bell Lake Granite, and imposed a set of subparallel faults in the Main Site of the research area.

Micro- and meso-scopic structural features all indicate these subparallel faults are thrusting faults with substantial dextral horizontal movement. Palaeopiezometry of recrystallized quartz grains reveals that the differential stress related to the thrusting ranged from 85 MPa to 146 MPa, with average of 100 MPa and standard deviation of 15 MPa, which is similar to the results obtained from other major thrusting zones. Fault-slip analysis suggests that the maximum compressive stress responsible for the thrusting came from the WNW direction, supporting the tectonic model that these faults were imposed by the indentation of the Superior craton.

The study of two fracture variations, namely, kinks and wedges, provides valuable insight into the palaeostress field and the regional structural development in the research area. From the theoretical and practical analysis of kinks, it is realized that a) if a straight fracture, subjected to mode I and mode II loading, begins to propagate, the resulting fracture will kink; b) the sign of kink angle is a reliable kinematic indicator: a clockwise kink angle indicates dextral sense of shear on the parent fracture while a counter-clockwise kink angle indicates sinistral sense of shear on the parent fracture; c)

the ratio of the effective shear stress and the effective normal stress determines the value of the kink angle; d) the kink angles in the research area suggest most parent fractures have had dextral sense of shear; e) the values of kink angles indicate that the effective shear stress was smaller than the effective normal stress responsible for kinking in the research area.

From the numerical modelling of stress distribution within wedges, fracture patterns developed in wedges can be predicted and the formation of wedges observed in the field can be explained. The model predicts that a) if the wedge angle is small ($<45°$), tensile fractures developed in the wedge will be curved, and the convex of the curves is toward the wedge apex; the fracture pattern is not sensitive to other parameters, such as the coefficient of friction (μ) and the pore fluid pressure ratio (λ); b) if the wedge angle is 45°, fractures developed in the wedge will be straight no matter how other parameters vary and no matter whether the fractures are tensile or shear; c) if the wedge angle is large ($>45°$), fracture patterns become dependent on the magnitude of the pore fluid pressure ratio (λ); tensile fractures developed in the wedge will be almost straight should λ be small (e.g., 0.1), whereas tensile fractures will be curved and the convex of the curves will be toward the wedge rear should λ be large (e.g., 0.5 or larger); d) the prime factor controlling the fracture patterns within wedges is the magnitude of the wedge angles. These predications regarding fracture patterns developed in wedges are substantiated by the field observations. The formation of wedges in the research area was related to the development of main faults. These faults cut and displaced the

existing non-systematic joints, which caused the stress disturbance around their conjunctions so that the secondary fractures were developed within them.

By considering that the GFTZ is the northwest limit of the effects the Grenville Orogeny, the position of the GFTZ seems justified to be suggested along the southeast edge of the KIC, excluding the KIC from the Grenville Province, because the Grenville Orogeny did not really affect the KIC except its southeast edge. This position is currently accepted by most workers, and has been applied to throughout this thesis.

8.2, Suggestions for Future Research

To test and modify the tectonic model proposed in chapter 7, an analogue experiment is needed to model the movement and rotation of the blocks representing the Superior Craton, the Grenville Province and the Huronian Supergroup, respectively, due to the southeasterly indentation of the block of the Superior Craton, and to investigate the structural features being developed in these blocks and evaluate the conditions (e.g., degrees of the rotation and the depth of the indentation, etc.) required to produce a transtension zone between the blocks of the Grenville Province and the Huronian Supergroup.

Palaeomagnetism is a powerful tool for identifying rotations of continental and intracontinental blocks about any axis, especially about vertical axis (McClelland and McCaig, 1989; Osete et al, 1989). Amin (1990) studied palaeomagnetism in Quebec and

suggested an anti-clockwise rotation for Rouyn-Noranda block in the Abitibi Belt about 100 KM northeast of the Killarney region. A detailed palaeomagnetic study in the region will help to recognize any rotations of the blocks representing the Huronian Supergroup, the Grenville Province and the Superior Craton, and shed light on relative movements among themselves.

A thorough geochemical analysis of rock samples from all parts of the KMB is required to verify their anorogenic nature. The timing of the thrusting can be further constrained or be proved to be coincident with the emplacement of the Bell Lake Granite if the mylonites developed along main faults are dated. Rink is trying to use the ESR (Electron Spin Resonance) technique to evaluate the age of the faulting.

It is clear that future work integrating palaeomagnetics, geochemistry and structural geology will contribute to a more detailed understanding of the region.

REFERENCES

Amin, M. T., 1990, Palaeomagnetic evidence for anti-clockwise rotation of Rouyn-Noranda structural block, Quebec, Canada: M.Sc. thesis, McMaster University, Hamilton, Ontario, 136p.

Anderson, E. M., 1942, The Dynamics of Faulting and Dyke Formation with Application to Britain, Oliver and Boyd, Edinburgh, Scotland, 191p.

Anderson, T. B., 1968, The geometry of a natural orthorhombic system of kink bands, Geological Survey of Canada Paper 68-52, 200-220.

Angelier, J., 1979, Determination of the mean principal directions of stresses for a given fault population, Tectonophysics, 56, T17-T26.

Angelier, J., 1984, Tectonic analysis of fault slip data sets, J. Geophys. Res., 89, 5835-5848.

Angelier, J., 1990, Inversion of field data in fault tectonics to obtain the regional stress-III: A new rapid direct inversion method by analytical means, Geophys. J. International, 103, 363-376.

Atkinson, B. K., 1987 (ed.), Fracture Mechanics of Rock, Academic Press, London, 534p.

Aydin, A., 1978, Small faults formed as deformation bands in sandstone, Pure & Appl. Geophys., 116, 913-930.

Aydin, A. and Johnson, A. M., 1978, Development of faults as zones of deformation bands and as slip surfaces in sandstones, Pure and Appl. Geophys., 116, 931-942.

Aydin, A. and Johnson, A. M., 1983, Analysis of faulting in porous sandstone, J. Struct. Geol., 5, 19-35.

Barlow, A. E., 1893, Relations of the Laurentian and Huronian rocks north of Lake Huron, Geol. Soc. Am. Bull., 4, 313-332.

Bell, R., 1878, Geology in the neighbourhood of Shiboananing, Geol. Surv. Can. Report

on Progress 1876-77, 208-210.

Bell, R., 1891, Sudbury Mining District, Geol. Surv. Can. Ann. Report V, Part F, 95p.

Bennett, G., Dresseler, B. O. and Robertson, J. A., 1991, The Huronian Supergroup and associated intrusive rocks, in: Geology of Ontario, Ontario Geological Survey, Special Volume 4, Part 1, 549-591.

Bergerat, F. and Vandycke, S., 1994, Palaeostress analysis and geodynamical implications of Cretaceous-Tertiary faulting in Kent and Boulonnais, J. Geological Soc., 151, 439-448.

Berthe, P., Choukroune, P. and Jegouze, P., 1979, Orthogneiss, mylonite and non-coaxial deformation of granites: the example of the Armorican shear zone, J. Struct. Geol., 1, 31-42.

Bickford, M. E., van Schmus, W. R. and Zeitz, I., 1986, Proterozoic history of the midcontinent region of North America, Geology, 14, 492-496.

Brooks, E. R., 1967, Multiple metamorphism along the Grenville Front north of Georgian Bay, Ontario, Geol. Soc. Am. Bull. 78, 1267-1280.

Burg, J. P. and Laurent, Ph., 1978, Strain analysis of a shear zone in a granodiorite, Tectonophysics, 47, 15-42.

Burg, J. P., 1986, Quartz shape fabric variations and c-axis fabrics in a ribbon-mylonite: arguments for an oscillating foliation, J. Struct. Geol., 8, 123-131.

Byerlee, J., 1978, Friction of rocks, Pure Appl. Geophys., 116, 615-626.

Card, K. D., Church, W. R. E., Franklin, J. M., Frarey, M. J., Robertson, J. A., West, G. F. and Young, G. M., 1972, The Southern Province, in: Price, R. A. and Douglas, R. J. W., eds., Variations in Tectonic Styles in Canada, Geological Association of Canada, Special Paper 11, 335-380.

Card, K. D., 1976, Geology of the McGregor Bay-Bay of Islands area, Districts of Sudbury and Manitoulin, Ontario Division of Mines Geoscience Report 138, 63p.

Card, K. D. and Lumbers, S. B., 1977, Sudbury-Cobalt, Ontario Geological Survey Map 2361, Geological Compilation Series.

Carreras, J., Estrada, A. and White, S. H., 1977, The effects of folding on the c-axis fabric of a quartz mylonite, Tectonophysics, 39, 3-24.

Choukroune, P. and Lagarde, J. L., 1977, Plans de schistosite et deformation rotationelle: exemple du gneiss de champtoceaux (Massif Armoricain), Comptes Rendus Academie de Science Paris, 284, Ser. D, 2331-2334.

Christie, J. M. and Ord, A., 1980, Flow stress from microstructures of mylonites: examples and current assessment, J. Geophys. Res., 85, 6253-6262.

Christie, J. M., Ord, A. and Koch, P. S., 1980, Relationship between recrystallized grain size and flow stress in experimentally deformed quartzite, EOS Trans. Am. Geophys. Un., 61, 377.

Clifford, P. M., 1986, Petrological and structural evolution of the rocks in the vicinity of Killarney, Ontario: an interim report, in: Current Research, Part B, Geological Survey of Canada Paper 86-1B, 147-155.

Clifford, P. M., 1991, Mid-Proterozoic deformational and intrusive events along the Grenville Front in the Sudbury-Killarney area, Ontario, and their implications, in: Gower, C. F., Rivers, T. and Ryan, B., eds., Mid-Proterozoic Laurentia-Baltica, Geological Association of Canada, Special Paper 38, 335-350.

Cloos, E., 1955, Experimental analysis of fracture patterns, Geol. Soc. Am. Bull., 66, 241-256.

Collier, M., 1978, Ultimate locking angles for conjugate and monoclinal kink bands, Tectonophysics, 48, T1-T6.

Collins, W. H., 1916, The age of the Killarney Granite, Geol. Surv. Can., Museum Bull. 8, 31p.

Collins, W. H., 1925, North shore of Lake Huron, Canada Geological Survey Memoir, 143, 160p.

Condie, K. C., 1989, Plate Tectonics And Crustal Evolution, 3rd ed., Pergamon, New York.

Costin, L. S., 1987, Time-dependent deformation and failure, in: Atkinson, B. K., ed., Fracture Mechanics of Rock, Academic Press, London, 167-216.

Cottrell, A. H., 1965, Mechanics of fracture, Tewksbury Symposium on Fracture, Eng. Faculty, University of Melbourne, 1-27.

Cottrell, B. and Rice, J. R., 1980, Slightly curved or kinked cracks, Int. J. Fract., 16, 155-169.

Cruikshank, K. M., Zhao, G. and Johnson, A. M., 1991, Analysis of minor fractures associated with joints and faulted joints, J. Struct. Geol., 13, 865-886.

Culshaw, N. G., Corrigan, D., Jamieson, R. A., Ketchum, J., Wallace, P. and Wodicka, N., 1991, Traverse of the Central Gneiss Belt, Grenville Province, Georgian Bay, Geological Association of Canada, Toronto'91, Guidebook, Field Trip B3, 40p.

Dahlen, F. A., Suppe, J. and Davis, D., 1984, Mechanics of fold-and thrust belts and accretionary wedges: Cohesive Coulomb theory, J. Geophys. Res., 89, 10,087-10,101.

Davidson, A., 1986a, New interpretations in the Southwestern Grenville Province, in: Moore, J. M., Davidson, A. and Baer, A. J., eds., The Grenville Province, Geological Association of Canada, Special Paper 31, 61-74.

Davidson, A., 1986b, Grenville Front relationships near Killarney, Ontario, in: Moore, J. M., Davidson, A. and Baer, A. J., eds., The Grenville Province, Geological Association of Canada, Special Paper 31, 107-117.

Davidson, A., 1991, Metamorphism and tectonic setting of gabbroic and related rocks in the Central Gneiss Belt, Grenville Province, Ontario, Geological Association of Canada, Toronto'91, Guidebook, Field Trip A.2, 60p.

Davidson, A., 1992, Relationship between faults in the South Province and the Grenville Front southeast of Sudbury, Ontario, in: Current Research, Part C, Geological Survey of Canada, Paper 92-1C, 121-127.

Davies, R. K. and Pollard, D. D., 1986, Relations between left-lateral strike-slip faults and right-lateral monoclinal kink bands in granodiorite, Mt. Abbot Quadrangle, Siera Nevada, California, Pure & Appl. Geophys., 124, 177-201.

Davis, D., Suppe, J. and Dahlen, F. A., 1983, Mechanics of fold-and-thrust belts and accretionary wedges, J. Geophys. Res., 88, 1153-1172.

Derry, D. R., 1950, A tectonic map of Canada, Geological Association of Canada Proceedings, 3, 39-53.

Dickin, A. P. and McNutt, R. H., 1989a, Nd model age mapping of the southeast margin of the Archean foreland in the Grenville Province of Ontario, Geology, 17, 299-303.

Dickin, A. P. and McNutt, R. H., 1989b, Nd model age mapping of Grenville lithotectonic domains: The Abitibi-Grenville Lithoprobe Project, 1989 Transect Report and Updated Proposal, Montreal, Quebec, 66-68.

Dickin, A. P., McNutt, R. H. and Clifford, P. M., 1990, A neodymium isotope study of plutons near the Grenville Front in Ontario, Canada, Chemical Geology, 83, 315-324.

Donath, F. A., 1969, The development of kink bands in brittle anistropic rocks, Geol. Soc. Am. Memoir, 115, 453-493.

Dunn, W. M. and Hancock, P. L., 1994, Palaeostress analysis of small-scale brittle structure, in: Hancock, P. L., ed., Continental Deformation, Pergamon Press, Oxford, 101-120.

Easton, R. M., 1986, Geochronology of the Grenville Province, Part I: compilation of data and Part II: synthesis and interpretation, in: Moore, J. M., Davidson, A. and Baer, A. J., eds., The Grenville Province, Geological Association of Canada, Special Paper 31, 127-173.

Easton, R. M., 1992, The Grenville Province and the Proterozoic history of central and southern Ontario, in: Geology of Ontario, Ontario Geological Survey, Special Volume 4, Part 2, 714-904.

Eisbacher, G. H., 1970, Deformation mechanics of mylonite rocks and fractured granites in Cobequid mountains, Nova Scotia, Canada, Geol. Soc. Am. Bull., 81, 2009-2020.

Emerman, S. H. and Turcott, D. L., 1983, A fluid model for the shape of accretionary wedges, Earth Planet. Sci. Lett., 63, 379-384.

Engelder, T., 1985, Loading paths to joint propagation during a tectonic cycle: an example from the Appalachian Plateau, U. S. A., J. Struct. Geol., 7, 459-476.

Engelder, T., 1987, Joints and shear fractures in rock, in: Atkinson, B. K., ed., Fracture Mechanics of Rocks, Academic Press, London, 27-69.

Etchecopar, A., 1977, A plane kinematic model of progressive deformation in a polycrystalline aggregate, Tectonophysics, 39, 121-139.

Fahrig, W. F. and West, T. D., 1986, Diabase dyke swarms of the Canadian Shield, Geological Survey of Canada, Map 1627A.

Fairbairn, H. W., 1949, Structural Petrology of Deformed Rocks, Addison-Wesley, Cambridge, Massachusetts.

Fan, X. and Clifford, P. M., 1993, Tectonic implication of the structural studies in the Killarney Igneous Complex, Ontario, Canada, GSA Program with Abstracts, 25, 168.

Fan, X. and Clifford, P. M., 1994, Structural analysis in the Killarney Igneous Complex, Ontario: A case study of secondary fractures, GAC/MAC Program with Abstracts, 19, A35.

Ferguson. C. C., Lloyd, G. E. and Knipe, R. J., 1987, Fracture mechanics and deformation processes in natural quartz: a combined Vickers indentation, SEM and TEM study, Can. J. Earth Sci., 24, 544-555.

Fletcher, R. C., 1989, Approximate analytical solutions for a cohesive fold-and-thrust wedge: Some results for lateral variation in wedge properties and for finite wedge angle, J. Geophys. Res., 94, 10,347-10,354.

Frarey, M. J. and Cannon, R. T., 1969, Notes to accompany a map of the geology of the Proterozoic rocks of Lake Panache-Collins inlet map-areas, Ontario (41I/3, H/14), Geological Survey of Canada Paper 68-63, 5p.

Frarey, M. J., 1985, Proterozoic geology of the Lake Panache-Collins inlet area, Ontario, Geological Survey of Canada Paper 83-22, 61p.

Fueten, F., Robin, P.-Y. F. and Stephens, R., 1991, A model for the development of a domainal quartz c-axis fabrics in a coarse-grained gneiss, J. Struct. Geol., 13, 1111-1124.

Fueten, F., 1992, Tectonic interpretations of systematic variations in quartz c-axis fabrics across the Thompson Belt, J. Struct. Geol., 14, 775-789.

Fung, Y. C., 1965, Foundations of Solid Mechanics, Chapman and Hall, London, 593p.

Garcia-Celma, A., 1982, c-axis fabric asymmetry in relation to curved shear planes in Cap de Creus quartz mylonites, in: International Conference on Planar and Linear Fabrics in Deformed Rocks Proceedings, Zurich, Mitteillungen aus dem Geologischem Institut der ETH und der Universitat Zurich, Neue Folge 239A, 111-114.

Grant, J. A., 1964, Rubidium-Strontium isochron study of the Grenville Front new Lake Timagami, Ontario, Science, 146, 1049-1053.

Griffith, A. A., 1921, The phenomena of rupture and flow in solids, Phil. Trans. R. Soc. Lond., 221, 163-178.

Groshong, R. H., 1988, Low-temperature deformation mechanisms and their interpretation, Geol. Soci. Am. Bull., 100, 1329-1360.

Hafner, W., 1951, Stress distribution and faulting, Geol. Soc. Am. Bull., 62, 373-398.

Handin, J., 1969, On the Coulomb-Mohr failure criterion, J. of Geophys. Research, 74, 5343-5349.

Hanmer, S., 1982, Microstructure and geochemistry of plagioclase and microcline in naturally deformed granite, J. Struct. Geol., 4, 197-213.

Hatcher, R. D., 1990, Structural Geology: Principles, Concepts, and Problems, Merrill Publishing Company, Ohio, 531p.

Hobbs, B. E., 1968, Recrystallization of single quartz crystals, Tectonophysics, 6, 353-401.

Hsu, M. Y., 1968, Structural analysis along the Grenville Front near Sudbury, Ontario: M.Sc. thesis, McMaster University, Hamilton, Ontario, 104p.

Irwin, G. R., 1957, Analysis of stresses and strain near the end of a crack traversing a plate, J. Appl. Mech., 24, 361-364.

Jaeger, J. C. and Cook, N. G. W., 1976, Fundamentals of Rock Mechanics, 2nd ed., Chapman and Hall Ltd., London, 585p.

Jones, W. A., 1930, The petrography of the rocks in the vicinity of Killarney, Ontario,

Univ. Tor. Studies, Geol. Ser., 29, 39-60.

Kamb, W. B., 1959, Ice petrofabric observations from Blue Glacier, Washington, in relation to theory and experiments, J. Geophys. Res., 64, 1891-1919.

Ketchum, J. W. F., Jamieson, R. A., Heaman, L. M., Culshaw, N. G. and Krogh, T. E., 1994, 1.45 Ga granulites in the southwestern Grenville Province: Geology setting, P-T conditions, and U-Pb geochronology, Geology, 22, 215-218.

Kirby, S. H., 1977, The effects of α-ß phase transfomation of the creep properties of hydrolytically-weakened synthetic quartz, Geophys. Res. Lett., 4, 97-100.

Knott, J. F., 1973, Fundamentals of Fracture Mechanics, Butterworths, London.

Kohlstedt, D. L. and Weathers, M. S., 1980, Deformation-induced microstructures, paleopiezometers, and differential stresses in deeply eroded fault zones, J. Geophys. Res., 85, 6269-6285.

Krogh, T. E. and Davis, G. L., 1969, Geochronology of the Grenville Province, Carnegie Institution of Washington Yearbook 67, 224-230.

Krogh, T. E. and Davis, G. L., 1970, Isotopic ages along the Grenville Front in Ontario, Carnegie Institution of Washington Yearbook 68, 309-313.

Krogh, T. E., Davis, G. L. and Frarey, M. J., 1971, Isotopic ages along the Grenville Front in the Bell Lake area, Southwest of Sudbury, Ontario, Carnegie Institution of Washington Yearbook 69, 337-339.

Krogh, T. E., Davis, D. W. and Corfu, F., 1984, Precise U-Pb zircon and baddeleyite ages for the Sudbury area, in: The Geology and Ore Deposits of the Sudbury Structure, Ontario Geological Survey, Special Volume 1, 431-446.

Krogh, T. E. and Wardle, R., 1984, U-Pb isotopic ages along Grenville Front, Geological Association of Canada Program with Abstracts, 9, 80.

Krogh, T. E., 1989, Terrane identification in the Grenville Province from detrital and metamorphic zircon ages: The Abitibi-Grenville Lithoprobe Project, 1989 Transect Report and Updated Proposal, Montreal, Quebec, 63-65.

Lapworth, C., 1885, The highland controversy in British history: Its causes, course, and consequences, Nature, 32, 558-559.

LaTour, T. E. and Fullager, P. D., 1986, Rb-Sr study of mylonite rocks at the Grenville Front near Coniston, Ontario: some preliminary results, in: The Grenville Province, Geological Association of Canada, Special Paper 31, 223-233.

Law, R. D., 1986, Relationships between strain and quartz crystallographic fabrics in the Roche Maurice quartzites of Plongastel, western Brittany, J. Struct. Geol., 8, 493-515.

Law, R. D., Casey, M. and Knipe, R. J., 1986, Kinematic and tectonic significance of microstructures and crystallographic fabrics within quartz mylonites from the Assynt and Eriboll regions of the Moine thrust zone, NW Scotland, Earth Sciences, 77, 99-125.

Lawn, B. R. and Wilshaw, T. R., 1975, Fracture of Brittle Solids, Cambridge University Press, Cambridge, 204p.

Lawn, B. R., 1983, Physics of fracture, J. Am. Ceram. Soc., 66, 83-91.

Lawson, A. C., 1929, Some Huronian problems, Geol. Soc. Am. Bull., 40, 361-383.

Lisle, R. J., 1987, Principal stress orientations from faults: an additional constraint, Annales Tectonicae, 1, 155-158.

Lisle, R. J., 1988, ROMSA: A basic program for palaeostress analysis using fault-striation data, Computers & Geosciences, 14, 255-259.

Lister, G. S., 1977, Crossed-girdle c-axis fabrics in quartzites plastically deformed by plane strain and progressive simple shear, Tectonophysics, 39, 51-54.

Lister, G. S., Paterson, M. S. and Hobbs, B. E., 1978, The simulation of fabric development in plastic deformation and its application to quartzite: the model, Tectonophysics, 45, 107-158.

Lister, G. S. and Price, G. P., 1978, Fabric development in a quartz-feldspar mylonite, Tectonophysics, 49, 37-78.

Lister, G. S., 1979, Fabric transitions in plastically deformed quartzites: competition between basal, prism and rhomb systems, Bull. Mineral, 102, 232-241.

Lister, G. S. and Paterson, M. S., 1979, The simulation of fabric development during plastic deformation and its application to quartzites: fabric transitions, J. Struct.

Geol., 1, 99-115.

Lister, G. S. and Williams, P. F., 1979, Fabric development in shear zones, theoretical controls and observed phenomena, J. Struct. Geol., 1, 283-297.

Lister, G. S. and Hobbs, B. E., 1980, The simulation of fabric development during plastic deformation and its application to quartzite: the influence of deformation history, J. Struct. Geol., 2, 355-370.

Lister, G. S. and Dornsiepen, U. F., 1982, Fabric transitions in the Saxony granulite terrain, J. Struct. Geol., 4, 81-92.

Lister, G. S. and Williams, P. F., 1983, The partitioning of deformation in flowing rock masses, Tectonophysics, 92, 1-33.

Liu, J. Y. and Ranalli, G., 1992, Stress in an overthrust sheet and propagation of thrusting: An Airy stress function solution, Tectonics, 11, 549-559.

Lumbers, S. B., 1975, Geology of the Burwash area, Districts of Nipissing, Parry Sound and Sudbury, Ontario Division of Mines Geological Report 116, 158p.

Lumbers, S. B., 1978, Geology of the Grenville Front Tectonic Zone in Ontario, in: Currie, A. L. and Mackasey, W. O., eds, Toronto'78, Field Trip Guidebook, Geological Association of Canada, 347-361.

Lumbers, S. B. and Vertolli, V. M., 1991, Proterozoic plutonism within the Central Gneiss Belt and Grenville Front Tectonic Zone, Grenville Province, Ontario, Geological Association of Canada, Program with Abstracts, 16, A77.

Lyell, C., 1834, Principles of Geology, 3rd ed., J. Murray, London.

McClelland, E. and McCaig, A. M., 1989, Palaeomagnetic estimates of rotations in compressional regimes and potential discrimination between thin-skinned and deep crustal deformation, in: Kissel, C. and Laj, C., eds., Palaeomagnetic Rotations and Continental Deformation, Kluwer Academic Publishers, the Netherlands, 365-379.

McKenzie, D. P., 1969, The relation between fault plane solutions and the directions of the principal stresses, Bull. Seismol. Soc. America, 59, 591-601.

Means, W. D., 1981, The concept of steady-state foliation, Tectonophysics, 78, 179-199.

Mercier, J. C., Anderson, D. A. and Carter, N. L., 1977, Stress in the lithosphere: inferences from the steady state flow of rocks, Pure & Appl. Geophys., 115, 199-226.

Miller, R. R., 1983, Age and petrological relationships of some igneous-textured and gneissic alkaline rocks in the Haliburton-Bancroft area: Ph.D thesis, University of Toronto, Toronto, Ontario, 345p.

Murray, A., 1849, Report of Alexander Murray, Esq., Asst. Geologist, Geol. Serv. Can. Ann. Rep. for 1847-48, 93-124.

Murray, A., 1857, Report of Alexander Murray for the year 1856, Geol. Surv. Can. Rep. of Prog. for the years 1853-56, 145-188.

O'Donnell, L. L., 1986, Characterization of the nature of deformation and metamorphic gradient across the Grenville Front Tectonic Zone in Carlyle Township, Ontario: M. Sc. thesis, McMaster University, Hamilton, Ontario, 199p.

Olson, J. and Pollard, D. D., 1988, Inferring stress state from detailed joint geometry, in: Key Questions in Rock Mechanics, Cundall, P. A., Sterling, R. L. and Starfield, A. M., eds., Proc. 29th U.S. Symp. on Rock Mechanics, A.A. Balkoma, Rotterdam, 159-167.

Olson, J. and Pollard, D. D., 1989, Inferring paleostresses from natural fracture patterns: A new method, Geology, 17, 345-348.

Ord, T. S. and Christie, J. M., 1984, Flow stresses from microstructures in mylonitic quartzite of the Moine thrust zone, Assynt area, Scotland, J. Struct. Geol., 6, 639-654.

Osete, M. L., Freeman, R. and Vegas, R., 1989, Palaeomagnetic evidence for block rotations and distributed deformation of the Iberian-African plate boundary, in: Kissel, C. and Laj, C., eds., Palaeomagnetic Rotations and Continental Deformation, Kluwer Academic Publishers, the Netherlands, 381-391.

Paris, P. and Sih, G., 1965, Stress analysis of cracks, in: Symposium on Fracture Toughness Testing and Applications, Spec. Tech. Publ., 30-81.

Passchier, C. W. and Simpson, C., 1986, Porphyroclast systems as kinematic indicators, J. Struct. Geol., 8, 831-843.

Platt, J. P., 1986, Dynamics of orogenic wedges and the uplift of high-pressure metamorphic rocks, Geol. Soc. Am. Bull., 97, 1037-1053.

Pollard, D. D. and Segall, P., 1987, Theoretical displacements and stresses near fractures in rock: With applications to faults, joints, veins, dikes, and solution surfaces, in: Atkinson, B. K., ed., Fracture Mechanics of Rock, Academic Press, London, 277-349.

Pollard, D. D. and Aydin, A., 1988, Progress in the understanding of jointing over the past century, Geol. Soc. Am. Bull., 100, 1181-1204.

Quirke, T. T., 1917, Espanola District, Ontario, Geol. Surv. Can. Memoir, 102, 87p.

Quirke, T. T. and Collins, W. H., 1930, The disappearance of the Huronian, Geol. Surv. Can. Memoir, 160, 129p.

Ragan, D. M., 1985, Structural Geology: An Introduction to Geometrical Techniques, 3rd ed., John Wiley & Sons Inc., New York, 393p.

Ramsay, J. G. and Graham, R. H., 1970, Strain variation in shear belts, Can. J. Earth Sci., 7, 786-813.

Ramsay, J. G., 1980, Shear zone geometry: a review, J. Struct. Geol., 2, 83-99.

Ramsay, J. G. and Huber, M. I., 1987, The Techniques of Modern Structural Geology, Volume 2: Folds and Fractures, Academic Press, London, 392p.

Ratschbacher, L., Merle, O., Davy, P. and Cobbold, P., 1991, Lateral extrusion in the Eastern Alps, Part 1: Boundary conditions and experiments scaled for gravity, Tectonics, 2, 245-256.

Ratschbacher, L., Frisch, W., Linzer, H. and Merle, O., 1991, Lateral extrusion in the Eastern Alps, Part 2: Structural analysis, Tectonics, 2, 257-271.

Riedel, W., 1929, Zur mechanik geologischer brucherscheinungen, Zent. Min. Geol. Pul. 1929, 354-368.

Rivers, T., Martingole, J., Gc er, C. F. and Davidson, A., 1989, New tectonic subdivisions of the Grenville Province, southeast Canadian Shield, Tectonics, 8, 63-84.

Robin, P.-Y. F. and Jowett, C. E., 1986, Computerized density contouring and statistical evaluation of orientation data using counting circles and continuous weighting functions, Tectonophysics, 121, 207-223.

Ron, H., Aydin, A. and Nur, A., 1986, Strike-slip faulting and block rotation in the Lake Mead fault zone, Geology, 14, 1020-1023.

Schmid, S. M., Casey, M. and Starkey, J., 1981, An illustration of the advantages of a complete texture analysis described by the orientation distribution function (OCD) using quartz pole figure data, Tectonophysics, 78, 101-117.

Schmid, S. M., 1982, Microfabric studies as indicators of deformation mechanisms and flow laws operating in mountain building, in: Hsu, K. J., ed., Mountain Building Processes, Academic Press, London, 95-110.

Segall, P. and Pollard, D. D., 1980, Mechanics of discontinuous faults, J. Geophys. Res., 85, 4337-4350.

Segall, P. and Pollard, D. D., 1983, Joint formation in granitic rock of the Sierra Nevada, Geol. Soc. Am. Bull., 94, 563-575.

Segall, P., 1984, Formation and growth of extensional fracture sets, Geol. Soc. Am. Bull., 95, 454-462.

Sibson, R. H., 1977, Fault rocks and fault mechanics, Geol. Soc. of London Journal, 133, 191-213.

Simpson, C. and Schmid, S. M., 1983, An evaluation of criteria to deduce the sense of movement in sheared rocks, Bull. Geol. Soc. Am., 94, 1281-1288.

Sokolnikoff, I. S., 1956, Mathematical Theory of Elasticity, 2nd ed., McGraw-Hill, New York, 476p.

Spaven, H. R., 1966, Granite tectonics in part of Eden Township, Sudbury District, Ontario: M.Sc thesis, McMaster University, Hamilton, Ontario, 80p.

Starkey, J., 1979, Petrofabric analysis of Saxony granulites by optical and X-ray diffraction methods, Tectonophysics, 58, 201-219.

Stockmal, G. S., 1983, Modelling of large-scale accretionary wedge deformation, J. Geophys. Res., 88, 8271-8287.

Stockwell, C. H., 1982, Proposals for the time classification and correlation of Precambrian rocks and events in Canada and adjacent areas of the Canadian Shield, Part I: A time classification of Precambrian rocks and events, Geol. Surv. Can. Paper 80-19, 135.

Suppe, J., 1985, Principles of Structural Geology, Prentice-Hall Inc., Englewood Cliffs, New Jersery, 537p.

Swain, M. V. and Hagan, J. T., 1978, Some observations of overlapping interacting cracks, Engineering Fracture Mech., 10, 299-304.

Sylvester, A. G., 1988, Strike-slip faults, Geol. Soc. Am. Bull., 100, 1666-1703.

Tada, H., Paris, P. C. and Irwin, G. R., 1973, The Stress Analysis of Cracks Handbook, Del Research Corporation, Hellertown, PA.

Tapponnier, P. and Molnar, P., 1976, Slip-line field theory and large-scale continental tectonics, Nature, 264, 319-324.

Tapponnier, P., Peltzer, G., Le Dain, A. Y., Armijo, R. and Cobbold, P., 1982, Propagating extrusion tectonics in Asia: New insights from simple experiments with plasticine, Geology, 10, 611-616.

Tchalenko, J. S., 1968, The evolution of kink-bands and the development of compression textures in sheared clays, Tectonophysics, 6, 159-174.

Timoshenko, S. P. and Goodier, J. N., 1951, Theory of Elasticity, 2nd ed., McGraw-Hill, New York, 506p.

Tjia, H. D., 1967, Sense of fault displacements, Geologie En Mijnbouw, 46, 392-396.

Tremblay, A. and Malo, M., 1991, Significance of brittle and plastic fabrics within the Massawippi Lake fault zone, Southern Canadian Appalachians, J. Struct. Geol., 9, 1013-1023.

Tullis, J., Christie, J. M. and Griggs, D. T., 1973, Microstructures and preferred orientations of experimentally deformed quartzites, Bull. Geol. Soc. Am., 84, 297-314.

Tullis, T. E. and Tullis, J., 1986, Experimental rock deformation techniques, Am. Geophys. Un. Geophys. Monogr., 36, 297-324.

Twiss, R. J., 1977, Theory and applicability of a recrystallized grain size paleopiezometer, Pure & Appl. Geophys., 115, 227-244.

Twiss, R. J. and Sellars, C. M., Limits of applicability of the recrystallized grain size geopiezometer, Geophys. Res. Letters, 5, 337-340.

Twiss, R. J. and Moores, E. M., 1992, Structural Geology, W. H. Freeman and Company, New York, 532p.

van Schmus, W. R., 1965, The geochronology of the Blind River-Bruce Mine area, Ontario, Canada, J. of Geol., 73, 755-780.

van Schmus, W. R., 1976, Early and middle Proterozoic history of the Great Lake area, North America, Royal Society of London Philosophical Transactions, Ser. A., 280, 605-628.

van Schmus, W. R. and Bickford, M. E., 1981, Proterozoic chronology and evolution of midcontinent region, North America, in: Kroner, A., ed., Precambrian Plate Tectonics, Elsevier, Amersterdam, Netherlands, 261-296.

van Breemen, O. and Davidson, A., 1988, Northeast extension of Proterozoic terranes of midcontinental North America, Geol. Soc. Am. Bull., 100, 630-638.

Wanless, R. K. and Loveridge, W. D., 1972, Rubidium-Strontium isochron age studies, Report 1, Geol. Surv. Can. Paper 72-23, 77p.

Weathers, M. S., Bird, J. M., Cooper, P. F. and Kohlstedt, D. L., 1979, Differential stress determined from deformation-induced mircostructures of the Moine thrust zone, J. Geophys. Res., 84, 7495-7509.

Wenk, H. R. and Christie, J. M., 1991, Comments on the interpretation of deformation textures in rocks, J. Struct. Geol., 13, 1091-1110.

Wetherill, G. W., Davis, G. L. and Tilton, G. R., 1960, Age measurements from the Culter Batholith, Culter, Ontario, J. Geophys. Research, 65, 2461-2466.

White, S. H., 1975, Tectonic deformation and recrystallization of oligoclase, Contrib. Mineral. Petrol., 50, 287-304.

White, S. H., 1976, The effects of strain on microstructures fabrics and deformation mechanisms in quartzites, Phil. Trans. Royal Soc. London, Ser. A, 283, 69-86.

White, S. H., 1977, Geological significance of recovery and recrystallization processes in quartz, Tectonophysics, 39, 143-170.

White, S. H., Burrows, S. E. and Carreras, J., 1978, Textural and microstructural development in a naturally deformed quartzite: A metallurgical approach, in: International Conference on Textures of Materials, 5th Procedings, Berlin, Germany, Springer, 211-220.

White, S. H., 1979, Difficulties associated with paleostress estimates, Bull, Miner., 102, 210-215.

White, S. H., Burrows, S. E., Carreras, J., Shaw, N. D. and Humphreys, F. J., 1980, On mylonites in ductile shear zones, J. Struct. Geol., 2, 175-188.

Wise, D. U., Dunn, D. E., Engelder, J. T., Geiser, P. A., Hatcher, R. D., Kish, S. A., Odom, A. L. and Schamel, S., 1984, Fault-related rocks: Suggestions for terminology, Geology, 12, 391-394.

Wynne-Edwards, H. R., 1972, The Grenville Province, in: Price, R. A. and Douglas, R. J. W., eds., Variations in Tectonic Styles in Canada, Geological Association of Canada, Special Paper 11, 263-334.

Xiao, H. B., Dahlen, F. A. and Suppe, J., 1991, Mechanics of extensional wedges, J. Geophys. Res., 96, 10,301-10,328.

Yin, A., 1986, A mechanical model for a wedge-shaped thrust sheet, EOS Trans. AGU, 67, 1242.

Yin, A., 1993, Mechanics of wedge-shaped fault blocks: 1. An elastic solution for compressional wedges, J. Geophys. Res., 98, 14,245-14,256.

Zolnai, A. I., Price, R. A. and Helmstaedt, H., 1984, Regional cross-section of the Southern Province adjacent to Lake Huron, Ontario: implications for the tectonic significance of the Murray fault zone, Canadian Journal of Earth Sciences, 21, 447-456.

Appendix A, Oreintation of main faults

NO.	Strike	Dip	NO.	Strike	Dip
1	237	80	34	242	83
2	240	90	35	238	82
3	239	80	36	238	81
4	238	84	37	240	84
5	242	80	38	239	80
6	241	78	39	241	78
7	241	82	40	241	80
8	236	80	41	241	81
9	242	82	42	240	81
10	239	84	43	240	80
11	236	81	44	241	79
12	240	79	45	240	83
13	242	80	46	239	81
14	240	79	47	239	81
15	240	79	48	239	82
16	242	82	49	240	82
17	241	82	50	239	81
18	240	79	51	239	82
19	243	80	52	240	82
20	241	80	53	241	80
21	239	82	54	239	82
22	239	82	55	236	81
23	239	82	56	239	79
24	239	79	57	237	80
25	238	82	58	243	84
26	241	79	59	235	81
27	238	82	60	245	80
28	240	87	61	240	78
29	236	83	62	240	80
30	239	82	63	242	84
31	240	82	64	240	83
32	238	80	65	241	80
33	237	80	66	239	82

Appendix B, Orientation of minor fractures in Main Site

No.	Strike	Dip	No.	Strike	Dip
1	2	84	99	2	82
2	4	82	100	18	78
3	21	85	101	25	85
4	22	86	102	20	84
5	21	85	103	34	60
6	32	64	104	32	60
7	42	68	105	41	62
8	52	70	106	57	70
9	55	70	107	50	69
10	55	68	108	55	72
11	51	69	109	56	68
12	52	68	110	55	82
13	53	70	111	54	85
14	56	85	112	50	72
15	50	78	113	51	85
16	52	84	114	78	70
17	80	70	115	80	72
18	75	78	116	73	77
19	75	76	117	77	72
20	81	64	118	85	76
21	82	90	119	95	72
22	101	70	120	95	90
23	96	90	121	75	77
24	93	66	122	92	88
25	98	86	123	105	88
26	91	84	124	90	64
27	101	75	125	100	71
28	103	71	126	101	71
29	116	56	127	100	88
30	100	88	128	102	84
31	105	75	129	110	74
32	101	80	130	110	74
33	125	80	131	125	79
34	125	90	132	115	90
35	122	70	133	120	70

(continued...)

36	121	71	134	135	72
37	140	76	135	136	72
38	138	85	136	165	90
39	171	90	137	174	85
40	164	70	138	205	90
41	256	62	139	257	62
42	296	90	140	230	78
43	300	89	141	295	88
44	298	84	142	301	87
45	305	80	143	310	84
46	300	84	144	297	82
47	36	63	145	302	78
48	32	61	146	2	84
49	51	70	147	32	64
50	57	69	148	25	57
51	53	75	149	49	67
52	57	69	150	42	69
53	38	59	151	42	64
54	50	70	152	43	60
55	78	71	153	40	54
56	91	89	154	83	70
57	82	67	155	82	60
58	84	43	156	87	70
59	90	80	157	77	55
60	109	89	158	90	81
61	99	86	159	105	85
62	106	90	160	110	87
63	112	90	161	106	88
64	115	82	162	108	90
65	122	75	163	101	89
66	121	75	164	125	75
67	120	78	165	120	78
68	120	85	166	115	85
69	131	83	167	130	85
70	132	85	168	124	85
71	160	44	169	125	81
72	160	85	170	147	50
73	170	90	171	166	83
74	283	88	172	168	69
75	296	89	173	282	88
76	290	84	174	290	87
77	321	65	175	300	85
78	311	85	176	275	80
79	337	62	177	320	73
80	335	57	178	333	29

(continued...)

81	343	58	179	346	72
82	349	61	180	338	83
83	345	31	181	337	69
84	333	34	182	339	62
85	336	54	183	330	82
86	348	86	184	350	58
87	355	53	185	304	86
88	300	81	186	297	81
89	300	86	187	282	88
90	282	86	188	281	87
91	282	90	189	314	50
92	270	84	190	325	48
93	312	50	191	321	70
94	310	82	192	310	75
95	317	81	193	350	77
96	320	78	194	344	79
97	348	85	195	350	55
98	345	88	196	342	84

Appendix C, Orientation of fractures in undeformed area

No.	Strike	Dip	No.	Strike	Dip
1	65	90	36	50	90
2	75	90	37	105	90
3	95	90	38	106	90
4	95	90	39	150	90
5	25	90	40	112	90
6	93	90	41	155	90
7	115	90	42	125	90
8	0	90	43	80	90
9	30	90	44	60	90
10	65	90	45	115	90
11	90	90	46	115	90
12	60	90	47	155	90
13	52	90	48	120	90
14	50	90	49	155	90
15	52	90	50	115	90
16	35	90	51	115	90
17	36	90	52	155	90
18	120	90	53	145	90
19	50	90	54	130	90
20	38	90	55	125	90
21	88	90	56	135	90
22	72	90	57	137	90
23	90	90	58	130	90
24	110	90	59	110	90
25	40	90	60	102	90
26	65	90	61	104	90
27	115	90	62	102	90
28	118	90	63	96	90
29	130	90	64	152	90
30	140	90	65	74	90
31	140	90	66	98	90
32	140	90	67	120	90
33	150	90	68	78	90
34	155	90	69	140	90
35	155	90	70	157	90